

A PLASTIC STRESS ANALYSIS OF CYLINDRICAL WAFERS  
UNDER ELASTICALLY DEFORMABLE COMPRESSION PLATES

Prepared by:

Dr. Robert L. Davis  
Prof. John W. Jackson

Mechanical Engineering  
University of Maryland

M.E. Dept. Report No. 1965-1

This report is based on a thesis submitted by Robert L. Davis to the University of Maryland in partial fulfillment of the requirements for the degree of Doctor of Philosophy.

Dr. Davis will be associated with the University of Missouri, Rolla Division, after September, 1965, as Assistant Professor of Mechanics.

A PLASTIC STRESS ANALYSIS OF CYLINDRICAL WAFERS  
UNDER ELASTICALLY DEFORMABLE COMPRESSION PLATES

Prepared by:

Dr. Robert L. Davis  
Prof. John W. Jackson

ABSTRACT

The use of an opposed-anvil apparatus as a mechanism for generating high-pressures in radially confined, circular specimens, has attracted the interest of many competent experimenters, and they have utilized the facility to explore the behavior of many materials in an environment of high pressure and temperature. The increased utility of the opposed-anvil device has demanded that a pressure calibration be made to determine the actual pressure gradient existing within the compressed specimen (pressure cell). It has long since been the general consensus of experimenters, that the pressure is not uniformly distributed across the cell, but agreement has not been achieved as to the location and magnitude of its maximum.

This report represents a combined analytical-experimental analysis of the pressure distribution occurring in a model, similar in structure and characteristics to the opposed-anvil or Bridgman-type pressure cell. From a mathematical necessity, the model has been constructed, and assumed to perform, in a manner consistent with the applicable laws presented in the theory of plasticity (von Mises yield criteria, St. Venant's flow laws, etc.). Such quantities as material compressibility, and pressure dependent properties, have been shelved in favor of examining the influence of radial constraints, material strain hardening, wafer diameter-to-height ratio, etc.

This report presents a method of solution that is traced from the results of a rigid-anvil analysis, to the establishment of two-dimensional stress and pressure distributions in compressed, low-shear, constrained and unconstrained wafers. A discussion is presented on the continuance of the solution for higher shear stress levels, and more general displacement patterns. The integrated axial normal stress distribution across the specimen surface has been verified with several materials, with and without radial constraints. Pressure levels in excess of the first bismuth transition have been recorded, and a possible high-volume, high-pressure generating device has been described. The future work that can, and will be attempted, is discussed briefly.

## TABLE OF CONTENTS

	Page
LIST OF TABLES . . . . .	iv
LIST OF FIGURES . . . . .	v
NOMENCLATURE . . . . .	vii
INTRODUCTION . . . . .	1
PURPOSE AND OBJECTIVES . . . . .	6
I.    STRESS ANALYSIS . . . . .	7
A.    Formulation of Governing Equations . . . . .	10
B.    Method of Solution . . . . .	15
C.    Resulting Stress Equations . . . . .	22
1.    Two-Dimensional Wafer Profile-With Shear . . . . .	22
2.    One-Dimensional Wafer Profile-Zero Shear . . . . .	38
3.    Rigid Anvils-Zero Shear . . . . .	42
4.    Two-Dimensional Hollow Wafer-With Shear . . . . .	43
II.    EXPERIMENTAL FACILITIES AND PROCEDURES . . . . .	46
III.   STRESS AND PRESSURE DISTRIBUTIONS . . . . .	56
IV.    FUTURE WORK . . . . .	85
SUMMARY AND CONCLUSIONS . . . . .	86
APPENDIX I.  COMPUTER PROGRAMS AND SAMPLE RESULTS . . . . .	88
REFERENCES . . . . .	117
SELECTED BIBLIOGRAPHY . . . . .	119

## LIST OF TABLES

	Page
TABLE 1. Experimental Data for Compression of Solid, Unconfined 303 Stainless Steel Wafers . . . . .	77
TABLE 2. Experimental Data for Compression of Solid, Confined 303 Stainless Steel Wafers . . . . .	78
TABLE 3. Experimental Data for Compression of Hollow, Unconfined 303 Stainless Steel Wafers . . . . .	79
TABLE 4. Experimental Data for Compression of Hollow, Confined 303 Stainless Steel Wafers . . . . .	80
TABLE 5. Experimental Data for Compression of Solid and Hollow, Unconfined Armco Iron Wafers . . . . .	81
TABLE 6. Experimental Data for Compression of Solid, Unconfined 6061 Aluminum Wafers . . . . .	82
TABLE 7. Experimental Data for Compression of Solid, Unconfined 2S Aluminum Wafers . . . . .	83

## LIST OF FIGURES

		Page
FIGURE	1. Postulated Wafer Profile for One- and Two-Dimensional Analysis . . . . .	8
FIGURE	2. 2500-Ton Hydraulic Press . . . . .	47
FIGURE	3. Component Parts of Confined Wafer Compression System . . . . .	49
FIGURE	4. Assembly View of Wafer-Containing Ring . . . . .	50
FIGURE	5. Complete Assembly of Confined Wafer Compression System . . . . .	54
FIGURE	6. Applied Force-Displacement Relation for an Unconfined 303 Stainless Steel Wafer . . . . .	57
FIGURE	7. Stress Distribution for 303 Stainless Steel. Case I-A . . . . .	59
FIGURE	8. Stress Distribution for 303 Stainless Steel. Case I-B . . . . .	60
FIGURE	9. Applied Force-Displacement Relation for an Unconfined 6061 Aluminum Wafer . . . . .	62
FIGURE	10. Stress Distribution for 6061 Aluminum Case I-A . . . . .	63
FIGURE	11. Applied Force-Displacement Relation for an Unconfined Armco Iron Wafer . . . . .	65
FIGURE	12. Stress Distribution for Armco Iron Case I-A . . . . .	66
FIGURE	13. Applied Force-Strain Relation for a Confined 303 Stainless Steel Wafer . . . . .	67
FIGURE	14. Stress Distribution for 303 Stainless Steel. Case II-A. $R_c/R_o = 1.012$ . . . . .	69
FIGURE	15. Stress Distribution for 303 Stainless Steel. Case II-A. $R_c/R_o = 1.024$ . . . . .	70
FIGURE	16. Stress Distribution for 303 Stainless Steel. Case II-A. $D/H = 6.5$ . . . . .	71
FIGURE	17. Stress Distribution for 303 Stainless Steel. Case II-A. $D/H = 13$ . . . . .	72

## LIST OF FIGURES (Continued)

		Page
FIGURE 18.	Influence of Wafer Shape on Axial Stress Gradient for 303 Stainless Steel . . . . .	73
FIGURE 19.	Applied Force-Displacement Relation for an Unconfined 2S Aluminum Wafer . .	75
FIGURE 20.	One-Dimensional Stress Distribution for 2S Aluminum . . . . .	76
FIGURE 21.	Computer Program for Determining Unknown Displacement Coefficients . . .	89
FIGURE 22.	Computer Program for Evaluating Applied Force on Wafer . . . . .	98
FIGURE 23.	Computer Program for Determining Stress Distribution in Wafer . . . . .	101
FIGURE 24.	Sample Input-Output Data for Coefficients Program. 303 Stainless Steel. Case I-A . . . . .	103
FIGURE 25.	Sample Input-Output Data for Applied Force Program. Information Used in Figure 6 . . . . .	104
FIGURE 26.	Sample Input-Output Data for Stress Distribution Program. Information Used in Figure 7 . . . . .	105
FIGURE 27.	Computer Program for Determining Unknown Displacement Coefficients-Hollow Wafer . . . . .	109

## NOMENCLATURE

$a_1, a_2, a_3$	. . . . .	displacement coefficients defined in two-dimensional analysis, in, in, dimensionless
$a_5, a_6$	. . . . .	displacement coefficients defined in one-dimensional analysis, in, dimensionless
$a_7$	. . . . .	displacement coefficient defined in rigid-anvil analysis, dimensionless
$b$	. . . . .	characteristic measure of wafer material strain hardening, psi
$D$	. . . . .	initial wafer diameter, in
$\dot{E}'$	. . . . .	deviator strain rate tensor, $\text{sec}^{-1}$
$E''$	. . . . .	spherical strain tensor, in/in
$f$	. . . . .	coefficient of friction
$F$	. . . . .	applied compressive force, lbs
$G$	. . . . .	shearing modulus of wafer material, psi
$2h_c$	. . . . .	wafer height measured along axis of revolution, in
$2h_o$	. . . . .	original wafer centerline height, in
$H$	. . . . .	initial wafer height, in
$n$	. . . . .	characteristic curvature of plastic strain hardening of wafer material in one-dimensional analysis
$P_1$	. . . . .	constraining pressure attributed to radial constraints, psi
$P_c$	. . . . .	constraining pressure at mid-meridian plane, psi
$r, \theta, z$	. . . . .	radial, circumferential, and tangential coordinates, in, rad, in
$R_o$	. . . . .	initial wafer radius, in
$R$	. . . . .	current wafer radius, in

## NOMENCLATURE (Continued)

$R_c$	. . . . .	mid-meridian wafer radius in two-dimensional analysis, in
$R_t$	. . . . .	wafer radius at anvil-wafer interface, in
$R_a$	. . . . .	radius at which surface shear stress exceeds wafer material shear <b>strength</b> , in
$S'$	. . . . .	deviator stress tensor, psi
$u, w$	. . . . .	radial and axial displacements, in
$\dot{u}, \dot{w}$	. . . . .	radial and axial velocities, in/sec
$\gamma_{rz}$	. . . . .	shearing strain, in/in
$\tau_{rz}$	. . . . .	shearing stress, psi
$\sigma_r, \sigma_\theta, \sigma_z$	. . . . .	radial, circumferential, and axial normal stress, psi
$\tau_0$	. . . . .	wafer material shear strength, psi
$\sigma_0$	. . . . .	yield stress of wafer material, psi
$\bar{\sigma}$	. . . . .	effective wafer material stress during plastic strain, psi
$\epsilon_r, \epsilon_\theta, \epsilon_z$	. . . . .	radial, circumferential, and axial normal strain, in/in
$\bar{\epsilon}$	. . . . .	effective wafer material strain during plastic deformation, $\text{sec}^{-1}$
$\dot{\bar{\epsilon}}$	. . . . .	effective wafer material strain rate during plastic deformation, $\text{sec}^{-1}$
$\epsilon_{\theta c}$	. . . . .	circumferential strain recorded at outer periphery of containing ring, in/in
$\Delta$	. . . . .	wafer centerline deflection, in
$\delta$	. . . . .	deformation occurring at inside diameter of wafer containing ring, in
$\mu$	. . . . .	coefficient of viscosity, lb-sec/in <sup>2</sup>
$\lambda$	. . . . .	scalar factor appearing in flow law equation, lb-sec/in

## NOMENCLATURE (Continued)

- $\nu$  . . . . . Poisson's ratio for anvil material
- $\psi$  . . . . . displacement function utilized in two-dimensional analysis,  $\text{in}^3$
- $\psi_1$  . . . . . displacement function as defined in one-dimensional analysis,  $\text{in}^3$
- $\psi_2$  . . . . . displacement function pertaining to rigid-anvil analysis,  $\text{in}^3$
- $\phi$  . . . . . stream function utilized in compression of viscous fluids,  $\text{in}^3/\text{sec}$

A PLASTIC STRESS ANALYSIS OF CYLINDRICAL WAFERS  
UNDER ELASTICALLY DEFORMABLE COMPRESSION PLATES

INTRODUCTION

The field of high-pressure research has stemmed primarily from the pioneering efforts of P.W. Bridgman, and is fast becoming one of the most lucrative areas of future research and development. The knowledge thus far acquired has led to the discovery of synthetic diamonds and emeralds, and has added evidence to the belief that other substances such as the metallic forms of ammonia and hydrogen can be created in the appropriate environment of ultra high-pressure and temperature. Even though the organizational unit of High-Pressure Technology is embodied in the structure of the American Society of Mechanical Engineers, the list of contributors to this field includes chemists, physicists, geophysicists, geo-chemist, metallurgist, geologists, engineers, and many others. The diversified knowledge of these researchers has manifest itself in terms of the many avenues of approach available to the solution of high-pressure problems. The utility of chemical, electrical, optical, and mechanical changes produced in high-pressure environments have been exploited to obtain a better understanding of the phenomenon involved.

The problem of specific interest here is the study of pressure gradients existing in a specimen situated between a pair of compression plates, called anvils. The resistance

change in manganin wire, as a function of pressure, has served as a basis for an experimental evaluation of pressure gradients in circular wafers of silver chloride; Reference (a). The manganin wire was formed into a hoop of constant radius in accordance with the assumed axial symmetry. This technique prevented any axial variations from influencing measurements of the radial gradients, and the converse is true for axial measurements. In Reference (b), the pressure induced phase change of bismuth wire was employed to obtain specific load-pressure data. The authors of this reference placed bismuth wires in both axial and radial positions in an effort to isolate and define the gradients occurring in these two directions. The results reported in Reference (a) indicate that pressure is lowest at the wafer center, and increases linearly with increase in radial position. Reference (b) suggests that this result is possible, but would be largely dependent on the diameter to thickness ratio ( $D/H$ ) of the wafer. The authors of Reference (c) have used the techniques described in Reference (b) with the result that the pressure is always highest at the center of pyrophyllite, talc, and boron nitride wafers. This reference also mentions the existence of axial variations in confined wafers of variable  $D/H$  ratios, and points out the influence of the anvil-wafer friction on this variation. These conclusions are definitely compatible with the results of this report. Since the actual pressure mechanism which generates these phase and resistance changes has not been conclusively described, most experi-

mentors have been compelled to define pressure in terms of total compressive load, divided by wafer area. This is actually a measure of the average axial normal stress, and would supposedly exist only at the mid-meridian plane by virtue of the presence of shearing stress on the deflected wafer surface. Pressure is usually defined as the average of the orthogonal stress state existing at a point, and will be referred to as such in this report. The purpose of discussing these reports is to point out the difficulty to be encountered by experimentors in attempting to isolate, and predict, the influence of changes in all of the probable parameters. Chief among the parameters needed to be studied are: diameter to thickness ratio; wafer material properties; anvil-wafer friction effect; anvil deflection; and influence of radial constraints.

The recent edition, Reference (d), of the Annotated Bibliography on High-Pressure Technology, by Alexander Zeitlin, has served as a very extensive and professional survey of the past contributions to high-pressure research. This reference, published in 1964, and containing over 275 pages, presents, in cross-reference form, a listing of P.W. Bridgman's papers, in addition to the numerous high-pressure oriented publications found in the various fields of science. A study of this reference indicated that the experimental techniques employed in References (a), (b), and (c), discussed earlier, provided the most recent and accurate data that has direct applicability to the subject problem. Reference (e) represents the

initial analytical work conducted in this area, and is the forerunner of the efforts presented herein. Several short articles, References (f), (g), (h), and (i), have appeared which present a simplified analytical discussion of the pressure distributions in opposed anvil systems. However, in each of these, the assumptions of rigid anvils, one-dimensional variations, pseudo-type materials, zero anvil friction, etc., were invoked at will in order to reduce the equations to an easily tractable form. The complexity of the problem prohibits the thought of abandoning the experimental approach; nevertheless, these efforts would be complimented with an analysis based on the appropriate equations contained in the theory of plasticity. This thesis presents a completely analytical solution for the compression of wafers under elastically deformable anvils, with due consideration given to the parameters listed above. A theoretically compatible experimental model has been developed and employed in an effort to assess the significance of the required mathematical assumptions, and to verify the resulting pressure gradients. The specific contribution of this thesis is the ability to examine, on an individual basis, both analytically and experimentally, the effects and influence of the parameters itemized in the previous paragraph. Several special cases have been treated to illustrate the scope and flexibility of this analysis. It is to be noted that the results of this thesis are in basic agreement with the conclusions of References (b), (c), and (j), and can be used, with the more exact definition

of pressure, to explain the apparent discrepancies found in earlier references.

## PURPOSE AND OBJECTIVES

The overall purpose of this analysis is to determine the state of stress existing within a short circular cylinder subjected to compressive loads by initially parallel plates, and to evaluate the effects of such parameters as; material strain-hardening, anvil (or plate) deflection, anvil-wafer surface shear, influence of an elastic radial confining ring, and the effect of the initial diameter-to-height ratio of the wafer.

The technical objectives are as follows:

1. To derive from the basic equations of plasticity, equilibrium, and continuity, a set of relations which will provide the state of stress in the wafer as a function of the above parameters, for a prescribed compressive load.
2. To design and develop an experimental system which is compatible with the mathematical model postulated in the analytical analysis.
3. To utilize results of the experimental system to obtain added verification of the predicted stress distributions within the wafer.

## I. STRESS ANALYSIS

The discussion of a stress analysis involving the compression of wafers in an opposed-anvil apparatus necessitates an agreement on the terminology to be employed. The wafer is initially in the form of a short, right circular cylinder, and is located between an identical pair of parallel plates, called anvils. As these anvils are brought closer together, a compressive force is generated on, and in a direction perpendicular to the parallel surfaces of the wafer. This loading causes the wafer to expand in the radial direction; however, the original cylindrical shape of the wafer is not necessarily maintained. The expanding wafer is retarded at the wafer-anvil interfaces by the inherent shearing action, and consequently deforms into a barrel shape (barrelling). If the compression plates are non-rigid, then they too will undergo a certain deformation pattern with change in load. The assumed elastic behavior of the anvils requires that they return to their initial parallel position upon unloading. However, the wafer is allowed to flow plastically and will, in general, be permanently distorted. Figure 1 is a qualitative view of the wafer in the deformed state. If the wafer maintains its cylindrical shape during expansion, then the single radial coordinate  $r$  can be used to describe the process. The possession of axial symmetry eliminates the variation of any parameters with the circumferential coordinate  $\theta$ . In

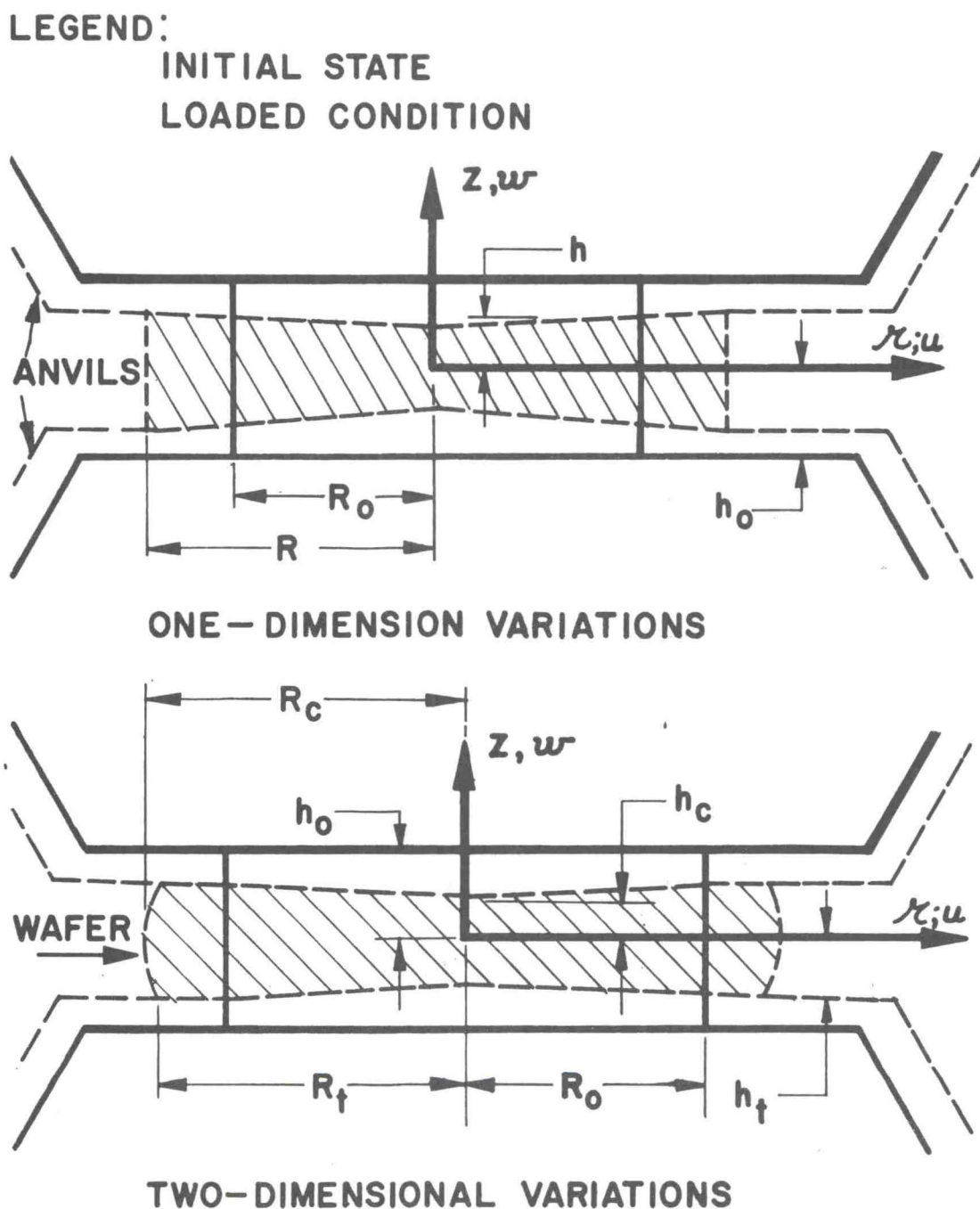


FIG. 1 POSTULATED WAFER PROFILE FOR ONE- AND TWO-DIMENSIONAL ANALYSIS.

the more general case, variations are occurring in the axial direction Z, and must be accounted for. The center of the wafer is shown to be the thinnest section; however, this is not a necessary assumption in that the analysis will dictate the required direction of curvature. As will be explained later, the variations in the one-dimensional analysis are assumed to be linear, while those in the two-dimensional case can be parabolic.

The admittance of an elastic containing ring around the wafer retards its motion, and significantly raises the stress level within the wafer. This, and other techniques, have been responsible for the generation of pressures of the magnitude required for bismuth phase changes as discussed earlier. The containing ring acts only on the wafer, hence the entire compressive force of the anvils is directed through the wafer. The actual design and construction of the containing ring is described in the section Experimental Facilities.

In order to effectively demonstrate the influence of the parameters under study, a single wafer material, called the primary material, was utilized in those tests where the material constants were not variable. Additional experiments were conducted with different wafer materials, called the secondary materials, to evaluate the material effect. The selection of the primary wafer material was based on the following factors: (1) high strain hardening; (2) high ductility; (3) incompressibility; and (4) essentially linear strain hardening. Strain hardening is one of the chief para-

meters to be studied, while the others are qualities which are compatible with the plasticity equations to be introduced later. The secondary wafer material should reflect changes only in those parameters under study. The above reasoning led to the selection of annealed 303 stainless steel for the primary material, and 2S aluminum, 6061 aluminum, and Armco iron for the secondary materials.

The approach to be taken here is to first describe the system of equations to be used, present the method of solution, and then show the resulting stress distributions for each of the situations under study.

A. Formulation of Governing Equations. The system of equations to be developed here are patterned from those given by Hoffman and Sachs in Reference (k). It has been determined experimentally in Reference (g), that for large plastic strains, such as occur in most metal-forming operations, the material may be considered incompressible. The condition of volume constancy may be written as

$$\epsilon_r + \epsilon_\theta + \epsilon_z = 0 \quad (1)$$

where  $\epsilon_r$ ,  $\epsilon_\theta$ , and  $\epsilon_z$  are the normal strains acting in the radial, tangential, and axial directions, respectively.

Since the wafer is axially symmetric, the strains are defined in terms of the displacements as

$$\epsilon_r = \frac{\partial u}{\partial r}, \quad \epsilon_\theta = \frac{u}{r}, \quad \epsilon_z = \frac{\partial w}{\partial z}$$

$$\gamma_{rz} = \frac{\partial u}{\partial z} + \frac{\partial w}{\partial r} \quad (2)$$

where  $u$  and  $w$  are the radial and axial displacement, respectively, and  $\gamma_{rz}$  is the shearing strain. If the displacements  $u$  and  $w$  are defined in terms of displacement function as

$$u = \frac{1}{r} \frac{\partial \psi}{\partial z}, \quad w = -\frac{1}{r} \frac{\partial \psi}{\partial r} \quad (3)$$

then the volume constancy equation is satisfied identically.

Using the assumptions of small finite strains (less than 20-30 percent) and the condition that the principal axes of stress and strain for a particle do not rotate with respect to the particle during the process of straining, Reference (k), the strains and strain increments may be written with the proportionality relationship as

$$\frac{d\epsilon_r}{\epsilon_r} = \frac{d\epsilon_\theta}{\epsilon_\theta} = \frac{d\epsilon_z}{\epsilon_z} = \frac{d\bar{\epsilon}}{\bar{\epsilon}} \quad (4)$$

This condition is achieved if there is no shear on any of the wafer surfaces, and the wafer maintains its cylindrical shape during loading. The same is approximately true for small amounts of shear at the wafer-anvil interfaces. A further discussion of this restriction is presented in the section Experimental Procedures and Results, and is supported in

part by the experimental results.

The flow laws identify the stress-strain state while the material is undergoing plastic deformation. St. Venant's theory may be written in tensor notation as

$$S' = 2\lambda \dot{E}', \quad E'' = 0 \quad (5)$$

where

$S'$  = deviator stress tensor

$\dot{E}'$  = deviator strain-rate tensor

$\lambda$  = variable scalar factor

$E''$  = spherical strain tensor

( $E'' = 0$  is a statement of volume constancy)

The expansion of this tensor equation is presented in References (k) and (l), and when combined with the law of proportional straining, equation (4), the resulting stress-strain relations, valid in the plastic domain, can be written as

$$\frac{2\sigma_{\theta} - \sigma_r - \sigma_z}{2\sigma_r - \sigma_{\theta} - \sigma_z} = \frac{\epsilon_{\theta}}{\epsilon_r} \quad (6)$$

$$\frac{2\sigma_z - \sigma_r - \sigma_{\theta}}{2\sigma_r - \sigma_{\theta} - \sigma_z} = \frac{\epsilon_z}{\epsilon_r}$$

$$\frac{6\tau_{rz}}{2\sigma_r - \sigma_{\theta} - \sigma_z} = \frac{\gamma_{rz}}{\epsilon_r} \quad (7)$$

where  $\sigma_r$ ,  $\sigma_\theta$ , and  $\sigma_z$  are the normal stresses acting in the radial, tangential, and axial directions, respectively, and  $\tau_{rz}$  is the only non-vanishing component of shearing stress. The first two of these equations are not independent, in that they reduce to a statement of volume constancy when combined. Thus, only two equations are obtained from the flow law.

The von Mises yield criteria can be used to predict the incipience of plastic yielding in ductile metals. This theory is independent of the hydrostatic component of stress and requires the knowledge of a single material constant, the "effective stress" in uniaxial state of stress, in order to predict the behavior under any given combination of principal stresses. The applicable yield criteria is written as

$$(\sigma_r - \sigma_\theta)^2 + (\sigma_\theta - \sigma_z)^2 + (\sigma_z - \sigma_r)^2 + 6 \tau_{rz}^2 = 2 \bar{\sigma}^2 \quad (8)$$

where  $\bar{\sigma}$  is the effective stress taken from a uniaxial compression test. The effective stress is assumed to be linear with respect to the effective strain as called for in the selection of the wafer material. Thus, the linear form of the Ludwig equation, Reference (n), becomes

$$\bar{\sigma} = \sigma_0 + b \bar{\epsilon} \quad (9)$$

where  $\sigma_0$  is the yield stress at the onset of plastic strain,  $b$  is the slope, and  $\bar{\epsilon}$  is the effective strain in the plastic region. An inherent implication here is that the wafer material be rigid until the incipience of plastic strain, and then strains in a linear fashion. Thus, the small elastic strains occurring in the wafer are neglected. The effective strain  $\bar{\epsilon}$  for a material that is rigid up to yield is given in Reference (f), and when combined with equation (4) can be written as

$$\bar{\epsilon} = \frac{\sqrt{2}}{3} \left[ (\epsilon_r - \epsilon_\theta)^2 + (\epsilon_\theta - \epsilon_z)^2 + (\epsilon_z - \epsilon_r)^2 + \frac{3}{2} \gamma_{rz}^2 \right]^{1/2} \quad (10)$$

The von Mises yield theory is thus a combination of equations (8), (9), and (10).

The two equilibrium equations for cylindrical coordinates are easily developed from the stress state acting on a differential volume element taken from the wafer in the loaded state. They are

$$\frac{\partial \sigma_r}{\partial r} + \frac{\sigma_r - \sigma_0}{r} + \frac{\partial \tau_{rz}}{\partial z} = 0 \quad (11)$$

$$\frac{\partial \tau_{rz}}{\partial r} + \frac{\partial \sigma_z}{\partial z} + \frac{\tau_{rz}}{r} = 0 \quad (12)$$

The above system of equations, combined with the appropriate boundary conditions, are sufficient for a complete determination of the displacements, strains, and stresses occurring in the plastically deformed wafer.

B. Method of Solution. The utility of a displacement function becomes apparent when it is realized that the previous system of equations can be reduced to a single equation, involving only the displacement function  $\psi$ , and the characteristics wafer material properties. Once the appropriate displacement function is determined, or assumed, the strains and displacements can be found directly. The first step will be to formulate this equation, and then discuss the available solutions in light of the various material parameters.

From the first flow law, equation (6), the expression

$$\sigma_z = \sigma_r \left( \frac{\epsilon_r + 2\epsilon_\theta}{\epsilon_\theta - \epsilon_r} \right) - \sigma_\theta \left( \frac{2\epsilon_r + \epsilon_\theta}{\epsilon_\theta - \epsilon_r} \right) \quad (13)$$

is obtained. Combining this with the second flow law equation (7), gives

$$\tau_{rz} = \frac{-1}{2} \left( \frac{\gamma r z}{\epsilon_\theta - \epsilon_r} \right) (\sigma_r - \sigma_\theta) \quad (14)$$

Using (13) and (14) in conjunction with the yield criteria, equation (8), the following stress difference is obtained,

$$\sigma_r - \sigma_\theta = \frac{\bar{\sigma} (\epsilon_\theta - \epsilon_r)}{\sqrt{3} [\epsilon_r^2 + \epsilon_r \epsilon_\theta + \epsilon_\theta^2 + \frac{1}{4} \gamma_{rz}^2]}^{1/2} \quad (15)$$

Substituting (15) into (14) yields

$$\tau_{rz} = \frac{\bar{\sigma} (\gamma_{rz})}{2\sqrt{3} [\epsilon_r^2 + \epsilon_r \epsilon_\theta + \epsilon_\theta^2 + \frac{1}{4} \gamma_{rz}^2]}^{1/2} \quad (16)$$

Equations (15) and (16) can be expressed in terms of the effective strain as

$$\sigma_r - \sigma_\theta = \frac{2\bar{\sigma}}{3\bar{\epsilon}} (\epsilon_r - \epsilon_\theta) \quad (17)$$

$$\tau_{rz} = \frac{\bar{\sigma}}{3\bar{\epsilon}} (\gamma_{rz}) \quad (18)$$

Using (13) and (15), the axial stress  $\sigma_z$  becomes

$$\sigma_z = \sigma_r - \frac{2\bar{\sigma}}{3\bar{\epsilon}} (2\epsilon_r + \epsilon_\theta) \quad (19)$$

These last three equations can be combined with the two equilibrium equations, (11) and (12), to give

$$\begin{aligned} \frac{\partial \sigma_r}{\partial r} + \frac{2\bar{\sigma}}{3r\bar{\epsilon}} (\epsilon_r - \epsilon_\theta) \\ + \frac{1}{3} \frac{\partial}{\partial z} \left( \frac{\bar{\sigma}}{\bar{\epsilon}} \gamma_{rz} \right) = 0 \end{aligned} \quad (20)$$

$$\begin{aligned} \frac{1}{3} \frac{\partial}{\partial r} \left( \frac{\bar{\sigma}}{\bar{\epsilon}} \gamma_{rz} \right) + \frac{\partial \sigma_r}{\partial z} + \frac{\bar{\sigma}}{3r\bar{\epsilon}} \gamma_{rz} \\ - \frac{2}{3} \frac{\partial}{\partial z} \left[ \frac{\bar{\sigma}}{\bar{\epsilon}} (2\epsilon_r - \epsilon_\theta) \right] = 0 \end{aligned} \quad (21)$$

Taking the partial derivatives of (20) and (21) with respect to  $z$  and  $r$ , respectively, and combining the resulting equations to eliminate  $\sigma_r$ , gives

$$\begin{aligned} & \frac{\partial^2}{\partial r^2} \left( \frac{\bar{\sigma}}{\bar{\epsilon}} \gamma_{rz} \right) - \frac{2}{r} \frac{\partial}{\partial z} \left[ \frac{\bar{\sigma}}{\bar{\epsilon}} (\epsilon_r - \epsilon_\theta) \right] \\ & - \frac{\partial^2}{\partial z^2} \left( \frac{\bar{\sigma}}{\bar{\epsilon}} \gamma_{rz} \right) - 2 \frac{\partial^2}{\partial r \partial z} \left[ \frac{\bar{\sigma}}{\bar{\epsilon}} (2\epsilon_r + \epsilon_\theta) \right] \quad (22) \\ & + \frac{1}{r} \frac{\partial}{\partial r} \left( \frac{\bar{\sigma}}{\bar{\epsilon}} \gamma_{rz} \right) - \frac{1}{r^2} \left( \frac{\bar{\sigma}}{\bar{\epsilon}} \gamma_{rz} \right) = 0 \end{aligned}$$

Using strain-displacement, and displacement-displacement function relations, equations (2) and (3), a single equation containing only the displacements function  $\psi$ , and the material strain parameters,  $\bar{\sigma}$  and  $\bar{\epsilon}$ , can be written in the form

$$\frac{\bar{\sigma}}{\bar{\epsilon}} \nabla_1^4 \psi + \nabla_3^2 \psi \nabla_2^2 \left( \frac{\bar{\sigma}}{\bar{\epsilon}} \right)$$

$$\begin{aligned}
& + \frac{2}{r} \frac{\partial}{\partial z} \left( \frac{\partial \psi}{\partial r} - \frac{2\psi}{r} \right) \frac{\partial}{\partial z} \left( \frac{\bar{\sigma}}{\epsilon} \right) \\
& + 2 \frac{\partial}{\partial z} \left( 2 \frac{\partial \psi}{\partial r} - \frac{\psi}{r} \right) \frac{\partial^2}{\partial r \partial z} \left( \frac{\bar{\sigma}}{\epsilon} \right) = 0
\end{aligned} \tag{23}$$

where the operators  $\nabla_1$ ,  $\nabla_2$  and  $\nabla_3$  are defined as (these operators are equivalent to the standard Laplacian operator, except for the indicated sign changes).

$$\nabla_1^2 = \frac{\partial^2}{\partial r^2} - \frac{1}{r} \frac{\partial}{\partial r} + \frac{\partial^2}{\partial z^2}$$

$$\nabla_2^2 = \frac{\partial^2}{\partial r^2} + \frac{1}{r} \frac{\partial}{\partial r} - \frac{\partial^2}{\partial z^2}$$

$$\nabla_3^2 = \frac{\partial^2}{\partial r^2} - \frac{1}{r} \frac{\partial}{\partial r} - \frac{\partial^2}{\partial z^2}$$

Equation (23) represents the governing equation for determining the displacement function  $\psi$ , and is predicated on the existence of proportional straining, equation (4). If the total derivatives had been retained in the flow law equations, and if the velocities  $\dot{u}$  and  $\dot{w}$ , acting in the radial and axial directions, respectively, are defined as

$$\dot{u} = \frac{1}{r} \frac{\partial \phi}{\partial z}, \quad \dot{\omega} = -\frac{1}{r} \frac{\partial \phi}{\partial r} \quad (24)$$

where  $\phi$  is a velocity function, then the analogous differential equation for the time dependent flow of an arbitrary material becomes

$$\begin{aligned} & \frac{\bar{\sigma}}{\dot{\epsilon}} \nabla_1^4 \phi + \nabla_3^2 \phi \nabla_2^2 \left( \frac{\bar{\sigma}}{\dot{\epsilon}} \right) \\ & + \frac{2}{r} \frac{\partial}{\partial z} \left( \frac{\partial \phi}{\partial r} - \frac{2\phi}{r} \right) \frac{\partial}{\partial z} \left( \frac{\bar{\sigma}}{\dot{\epsilon}} \right) \\ & + 2 \frac{\partial}{\partial z} \left( 2 \frac{\partial \phi}{\partial r} - \frac{\phi}{r} \right) \frac{\partial}{\partial r \partial z} \left( \frac{\bar{\sigma}}{\dot{\epsilon}} \right) = 0 \end{aligned} \quad (25)$$

In the case of a Newtonian fluid, the ratio of the shearing stress to the rate of shear strain is a constant; and this constant is usually called the coefficient of viscosity  $\mu$ . Using analogous terms, the following relation can be written for a Newtonian fluid.

$$\bar{\sigma} = \mu \dot{\epsilon} \quad (26)$$

Combining equations (25) and (26) gives

$$\nabla_r^4 \phi = 0 \quad (27)$$

The solution of (27) for the compression of a circular layer of viscous fluid, by parallel plates moving with constant velocity, is presented in Reference (g). This reference indicates that the pressure is greatest at the center of the specimen; a result which is consistent with the results of this report. An equivalent solution could be obtained from (23), providing that the ratio of the effective stress and strain remains constant. This is the requirement for an elastic material, which is not of interest here. The prospect of obtaining an exact solution of (23) is improbable at this point, and a numerical solution would likewise be difficult by virtue of the mixed boundary conditions. An alternate approach, and the one to be used here, is to select an approximate displacement function  $\psi$  that will yield a prescribed displacement pattern which is consistent with the observed shape of the loaded wafer.

C. Resulting Stress Equations. Depending on the assumptions that are applied, different stress solutions are obtainable. These solutions are derivable from the same basic equations, but are presented under separate headings to preserve and emphasize the effects and influence of each assumption. The more general solution is presented first, followed by the results of a simpler analysis. The last topic of this group is concerned with the extension of the present analysis to include the effects of a concentric hole located along the axis of the wafer.

1. Two-Dimensional Wafer Profile-With Shear. The assumed profile of the wafer in the loaded state has been portrayed in Figure 1, and leads to the following trial for the displacement function  $\psi$ .

$$\psi = a_1 r^4 z + a_2 r^2 z^3 + a_3 r^2 z \quad (28)$$

where  $a_1$ ,  $a_2$ , and  $a_3$  are constants, and will be referred to as displacement coefficients. Using this function with equations (3), the displacements become

$$u = a_1 r^3 + (3a_2 z^2 + a_3) r \quad (29)$$

$$\omega = -2z (2a_1 r^2 + a_2 z^2 + a_3) \quad (30)$$

An examination of (29) indicates that the wafer can barrel in a parabolic fashion, having symmetry with respect to the mid-meridian wafer plane. Equation (30) shows that the wafer-anvil interface can likewise be deformed into a parabola; the line of symmetry being coincident with the wafer axis. It should be noted that no restriction has been placed on the wafer diameter-to-height ratio (D/H).

By taking the appropriate derivatives of the displacements, the strains are found to be

$$\epsilon_r = 3a_1 r^2 + 3a_2 z^2 + a_3 \quad (31)$$

$$\epsilon_\theta = a_1 r^2 + 3a_2 z^2 + a_3 \quad (32)$$

$$\epsilon_z = -4a_1 r^2 - 6a_2 z^2 - 2a_3 \quad (33)$$

$$\gamma_{rz} = 2rz (3a_2 - 4a_1) \quad (34)$$

When equations (31) through (34) are combined with (10), the effective strain becomes

$$\bar{\epsilon} = (\alpha_1 r^4 + \beta_1 r^2 + \gamma_1)^{1/2} \quad (35)$$

where

$$\alpha_1 = \frac{52}{3} a_1^2, \quad \gamma_1 = 4(3a_2 z^2 + a_3)^2 \quad (36)$$

$$\beta_1 = \frac{4}{3} [(12a_1 a_2 + 9a_2^2 + 16a_1^2) z^2 + 12a_1 a_3]$$

The first derivative with respect to  $z$  of the above coefficients will be required later, and are documented here as

$$\beta_1' = \frac{8}{3} (12a_1 a_2 + 9a_2^2 + 16a_1^2) z \quad (37)$$

$$\gamma_1' = 48a_2 (3a_2 z^2 + a_3) z$$

With the strains now known, the equilibrium equation, (20), can be integrated, with the aid of (9), to give the radial stress result shown in (38). The integration is lengthy, but can be accomplished with the formulas appearing in a short table of integrals. The constant of integration is assessed by requiring that the radial stress be equal to the containing pressure  $P_1$  at the external wafer surface. If the containing ring is absent,  $P_1$  vanishes. The remaining stresses are easily found from the use of equations (17), (18), and (19). The tangential and axial normal stresses are given in (39) and (40), respectively, and equation (41) is the shearing stress. The foregoing three normal stress equations represent the orthogonal stress state existing at any point in the wafer, and are based on the assumptions of low shear stress, elastic deflection of the anvil and containing ring, and linear strain hardening of the wafer material. The mean stress or pressure distribution across the diameter of the wafer may be obtained by taking the average of (38), (39), and (40).

The area under the axial normal stress  $\sigma_z$  curve, evaluated at the mid-meridian wafer plane, ( $Z = 0$ ) corresponds to the applied force transmitted to the wafer from the anvils. The mid-meridian is selected, since at any other plane the wafer is distorted, and is under the influence of shearing stresses, which can support a portion of the applied load. In integral form, the area is expressed as

$$\sigma_r = \frac{\sigma_0}{3\sqrt{\alpha_1}} (2a_1 - 3a_2) \operatorname{Ln} \left\{ \frac{2\alpha_1 r^2 + \beta_1 + 2\sqrt{\alpha_1} [\alpha_1 r^4 + \beta_1 r^2 + \gamma_1]^{1/2}}{2\alpha_1 R^2 + \beta_1 + 2\sqrt{\alpha_1} [\alpha_1 R^4 + \beta_1 R^2 + \gamma_1]^{1/2}} \right\}$$

$$+ \frac{\sigma_0 z (3a_2 - 4a_1)}{3(\beta_1^2 - 4\alpha_1 \gamma_1)} \left\{ \frac{(\beta_1 \beta_1' - 2\alpha_1 \gamma_1') r^2 - (\beta_1 \gamma_1' - 2\gamma_1 \beta_1')}{[\alpha_1 r^4 + \beta_1 r^2 + \gamma_1]^{1/2}} \right. \quad (38)$$

$$\left. - \frac{(\beta_1 \beta_1' - 2\alpha_1 \gamma_1') R^2 - (\beta_1 \gamma_1' - 2\gamma_1 \beta_1')}{[\alpha_1 R^4 + \beta_1 R^2 + \gamma_1]^{1/2}} \right\} + \frac{b}{3} (2a_1 - 3a_2) (r^2 - R^2) - P_1$$

$$\tau_{rz} = \frac{2}{3} b (3a_2 - 4a_1) rz + \frac{2}{3} \sigma_0 (3a_2 - 4a_1) \left\{ \frac{rz}{[\alpha_1 r^4 + \beta_1 r^2 + \gamma_1]^{1/2}} \right\} \quad (41)$$

$$\sigma_{\theta} = \frac{\sigma_0}{3\sqrt{\alpha_1}} (2a_1 - 3a_2) \operatorname{Ln} \left\{ \frac{2\alpha_1 r^2 + \beta_1 + 2\sqrt{\alpha_1} [\alpha_1 r^4 + \beta_1 r^2 + \gamma_1]^{1/2}}{2\alpha_1 R^2 + \beta_1 + 2\sqrt{\alpha_1} [\alpha_1 R^4 + \beta_1 R^2 + \gamma_1]^{1/2}} \right\}$$

$$+ \frac{\sigma_0 z (3a_2 - 4a_1)}{3(\beta_1^2 - 4\alpha_1 \gamma_1)} \left\{ \frac{(\beta_1 \beta_1' - 2\alpha_1 \gamma_1') r^2 - (\beta_1 \gamma_1' - 2\gamma_1 \beta_1')}{[\alpha_1 r^4 + \beta_1 r^2 + \gamma_1]^{1/2}} \right. \quad (39)$$

$$\left. - \frac{(\beta_1 \beta_1' - 2\alpha_1 \gamma_1') R^2 - (\beta_1 \gamma_1' - 2\gamma_1 \beta_1')}{[\alpha_1 R^4 + \beta_1 R^2 + \gamma_1]^{1/2}} \right\} - \frac{4}{3} a_1 \sigma_0 \left\{ \frac{r^2}{[\alpha_1 r^4 + \beta_1 r^2 + \gamma_1]^{1/2}} \right\}$$

$$- \frac{2}{3} a_1 b (r^2 + R^2) \quad - a_2 b (r^2 - R^2) - P_1$$

$$\sigma_z = \frac{\sigma_0}{3\sqrt{\alpha_1}} (2a_1 - 3a_2) \operatorname{Ln} \left\{ \frac{2\alpha_1 r^2 + \beta_1 + 2\sqrt{\alpha_1} [\alpha_1 r^4 + \beta_1 r^2 + \gamma_1]^{1/2}}{2\alpha_1 R^2 + \beta_1 + 2\sqrt{\alpha_1} [\alpha_1 R^4 + \beta_1 R^2 + \gamma_1]^{1/2}} \right\}$$

$$+ \frac{\sigma_0 z (3a_2 - 4a_1)}{3(\beta_1^2 - 4\alpha_1 \gamma_1)} \left\{ \frac{(\beta_1 \beta_1' - 2\alpha_1 \gamma_1') r^2 - (\beta_1 \gamma_1' - 2\gamma_1 \beta_1')}{[\alpha_1 r^4 + \beta_1 r^2 + \gamma_1]^{1/2}} \right. \quad (40)$$

$$\left. - \frac{(\beta_1 \beta_1' - 2\alpha_1 \gamma_1') R^2 - (\beta_1 \gamma_1' - 2\gamma_1 \beta_1')}{[\alpha_1 R^4 + \beta_1 R^2 + \gamma_1]^{1/2}} \right\} - \frac{2\sigma_0}{3} \left\{ \frac{7a_1 r^2 + 9a_2 z^2 + 3a_3}{[\alpha_1 r^4 + \beta_1 r^2 + \gamma_1]^{1/2}} \right\}$$

$$- \frac{2}{3} a_1 b (6r^2 + R^2) - a_2 b (r^2 - R^2) - 6a_2 b z^2 - 2a_3 b - P_1$$

$$F = 2\pi \int_0^{R_c} (\sigma_z)_{z=0} r dr \quad (42)$$

where  $R_c$  is the maximum wafer radius in the mid-meridian plane. Substituting equation (40) into (42), and performing the indicated integration, the results shown in equation (43) are obtained. The subscript "c" indicates that the quantity in question has been evaluated at a radius of magnitude  $R_c$ .

The boundary conditions imposed on the problem by its physical constraints are itemized in the following paragraphs. The boundary conditions shown apply to the compression of a solid, radially retarded wafer via elastically deformable compression plates. The applicable conditions for the case of no containing ring, or for a hollow wafer, will be pointed out at the appropriate place.

The first boundary condition pertains to the radial deformation at the mid-meridian wafer plane. This condition requires that at

$$r = R_c, \quad z = 0; \quad U = R_c - R_0 \quad (44)$$

where  $R_0$  is the initial wafer radius. A combination of (29)

$$\begin{aligned}
F = & \frac{2\sigma_0\pi}{3\sqrt{\alpha_c}} (2a_1 - 3a_2) \left\{ \frac{2\alpha_c R_c^2 + \beta_c}{4\alpha_c} \left[ \text{Ln}(2\alpha_c R_c^2 + \beta_c) - 1 \right] \right. \\
& - \frac{\beta_c}{4\alpha_c} \left[ \text{Ln}(\beta_c) - 1 \right] - \frac{1}{2} R_c^2 \text{Ln}(2\alpha_c R_c^2 + \beta_c) \left. \right\} - \frac{1}{2} (4a_1 + a_2) \pi b R_c^4 \\
& - \frac{4}{3} \pi \sigma_0 \left\{ 7a_1 \left[ \frac{1}{2\alpha_c} (\alpha_c R_c^4 + \beta_c R_c^2 + \gamma_c)^{1/2} - \frac{1}{4} \beta_c \alpha_c^{-3/2} \text{Ln} \left\{ \frac{\beta_c}{2\sqrt{\alpha_c}} \right. \right. \right. \\
& + \sqrt{\alpha_c} R_c^2 + (\alpha_c R_c^4 + \beta_c R_c^2 + \gamma_c)^{1/2} \left. \left. \right\} - \frac{\sqrt{\gamma_c}}{2\alpha_c} + \frac{1}{4} \beta_c \alpha_c^{-3/2} \right. \\
& \left. \left. \text{Ln} \left( \frac{\beta_c}{2\sqrt{\alpha_c}} + \sqrt{\gamma_c} \right) \right] + 3a_3 \left[ \frac{1}{2\sqrt{\alpha_c}} \text{Ln} \left\{ \frac{\beta_c}{2\sqrt{\alpha_c}} + \sqrt{\alpha_c} R_c^2 \right. \right. \right. \\
& \left. \left. + (\alpha_c R_c^4 + \beta_c R_c^2 + \gamma_c)^{1/2} \right\} - \frac{1}{2\sqrt{\alpha_c}} \text{Ln} \left( \frac{\beta_c}{2\sqrt{\alpha_c}} + \sqrt{\gamma_c} \right) \right] \left. \right\} \\
& - \pi \left( \frac{2}{3} a_1 b R_c^2 - a_2 b R_c^2 + 2a_3 b + P_c \right) R_c^2
\end{aligned} \tag{43}$$

and (44) gives

$$a_1 = \left( \frac{R_c - R_0}{R_c} - a_3 \right) / R_c^2 \quad (45)$$

The second condition relates the radial wafer deflection to the constraining pressure. If  $\delta$  is the radial deflection at the mid-meridian plane, then

$$\delta = R_c - R_0 = (5.32 \times 10^{-8}) P_c \quad (46)$$

where  $P_c$  is the restraining pressure exerted on the wafer, at  $Z = 0$ , by the containing ring. The numerical factor appearing in (46) is obtained from an application of the well-known Lamé equation for the elastic deformation of a thick-wall cylinder. These equations can also be used to describe the amount of tangential strain  $\epsilon_{\theta c}$  occurring at the outer surface of the containing ring, due to the influence of the internal pressure  $P_c$ . The relation found for the ring used in this program is

$$\epsilon_{\theta c} = (3.02 \times 10^{-9}) P_c \quad (47)$$

A more detailed description of the containing ring and its use is given in the section "Experimental Facilities and Procedures". Using equations (29) and (46), the mid-meridian constraint pressure becomes

$$P_c = \left( \frac{R_c}{5.32 \times 10^{-8}} \right) [a_1 R_c^2 + a_3] \quad (48)$$

In the absence of a constraining ring,  $P_c$  is zero. If the total axial deflection along the wafer axis is defined as  $\Delta$ , the third boundary condition becomes

$$r = 0, \quad z = h_c; \quad w = -\Delta/2 \quad (49)$$

where  $h_c$  is one-half the wafer height, measured along its axis, at any given load. Substituting the conditions of (49) into (30) gives

$$a_3 = \frac{\Delta}{2(2h_o - \Delta)} - \frac{a_2}{4} (2h_o - \Delta)^2 \quad (50)$$

where  $2h_o$  is the initial wafer height.

The assumption is now made that the amount of shear

stress existing on the wafer-anvil interface is directly proportional to the magnitude of the normal stress acting on this same surface. (Coulomb law of friction). The coefficients of friction for various materials, under a pressure of 25 Kb, have been documented in Reference (m). The manner in which these experiments were conducted requires that the integrated effects of the normal and shear stresses be related as follows.

$$\int_0^{R_t} (\tau_{rz})_{z=hc} r dr = f \int_0^{R_t} (\sigma_z)_{z=hc} r dr \quad (51)$$

where  $R_t$  is the external radius, evaluated at the top surface of the loaded wafer. If the shear stress  $\tau_{rz}$  exceeds the shear strength  $\tau_0$  of the wafer material, then equation (51) must be written in the form

$$\begin{aligned} & \int_0^{R_0} (\tau_{rz})_{z=hc} r dr + \int_{R_0}^{R_t} \tau_0 r dr \\ & = f \int_0^{R_t} (\sigma_z)_{z=hc} r dr \end{aligned} \quad (52)$$

where  $R_a$  is the radial position where  $\tau_{rz}$  becomes equivalent to  $\tau_0$ . The value of  $\tau_0$  is considered to be one-half of the effective stress  $\bar{\sigma}$  at any given stage of strain. The limits of integration are taken as shown since the shear stress is zero at the wafer axis, and increases with increase in radial position. The computer program used in solving this problem first calculates the shear stress  $\tau_{rz}$  at the top surface of the wafer, and then runs a comparison check between  $\tau_{rz}$  and  $\tau_0$  at ten equally spaced intervals across the wafer. If  $\tau_{rz}$  is less than  $\tau_0$  at all radial positions, then  $R_a$  is set equal to  $R_t$  and equation (52) reduces to (51), thus eliminating the need of equation (51). Combining the known stress equations with (52), and performing the indicated integration yields the results shown in equation (53).

$$\begin{aligned} & \frac{2}{3} hc (3a_2 - 4a_1) \left( \frac{1}{3} R_0^3 + \sigma_0 N_0 \right) \\ & + \frac{1}{4} \sigma_0 (R_t^2 - R_0^2) + \frac{1}{2} b \left[ (K_t \bar{\epsilon}_t - K_0 \bar{\epsilon}_0) / 8\alpha_t \right. \\ & \left. + M (L_t - L_0) \right] = f F_t / 2\pi \quad (53) \end{aligned}$$

The terms  $J$ ,  $K$ ,  $L$ ,  $M$ ,  $N$ , and  $h_c$  are defined as follows, and the subscripts "t" and "a" indicate that these terms have been evaluated at the radii  $R_t$  and  $R_a$ , respectively.

$$h_c = h_o - \Delta/2$$

$$J = \left[ \sqrt[4]{\gamma_t} + R \sqrt[4]{\alpha_t} \right] / \left[ \sqrt[4]{\gamma_t} - R \sqrt[4]{\alpha_t} \right]$$

$$K = 2\alpha_t R_t^2 + \beta_t$$

(54)

$$L = \text{Ln} (K + 2 \sqrt{\alpha_t} \bar{\epsilon})$$

$$M = (4\alpha_t \gamma_t - \beta_t^2) / 16\alpha_t^{1.5}$$

$$N = R / \sqrt{\alpha_t} - (\gamma_t / \alpha_t^3)^{0.25} \text{Ln} (J_t)$$

The last boundary condition is concerned with the compatible deformations of the wafer and anvil at their mating surface. An approximate relation which relates the average slope of the anvil to that of the wafer is given as

$$\left[ (\omega)_{r=0} - (\omega)_{r=R_t} \right]_{\text{ANVIL}} = \quad (55)$$

$$\left[ (\omega)_{r=0} - (\omega)_{r=R_t} \right]_{z=h} \text{ WAFER}$$

If the anvils are considered to be semi-infinite elastic bodies, the deflections due to a normal stress, continuously distributed within a circular region, are given in Reference (g) as

$$\left[ (\omega)_{r=0} \right]_{\text{ANVIL}} = \frac{1-\nu}{G} \int_0^{R_t} \sigma_z \, dr \quad (56)$$

$$\left[ (\omega)_{r=R_t} \right]_{\text{ANVIL}} = \frac{1-\nu}{GR_t} \int_0^{R_t} \sigma_z \, r \, dr$$

A combination of equations (30), (40), (55), and (56) results, after lengthy computations, in the expression shown in equation (57). The terms  $D_1$ ,  $E_1$ , and  $H_1$ , appearing in (57), are defined in equations (58). The integral term ap-

$$\begin{aligned}
\left(\frac{G}{1-\nu}\right)(h_c - h_t) &= \frac{\sigma_0}{3\sqrt{\alpha_t}} (2a_1 - 3a_2) \left\{ \int_0^{R_t} \text{Ln}(K) dr \right. \\
&- R_t \text{Ln}(K_t) \left. \right\} - \frac{2\sigma_0}{3} \left\{ 7a_1 N_t - J_t (9a_2 h_c^2 + 3a_3) / H_1 \right\} \\
&+ \frac{1}{3} \sigma_0 h_c \left[ (3a_2 - 4a_1) / (\beta_t^2 - 4\alpha_t \gamma_t) \right] \left\{ (D_1 N_t + E J_t / H_1) \right. \\
&- R_t (D_1 R_t^2 - E) / (\sqrt{\alpha_t} R_t^2 - \sqrt{\gamma_t}) \left. \right\} - \frac{1}{3} b R_t^3 (4a_1 + a_2) \\
&- b R_t \left[ R_t^2 \left( \frac{2}{3} a_1 - a_2 \right) + 6a_2 h_c^2 + 2a_3 + P_t / b \right] - F_t \gamma_{R_t}
\end{aligned} \tag{57}$$

$$\begin{aligned}
D_1 &= \beta_t \beta_t^1 - 2\alpha_t \gamma_t^1 \\
E_1 &= \beta_t \gamma_t^1 - 2\gamma_t \beta_t^1 \\
H_1 &= 2(\alpha_t \gamma_t^1)^{0.25}
\end{aligned} \tag{58}$$

peating in (58) does not possess a simple closed-form solution, and is therefore evaluated in the computer program by an application of Simpson's Rule. An explanation of this computer program is given later.

The equations (45), (48), (50), (53), and (57) represent five independent equations for the determination of the three displacement coefficients,  $a_1$ ,  $a_2$ ,  $a_3$ , the mid-meridian constraining pressure,  $P_c$ , and the wafer centerline deflection,  $\Delta$ . Once these quantities are known, the displacements, strains, stresses, and applied force can all be found by utilizing the appropriate equations. When each of the above equations are expanded, the thought of obtaining an explicit equation for each of the unknowns is out of the question. The complexity of these equations provided the motivation for writing a computer program that would solve for the unknowns, using an iteration scheme. Appendix I has been reserved for a discussion of the use and operation of the programs utilized in determining the unknown coefficients, and evaluating the stresses, applied force and strains pertaining to the two-dimensional analysis of a compressed wafer.

2. One-Dimensional Wafer Profile- Zero Shear. The displacement function that will yield the deformation pattern shown in the first part of Figure 1 is written as

$$\psi_1 = a_5 r^3 z + a_6 r^2 z \quad (59)$$

where  $a_5$  and  $a_6$  are the constant displacement coefficients. Combining (59) with equations (3) leads to the following expressions for the displacements.

$$u = a_5 r^2 + a_6 r \quad (60)$$

$$w = -z (3a_5 r + 2a_6) \quad (61)$$

The undesirable feature associated with these displacements is that the curvature at the top surface of the wafer is discontinuous at the axis. This situation could have been remedied by replacing the  $r^3$  term in (59) with an  $r^4$ ; however, the resulting equations were not deemed tractable at the time this part of the problem was worked. If the above displacements are combined with the strain definitions, (2), the results are

$$\begin{aligned} \epsilon_r &= 2a_5 r + a_6 \\ \epsilon_\theta &= a_5 r + a_6 \\ \epsilon_z &= -3a_5 r - 2a_6 \end{aligned} \quad (62)$$

The assumption is made that a perfect lubricant is applied to the wafer-anvil interface, thus creating a condition of zero shear. The simpler form of the strain equations permits the use of the Ludwig equation for relating the effective stress and strain, which is written as

$$\sigma_o = b + (\bar{\epsilon})^n \quad (63)$$

where "n" is a constant exponent which characterizes the shape of the experimentally determined stress-strain curve. Utilizing equations (62) and (63), and following precisely the same steps as shown in the two-dimensional analysis, the resulting normal stress equations for one-dimensional variations, and zero shear, are found to be of the form shown in equations (64), (65), and (66). The coefficients  $\alpha$  and  $\beta$  appearing in these equations are defined as

$$\alpha = \sqrt{7} \left[ \left( \frac{R - R_0}{R^2} \right) - \frac{\Delta}{2R(2h_0 - \Delta)} \right]$$

$$\beta = \frac{\sqrt{3} \Delta}{2(2h_0 - \Delta)} \quad (67)$$

$$\sigma_r = \frac{\sigma_0}{\sqrt{21}} \operatorname{Ln} \left( \frac{\alpha_r + \beta}{\alpha_R + \beta} \right) + \frac{b}{n\sqrt{21}} \cdot \left( \frac{2}{\sqrt{3}} \right)^n \left[ (\alpha_r + \beta)^n - (\alpha_R + \beta)^n \right] \quad (64)$$

$$\sigma_\theta = \frac{\sigma_0}{\sqrt{21}} \left[ \operatorname{Ln} \left( \frac{\alpha_r + \beta}{\alpha_R + \beta} \right) - \left( \frac{\alpha_r}{\alpha_r + \beta} \right) \right] + \frac{b}{n\sqrt{21}} \left( \frac{2}{\sqrt{3}} \right)^n \left[ (\alpha_r + \beta)^n - \alpha_n r (\alpha_r + \beta)^{n-1} - (\alpha_R + \beta)^n \right] \quad (65)$$

$$\sigma_z = \frac{\sigma_0}{\sqrt{21}} \left[ \operatorname{Ln} \left( \frac{\alpha_r + \beta}{\alpha_R + \beta} \right) - \left( 5r + \sqrt{21} \frac{\beta}{\alpha} \right) \cdot \left( \frac{\alpha}{\alpha_r + \beta} \right) \right] + \frac{b}{n\sqrt{21}} \left( \frac{2}{\sqrt{3}} \right)^n \left[ (\alpha_r + \beta)^n - \left( 5r + \sqrt{21} \frac{\beta}{\alpha} \right) \alpha_n (\alpha_r + \beta)^{n-1} - (\alpha_R + \beta)^n \right] \quad (66)$$

The boundary conditions used to determine the two displacement coefficients  $a_5$  and  $a_6$ , the constraint pressure  $P_1$ , and the wafer centerline deflection are the same as those invoked previously. Once these factors are known, the displacements, strains, stresses, and applied force can all be found by utilizing the appropriate equations.

A complete description of the one-dimensional analysis, together with the computer programs used in computing the coefficients, stresses, and applied force, is presented in Reference (1), and will not be repeated here.

3. Rigid Anvils - Zero Shear. If only the last term appearing in the previous two displacement functions is retained, a new function

$$\psi_2 = a_7 r^2 z \quad (68)$$

is thus defined. It will be shown that this function leads to the results obtained from the analysis of rigid, perfectly lubricated anvils.

Taking the appropriate derivatives of (68), the displacements become

$$u = a_7 r \quad w = -2a_7 z \quad (69)$$

The strains are found to be of the form

$$\begin{aligned}\epsilon_r &= \epsilon_\theta = a_7 \\ \epsilon_z &= -2a_7, \quad \gamma_{rz} = 0\end{aligned}\tag{70}$$

Using, once again, the format given previously, the stresses become

$$\begin{aligned}\sigma_r &= \sigma_\theta = \tau_{rz} = 0 \\ \sigma_z &= \sigma_0 + b(2a_7)^n\end{aligned}\tag{71}$$

and  $a_7$  is determined from the radial boundary condition.

$$a_7 = (R - R_0)/R\tag{72}$$

4. Two-Dimensional Hollow Wafer - With Shear. The admittance of a concentric hole along the wafer axis does not alter the form of the normal and shear stress equations, although the displacement coefficients will be different

by virtue of the added boundary condition at the inside surface of the wafer hole. Some of the practical advantages to be gained from the analysis of a hollow wafer are: (1) an understanding of the influence of a plastic containing ring on an elastic, plastic, or hydrostatic medium; (2) A feasibility study of a high-pressure generating device consisting of a hollow, plastically deformable compression gasket (or wafer), located within an elastic containing ring, and filled with a hydrostatic fluid. The high-strength containing ring will force the compressively loaded wafer to extrude into the central cavity with an accompanying increase in the fluid pressure. The wafer design that exhibits the largest gradient of radial stress, from outer to inner surface, for a given press capacity, will result in the highest cavity pressure.

The boundary condition previously used to assess the effect of anvil deflections will be eliminated in favor of having the radial stress at the surface of the hole be equivalent to the cavity fluid pressure. Since the cavity contains a pressure sensing element, as well as the fluid medium, the compressibility of each substance must be utilized in order to predict the cavity pressure as a function of cavity volume. Denoting the radius of the wafer hole (at the top surface) by  $R_{it}$ , the applied force on the wafer is found by integrating the axial stress from  $R_{it}$  to  $R_t$ , and then adding the force created by the cavity pressure, acting over a circular area of radius  $R_{it}$ .

A computer program for finding the displacement coefficients, constraint pressure, cavity pressure, and wafer axial deflection from the boundary condition equations has been written, and is shown in Appendix I. Since this program overflows the memory storage of the IBM 1620 digital computer, no actual results have been tabulated at this time. The hopes of obtaining the required design criteria for an ultra high-pressure system, and the analogy existing between the solid and hollow wafer analysis, provided the stimulus to carry the problem to this stage of completion. A further discussion of the hollow wafer computer program is presented in the section Future Work.

## II. EXPERIMENTAL FACILITIES AND PROCEDURES

The compressive loads applied to the wafer assembly are supplied by a 2500-ton hydraulic ram press. A view of this press, and the associated controls, is presented in Figure 2. This press constitutes a part of the general research facilities employed at Pressure Science, Inc., 11642 Old Baltimore Pike, Beltsville, Maryland, for the long range study of high-pressure phenomenon, and the design of ultra-high pressure test equipment. The purpose of having such a massive press is twofold. First, the increased tonnage provides an access to ultra-high pressures (providing the anvil design is adequate), and secondly, the wafer size can be scaled-up to sizes that are easily manufactured and handled.

The top of the press is maintained in a permanent position by four 10-inch diameter steel posters. The bottom section of the press (ram) is raised through the action of fluid pressure generated by hydraulic pumps. A high- and a low-volume pump is connected to the ram in order to obtain a more deliberate control of the applied force. The approximate magnitude of the applied force can be found by recording the ram gage pressure, and multiplying by the projected ram area. This method does not account for the friction created by the sliding seals, and other effects; thus, a standard load-cell was acquired from the National Bureau of Standards, and used to calibrate the ram pressure gage directly in terms

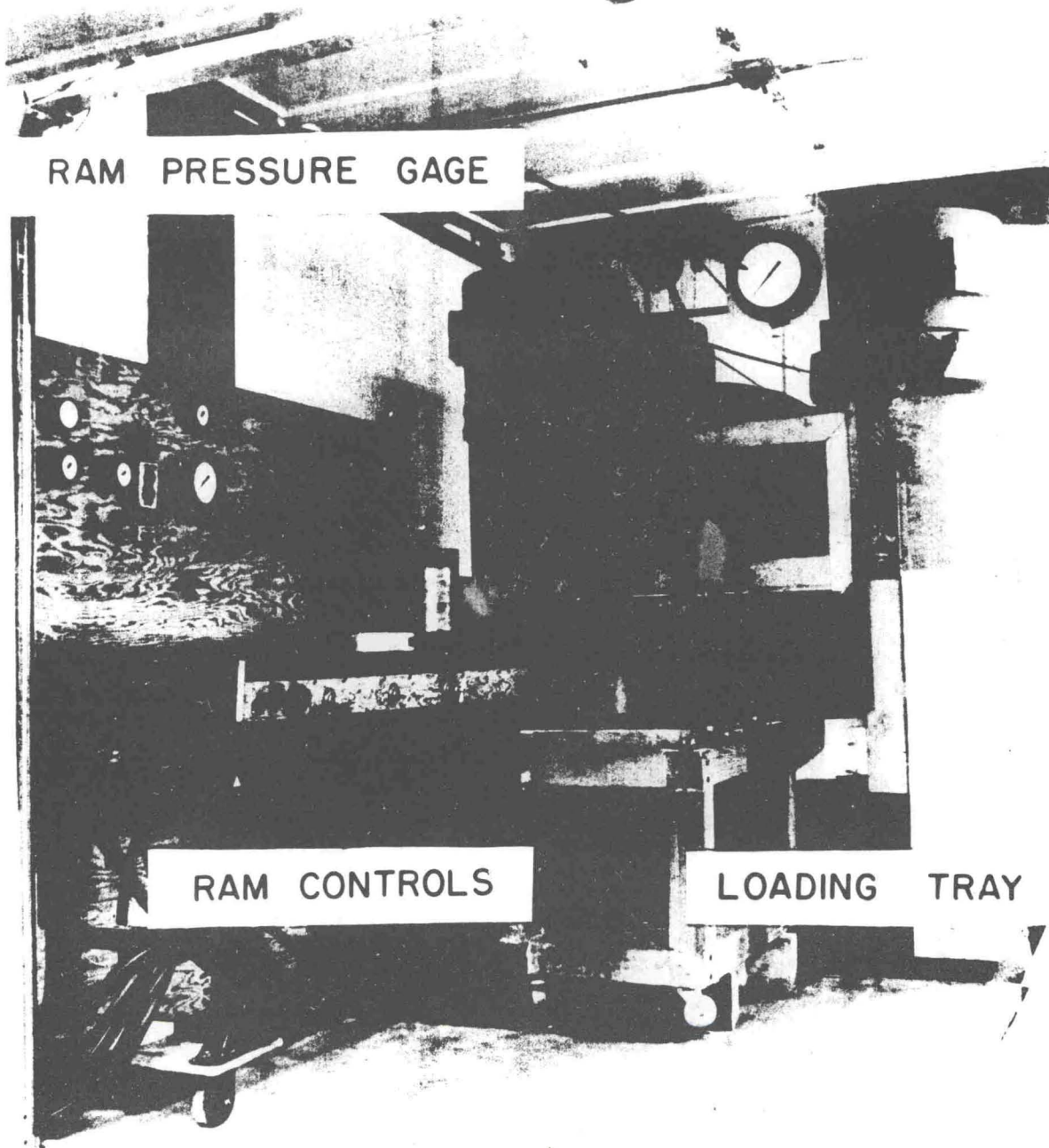


FIG. 2 2500 - TON HYDRAULIC PRESS

of force.

The loading tray, appearing in Figure 2, provides an assembly area at a position external to the press. After the anvil-wafer-containing ring system has been completely assembled, the spring-loaded, roller mounted, loading tray can be positioned over the ram center. The initial compressive load applied through the wafer system deflects the rollers, allowing the loading tray to sit flush on the ram. Upon removal of the load, the tray is once again free to roll. The weights of the component parts, together with the restricted space under the press superstructure, not to mention safety, illustrate the desirability of having the loading tray.

The complete wafer compression system consists of the following components, shown in Figure 3 and 4.

(1) Wafer - As defined previously, the wafer is a short circular cylinder, having a D/H ratio ranging from 3 to 13. The primary wafer material is annealed 303 stainless steel, and the secondary materials are 2S aluminum, 6061 aluminum, and Armco iron. The materials were purchased as bar stock, and all wafers of a particular material were taken with identically cuts from the same bar. Standard compression tests were conducted on specimens of each material to obtain the desired material constants. The compression specimens have a D/H ration of 0.4, and are coated with molybdenum disulphide to minimize the end-effects. The material constants determined by fitting equation (9), or (63), to the

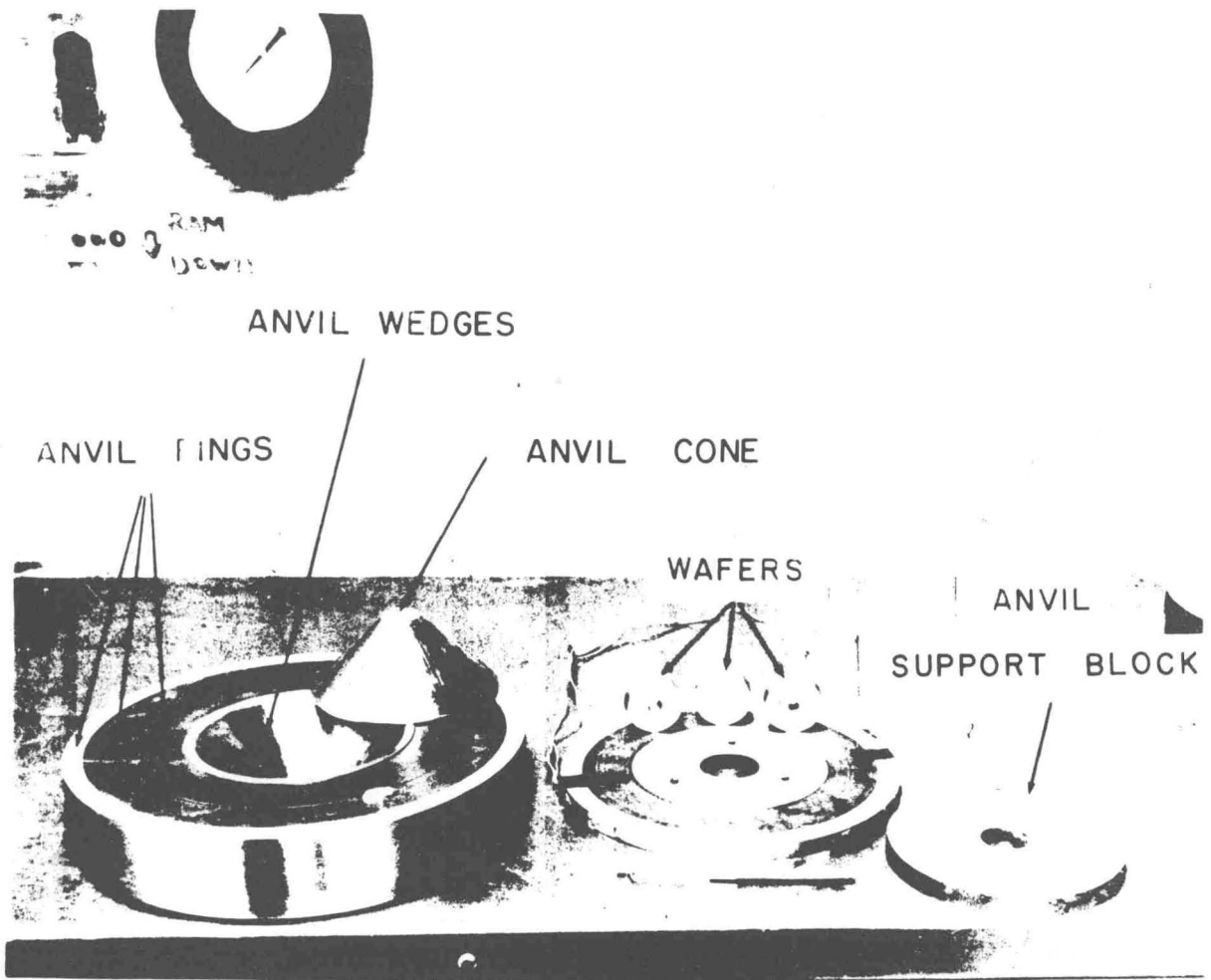


FIG. 3 COMPONENT PARTS OF CONFINED  
WAFER COMPRESSION SYSTEM

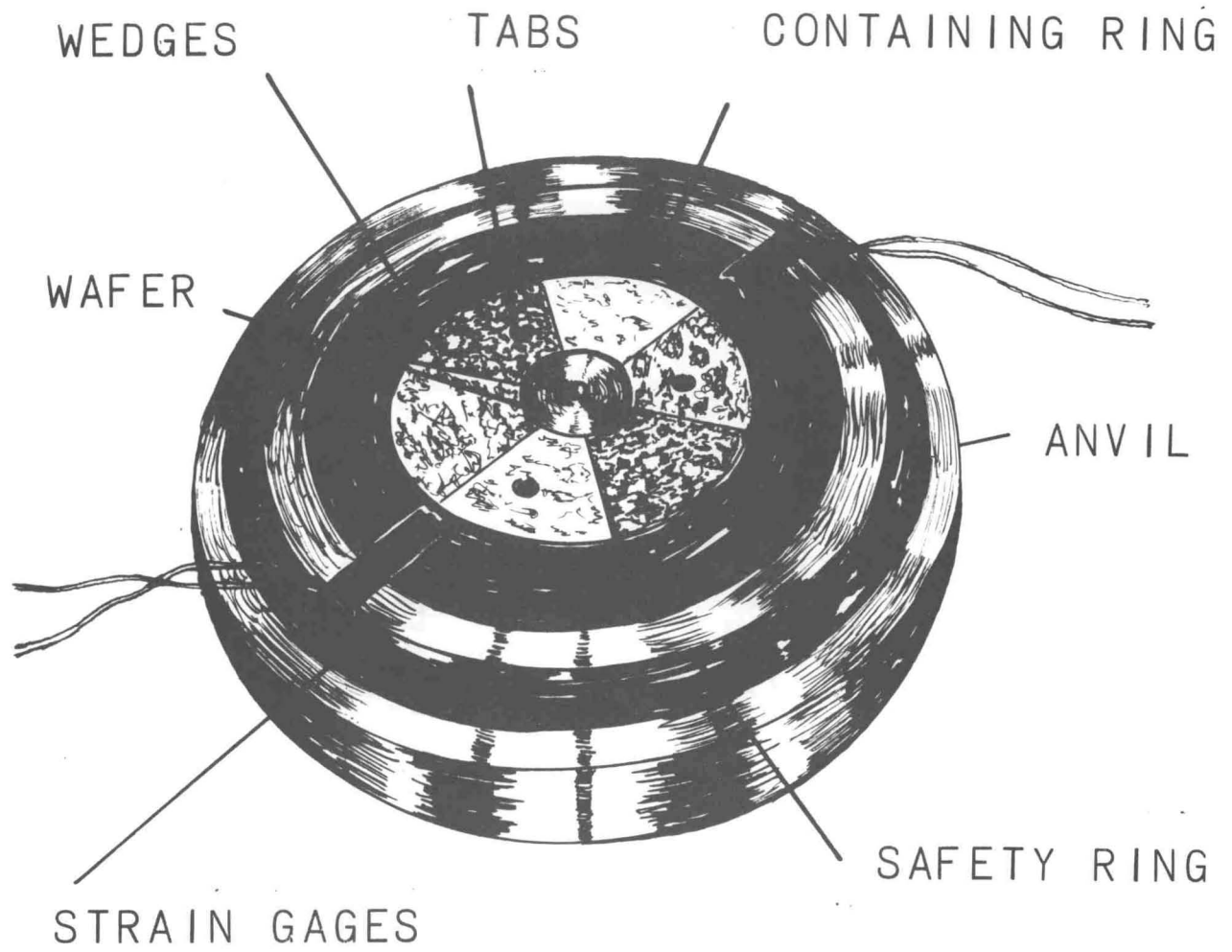


FIG. 4 ASSEMBLY VIEW OF WAFER  
CONTAINING RING

experimental stress-strain curves are documented in the following table.

Material	$\sigma_0$ -psi	b-psi	n
303 Stainless Steel	38,000	340,000	1
2S Aluminum	10,500	11,000	0.377
6061 Aluminum	15,000	33,000	1
Armco Iron	30,000	150,000	1

The two hollow wafers appearing in Figure 3 serve to illustrate the possible reduction in cavity volume as referred to earlier. These two annealed, 303 stainless steel wafers were initially the same size (1.500" O.D., 0.375" I.D., 0.466" ht.), but after being subjected to a 0.5 million pound load, in the ring assembly, the wafer on the right assumed the form as shown (1.525" O.D., 0.264" I.D., 0.436" ht.). This change in the hole diameter represents a 50% reduction in cavity volume, which is sufficiently large to create extremely high pressures in the cavity fluid.

(2) Wedges - The purpose of the wedges is to transmit, in an elastic manner, the high-intensity restraining pressure existing at the external wafer surface, to a low-intensity pressure level at the larger inner surface of the steel containing ring. This intensification is inversely proportional to the radial position. Since the wedges are not joined to one another, no hoop stresses are developed, and

the wedges are in a state of compressive stress. The high compressive strengths available in Graph-Air metals suggested their use as the wedge material. By employing an ambient air quench from  $1475^{\circ}\text{F}$ , and a further air quench to  $-11^{\circ}\text{F}$  with dry-ice, the compressive elastic limit of the Graph-Air was raised to 400,000 psi. These precautions were taken to assure that the wafer is confined in an elastically deformable surrounding, consistent with the assumption employed in the analysis.

(3) Steel Containing Ring. This ring serves as a radial support for the wedges, and was designed to withstand an internal pressure of 50,000 psi. 4140 steel, heat treated to a 190,000 psi yield strength, was used as the ring material. A slight interference fit between the steel containing ring and wedges was provided to maintain the assembly as an integral unit.

(4) Safety Ring - As the name implies, the safety ring is constructed of a ductile material (303 stainless steel), and serves to restrain the motion of the internal parts in case a fracture should occur.

The anvil design is shown in Figure 3 with the containing ring. The wafer makes actual contact with the anvil cones, which in turn are seated in a conical wedge assembly. The anvil wedges are supported by two press-fitted containing rings and an outer safety ring. The anvil cones were fabricated from Graph-Air, and were designed in the conical shape to take advantage of the supporting stresses.

An assembly view of the wafer-containing ring system appears in Figure 4. It can be seen here that the wafer thickness is slightly greater than the corresponding thickness of the containing ring, which prevents the anvils from making contact with the ring. Three equally spaced rubber tabs are placed on the upper and lower sides of the containing ring to keep it centered until the expanding wafer makes contact. Two SR-4 foil-type strain gages have been mounted at diametrically opposed positions on the outer surface of the containing ring such that an average circumferential strain can be recorded as a function of the applied force.

The complete assembly of anvils, wafer, and containing ring is shown in place on the ram in Figure 5. Since the ram moves at a maximum rate of 0.5 inches per minute, additional parallel cylindrical blocks were placed above the top anvil to reduce the ram travel required for contact. The large area of these blocks prevents the stress level from exceeding their elastic limit. The strain gage leads are connected to a switching circuit such that readings can be taken from both gages without having to reach under the press. The leads from the switching circuit are then placed across the terminals of a Baldwin static strain gage indicator. A temperature compensating strain gage is also employed in the usual fashion. In conducting compression tests on confined wafers, the ram load was increased in even increments, and the circumferential strain, as read on the Baldwin indicator, was recorded at each increment. In the unconfined wafer

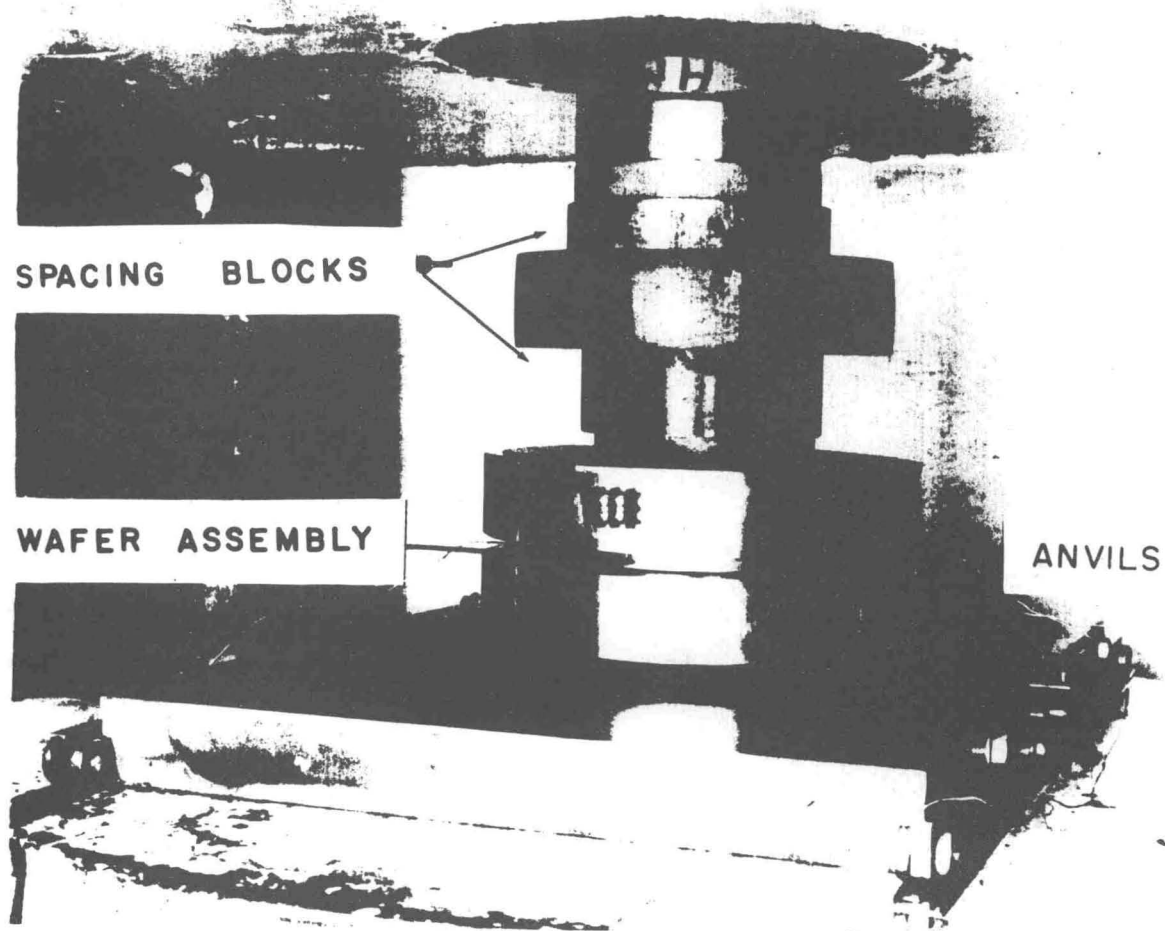


FIG. 5 COMPLETE ASSEMBLY OF  
CONFINED WAFER COMPRESSION  
SYSTEM

tests, the mid-meridian wafer diameter was measured with micrometers, and documented against the corresponding axial load. The loss of axial symmetry occurring with large (greater than 30%) radial deformations required that several diametral measurements be made, and the average recorded.

The lubricants used were molybdenum disulphide and iron oxide. According to Reference (m), these lubricants have coefficients of friction of 0.04 and 0.71, respectively. These lubricating powders were first mixed with an alcohol solution, and then brush-coated on the wafer-anvil surfaces. Upon drying, a thin, uniform coat of lubricant was deposited on the desired surfaces.

The applied force-strain data taken from the confined wafer, and the applied force-radial deformation measurements acquired from the compression of unconfined wafers, has been documented in the various tables and figures of the following section. This procedure permits a direct comparison between the experimental data and that which has been determined from the preceding analysis.

### III. STRESS AND PRESSURE DISTRIBUTIONS

This section is devoted to the presentation of the resulting stress and pressure gradients existing throughout the wafer, with emphasis placed on the effects of the following parameters: (1) diameter-to-thickness ratio; (2) wafer material properties; (3) anvil-wafer friction factor; and (4) influence of elastically deformable radial constraints.

The experimental and analytical applied force-displacement results achieved in the compression of an unconfined 303 stainless steel wafer are shown in Figure 6. The ordinate of this, and subsequent force-displacement diagrams, has been non-dimensionalized by dividing the applied force, equation (43), by the wafer surface area and the material yield strength  $\sigma_0$ . The abscissa has likewise been non-dimensionalized by forming the ratio of current radius to initial radius. The predicted curve is in good agreement with the data for the low-friction lubricant (molybdenum disulphide), but the same comparison for the high-friction lubricant is not as favorable, except perhaps, at the approach of higher loads. This latter disagreement is to be expected since the analysis was predicated on the concept of proportional straining, which in turn requires that the surface shear stress be small. Since the applied force corresponds to the area under the axial normal stress curve, its agreement with the experimental data suggests strongly that the

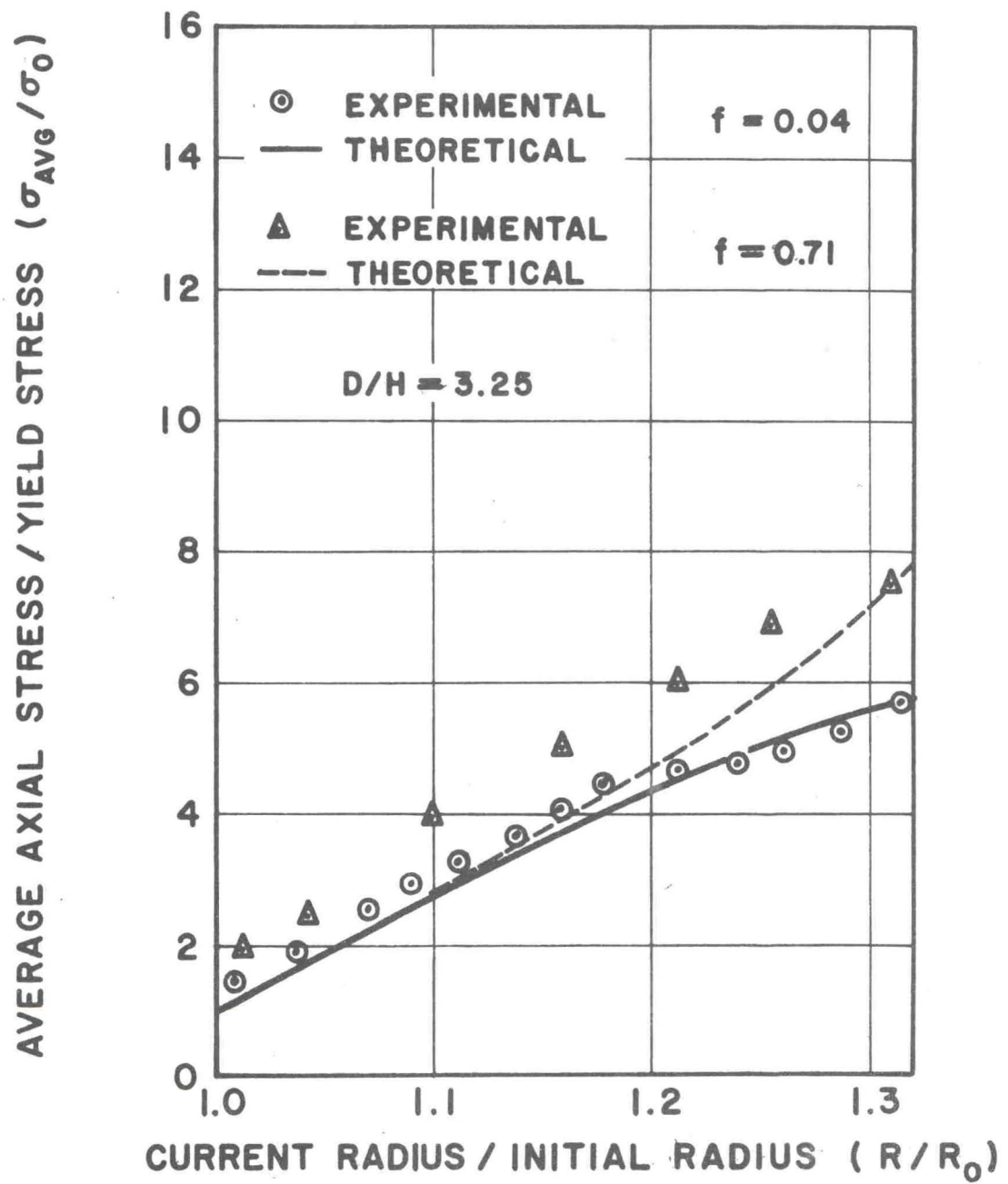


**FIG. 6 APPLIED FORCE DISPLACEMENT RELATION FOR AN UNCONFINED 303 STAINLESS STEEL WAFER**

stress distributions are also valid.

The stress distributions occurring in a radial direction across the top and mid-meridian surfaces of a compressed, unconfined 303 stainless steel wafer are shown in Figure 7. To aid in the identification of the type of compression test, a case number has been assigned to each of the stress distribution diagrams. The first character is a I or II, with the I meaning unconfined, and II represents a confined wafer. The second character is an A or B, where A indicates that the anvil lubricant is molybdenum disulphide, and B represents iron oxide. Since the stresses are symmetrical about the wafer axis, the second half of the diagram is reserved for showing the results of an increased load. In Figure 7, the stresses induced by the loads required to cause 16% and 32% increases in the initial radius are shown on the left and right sides, respectively. The axial stress  $\sigma_z$  and shearing stress  $\tau_{rz}$  are obtained from equations (40) and (41), respectively, and the pressure P is found by taking the average of the normal stresses, equations (38), (39), and (40). The computer programs used in finding the appropriate displacement coefficients, stresses and applied forces are given in Appendix I. In order to better illustrate the use and operation of these programs, a single problem, namely, the one now in question, is presented in Appendix I, with the output being that required for the construction of Figures 6 and 7.

A comparison of Figures 7 and 8 illustrates the influ-

CASE I-A SOLID WAFER, UNCONFINED  
 COEF. OF FRICTION = 0.04 D/H = 3.25

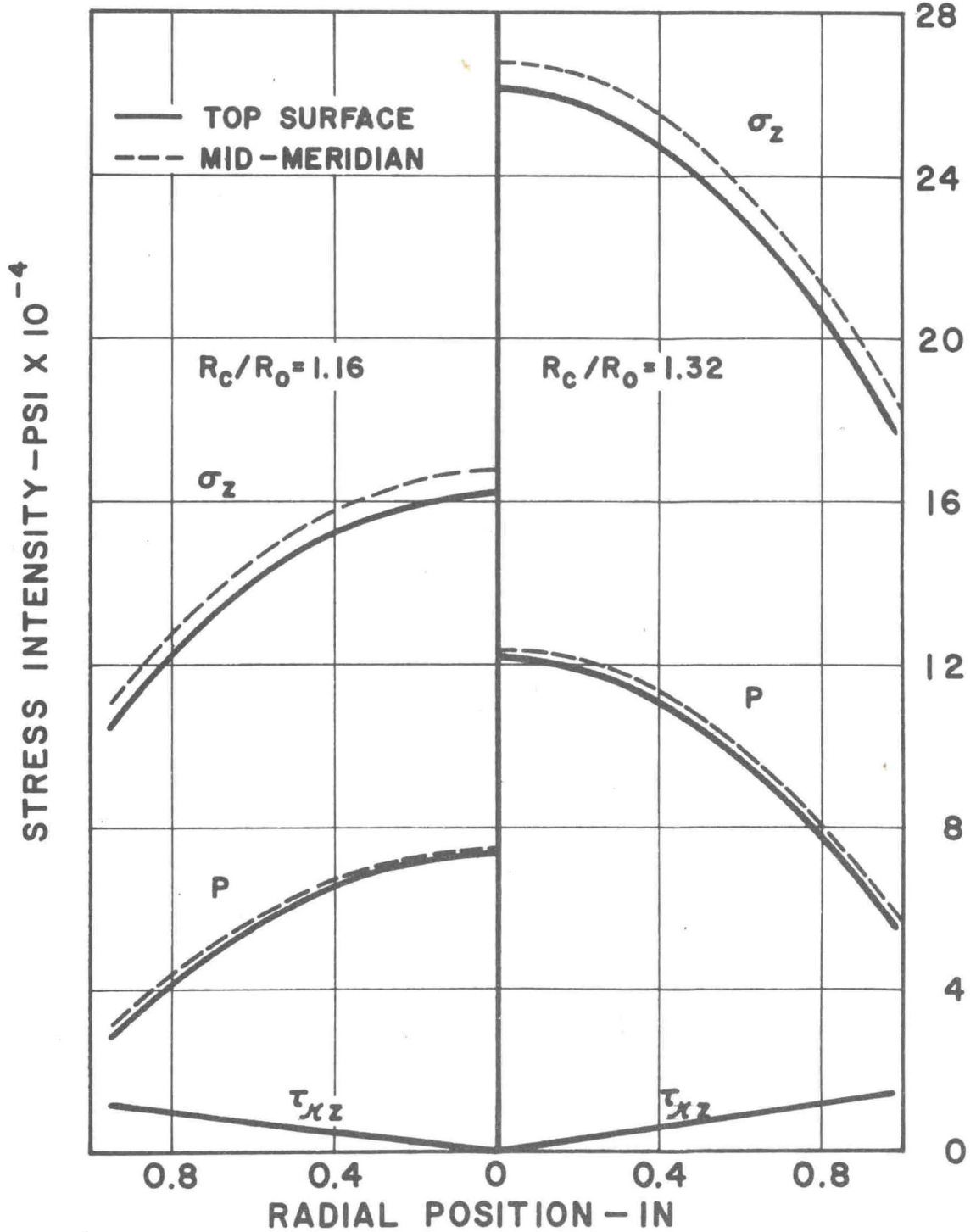


FIG. 7 STRESS DISTRIBUTION FOR 303 STAINLESS STEEL. CASE I-A

CASE I-B SOLID WAFER, UNCONFINED  
 COEF. OF FRICTION = 0.71 D/H = 3.25

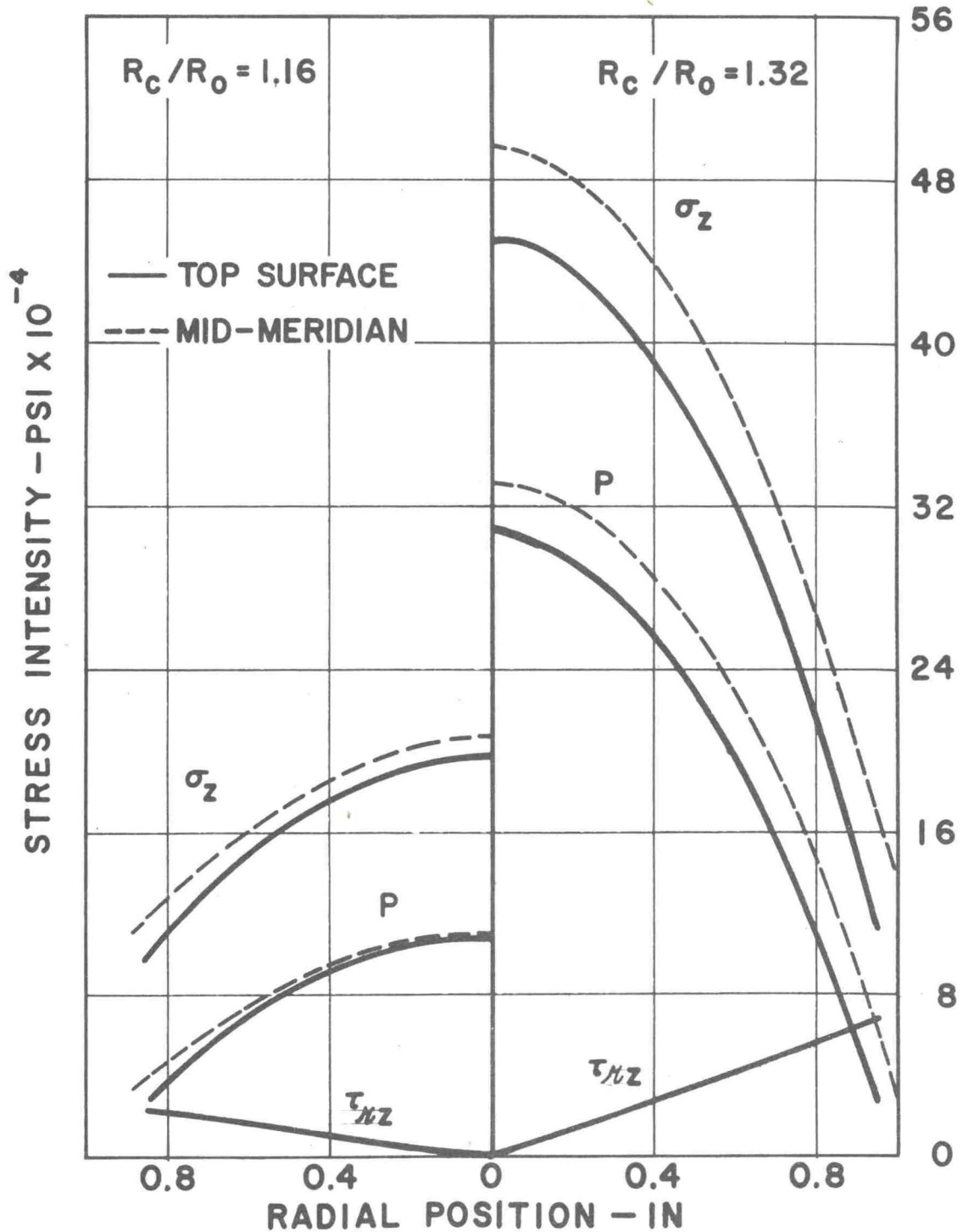


FIG. 8 STRESS DISTRIBUTION FOR 303  
 STAINLESS STEEL. CASE I-B

ence of different anvil lubricants on the stress distribution. Molybdenum disulphide (coefficient of friction = 0.04) was used in Figure 7, and iron oxide (coefficient of friction = 0.71) was the lubricant for Figure 8. The higher surface friction retards the radial expansion, and causes an intensification of the stresses at the wafer center. The shearing stress vanishes along the wafer axis and on the mid-meridian plane by virtue of symmetry. Both of these figures indicate that the axial variations are not significant for the unconfined wafer, especially in the low shear case. This latter case also points the discrepancy involved in assuming that the pressure in the wafer is the total force divided by wafer area, or what is equivalent, the average value of the normal axial stress  $\sigma_z$ .

The influence of wafer material properties has been examined from the results of compression tests on 6061 aluminum and Armco iron. Typical applied force-displacement, and stress distribution diagrams have been constructed in the manner described earlier, and are shown in the following figures. Wafers having two different D/H ratios were constructed from 6061 aluminum, and their applied force test results were superposed on Figure 9 to show the apparent agreement with the analysis. This figure indicates that the wafer shape (D/H ratio) does not play a major role in the compression of unconfined wafers, within the range studied herein. Figure 10 represents the corresponding stress and pressure distributions for 6061 aluminum, and it is noted

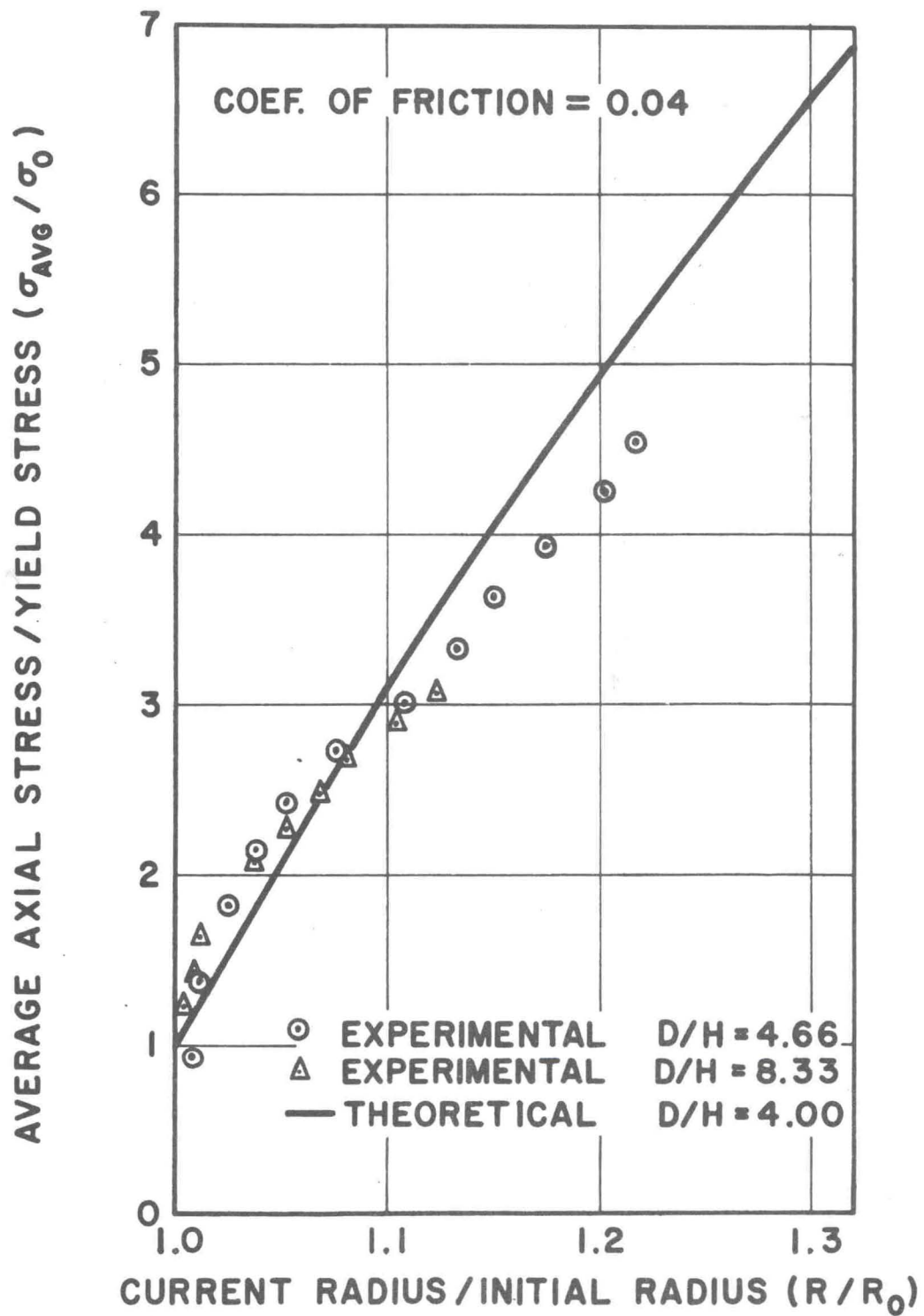


FIG. 9

APPLIED FORCE DISPLACEMENT  
RELATION FOR AN UNCONFINED  
6061 ALUMINUM WAFER.

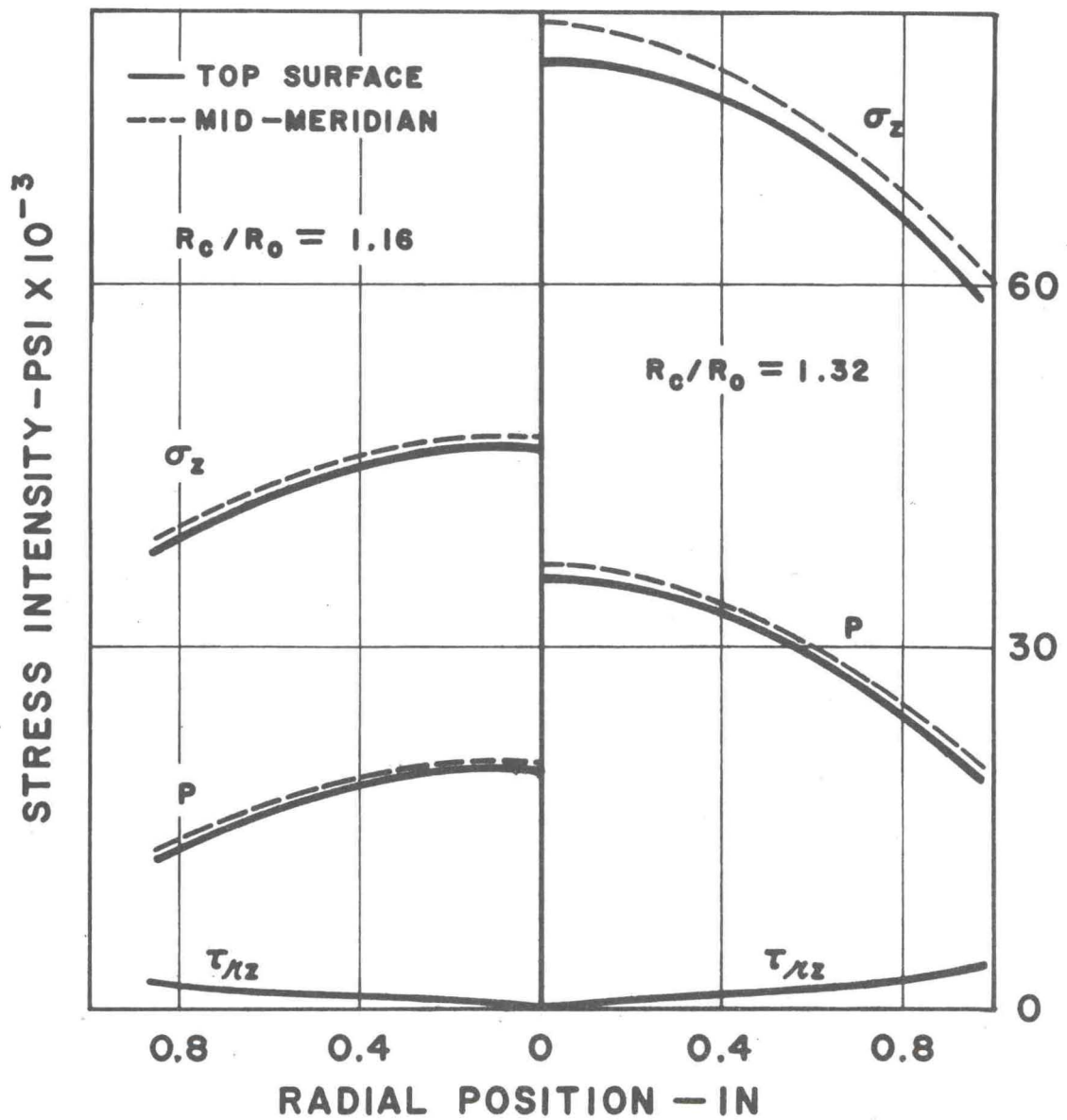


FIG. 10 STRESS DISTRIBUTION FOR 6061 ALUMINUM. CASE 1-A

that the stresses are still highest at the wafer center, and that the axial variations are small. The applied force-displacement and stress distribution results for Armco iron are shown in Figure 11 and 12, respectively. The inability to replace the actual stress-strain curve of Armco iron with a linear equation prohibits the extension of agreement between experiments and analysis beyond a 15 per cent radial deformation. The earlier comments made on stress distributions applies also to Figure 12.

The tangential strain occurring at the center surface of the containing ring has been documented against the applied force required for the compression of a confined 303 stainless steel wafer, and the results are shown with the analytical data in Figure 13. The excellent agreement shown here is especially encouraging in view of the magnitude of the applied load (one million pounds). The experimental results do not pass through the origin since a certain minimum initial clearance must exist between the wafer and ring to provide for assembly. The analytical curve also starts above the origin since it was assumed that the wafer material is rigid until the onset of plastic straining. If the initial clearance and the elastic deformation of the wafer are the same, the two results should be compatible at the start. The stress distributions occurring across the top and mid-meridian surfaces of confined 303 stainless steel wafer, subjected to a load corresponding to a 1.2 per cent increase in initial radius, are shown

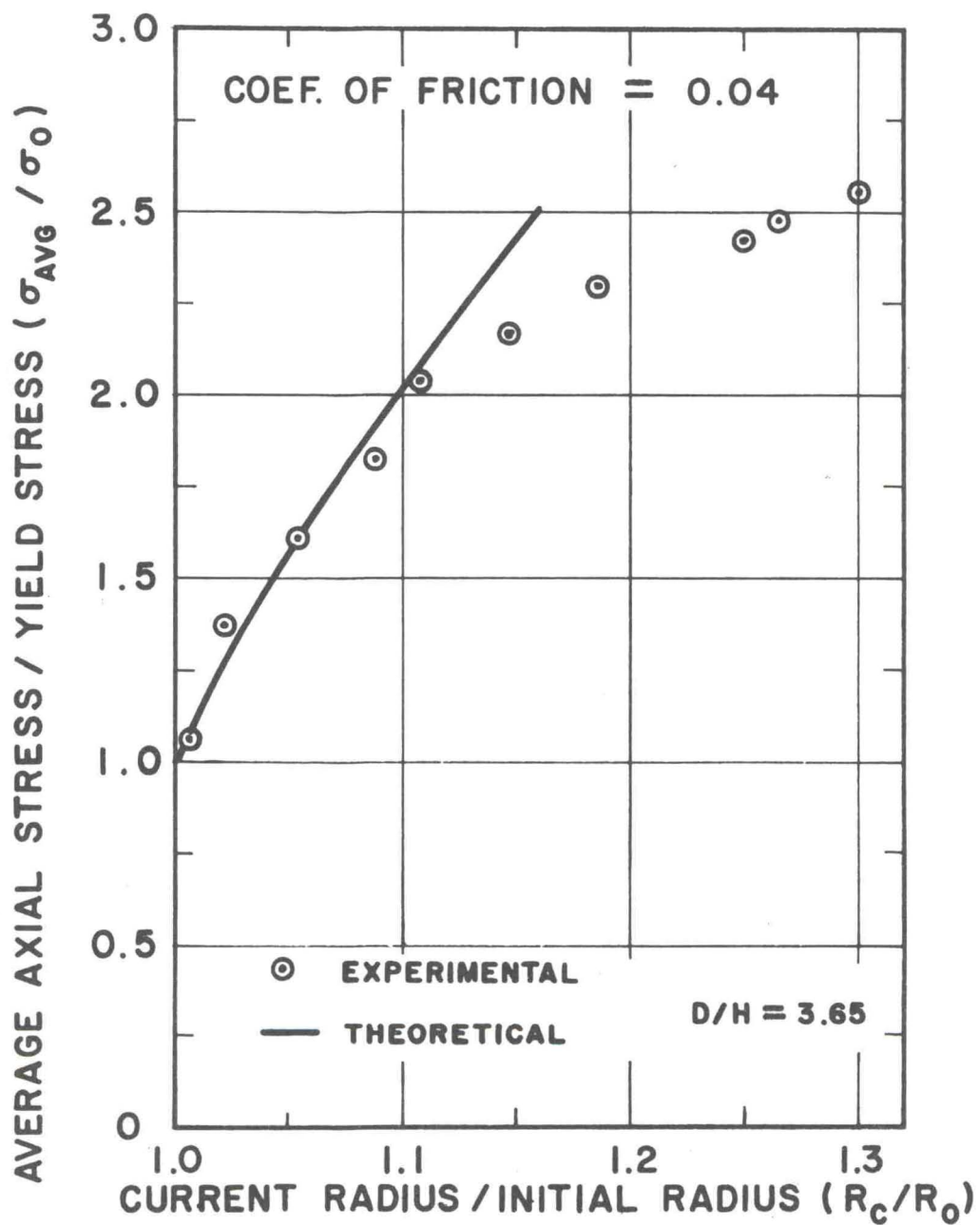


FIG. II APPLIED FORCE DISPLACEMENT RELATION FOR AN UNCONFINED ARMCO IRON WAFER.

CASE I-A SOLID WAFER, UNCONFINED  
 COEF. OF FRICTION = 0.04 D/H = 3.65

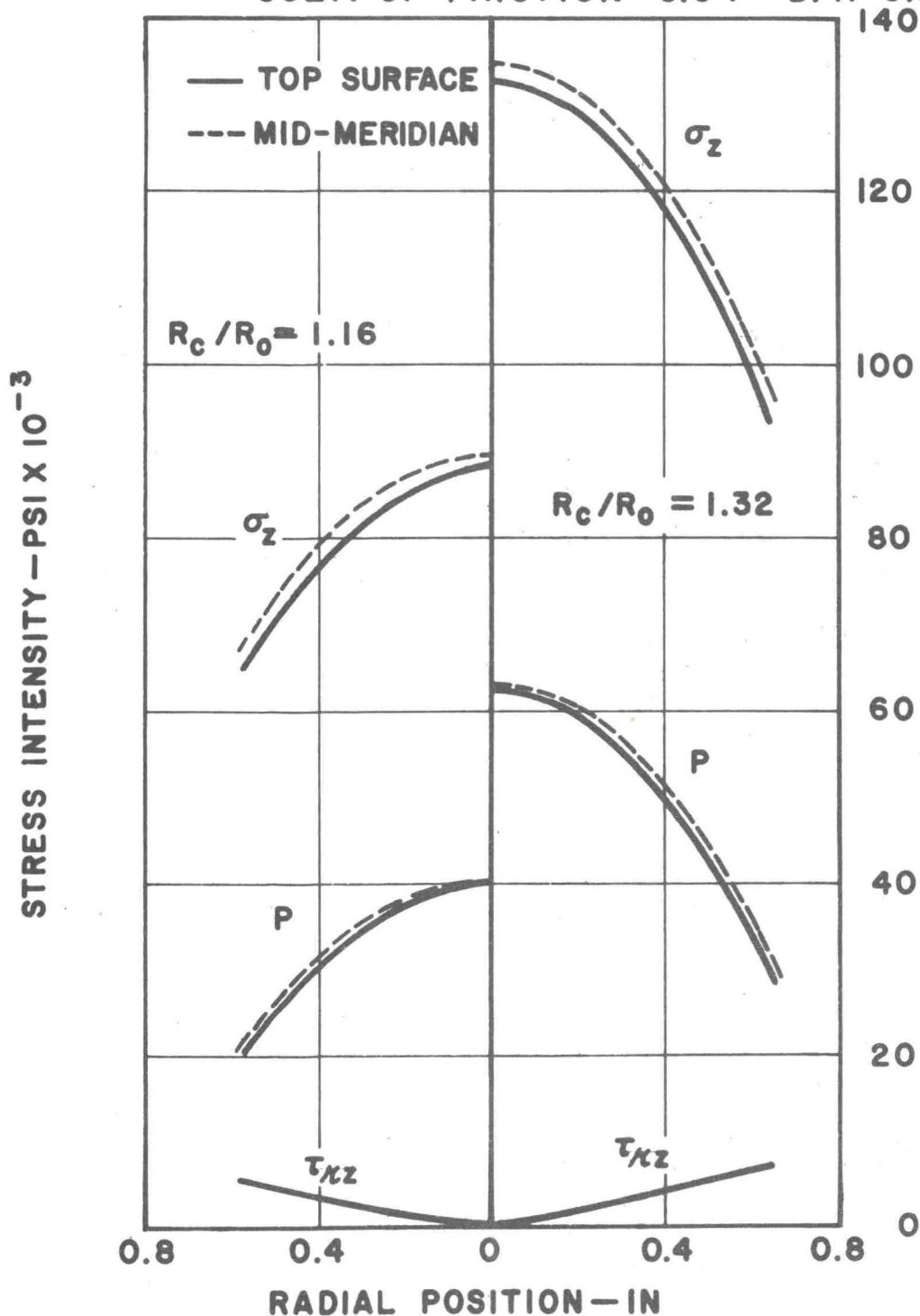


FIG. 12 STRESS DISTRIBUTION FOR  
 ARMCO IRON. CASE I-A

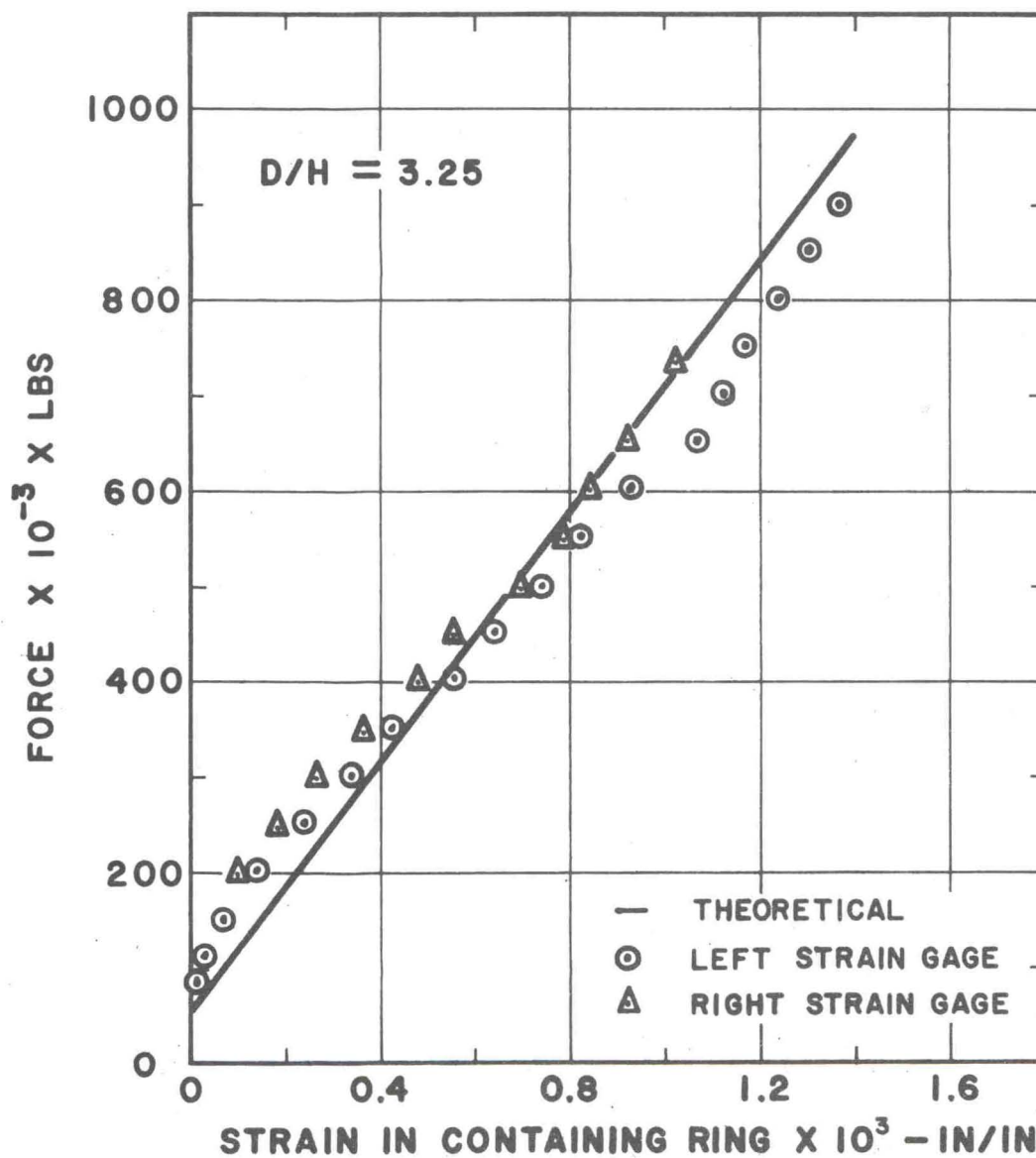


FIG. 13 APPLIED FORCE STRAIN RELATION FOR A CONFINED 303 STAINLESS STEEL WAFER.

in Figure 14. Both sides of the diagram are employed to effectively illustrate the large stress gradients which occur in both the radial and axial directions of a confined wafer. The radial stress gradients are of the type encountered in the unconfined wafer; however, the axial gradients are appreciably greater, and this observation will be commented on later. Figure 15 illustrates the stress gradients within the above wafer after the load has been increased until the mid-meridian wafer radius is 2.4 per cent larger than its original value. These last two figures indicate that the radial gradients tend to level out with increase in load, and that the entire stress state approaches more closely to a hydrostatic condition.

In order to evaluate the effects of wafer shape ( $D/H$  ratio) on the stress distribution in confined wafers, two additional calculations were made with all parameters, except wafer shape, being the same as those utilized in Figure 15. The new diameter-to-height ratios were 6.5 and 13, and their resulting stress distributions are shown in Figures 16 and 17, respectively. The results of these last three figures have been combined to give a descriptive account of the influence of wafer shape on the profile of the axial normal stress distribution. Using the ratio of the axial stress at the wafer center to the average axial stress as the parameter for describing the stress profile, the curve appearing in Figure 18 shows, for  $D/H$  in the range of 3 to 13, that the normal axial stress distribution across the wafer surface is

CASE II-A SOLID WAFER, CONFINED  
 COEF. OF FRICTION = 0.04  
 $R_c/R_0 = 1.012$ ,  $D/H = 3.25$

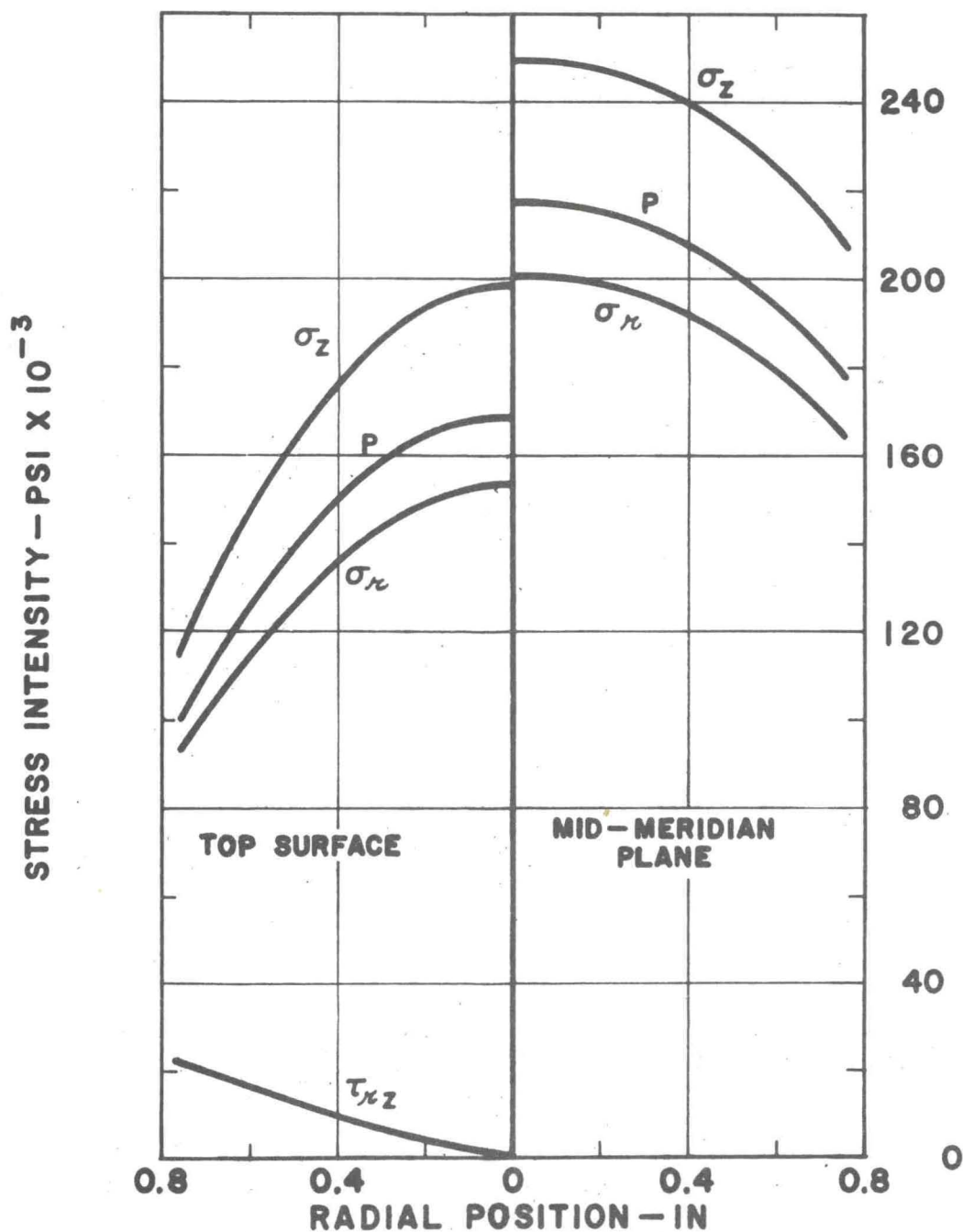


FIG. 14 STRESS DISTRIBUTION FOR 303  
 STAINLESS STEEL. CASE II - A  
 $R_c/R_0 = 1.012$ .

CASE II-A SOLID WAFER, CONFINED  
 COEF. OF FRICTION=0.04  
 $R_c/R_0 = 1.024$ ,  $D/H=3.25$

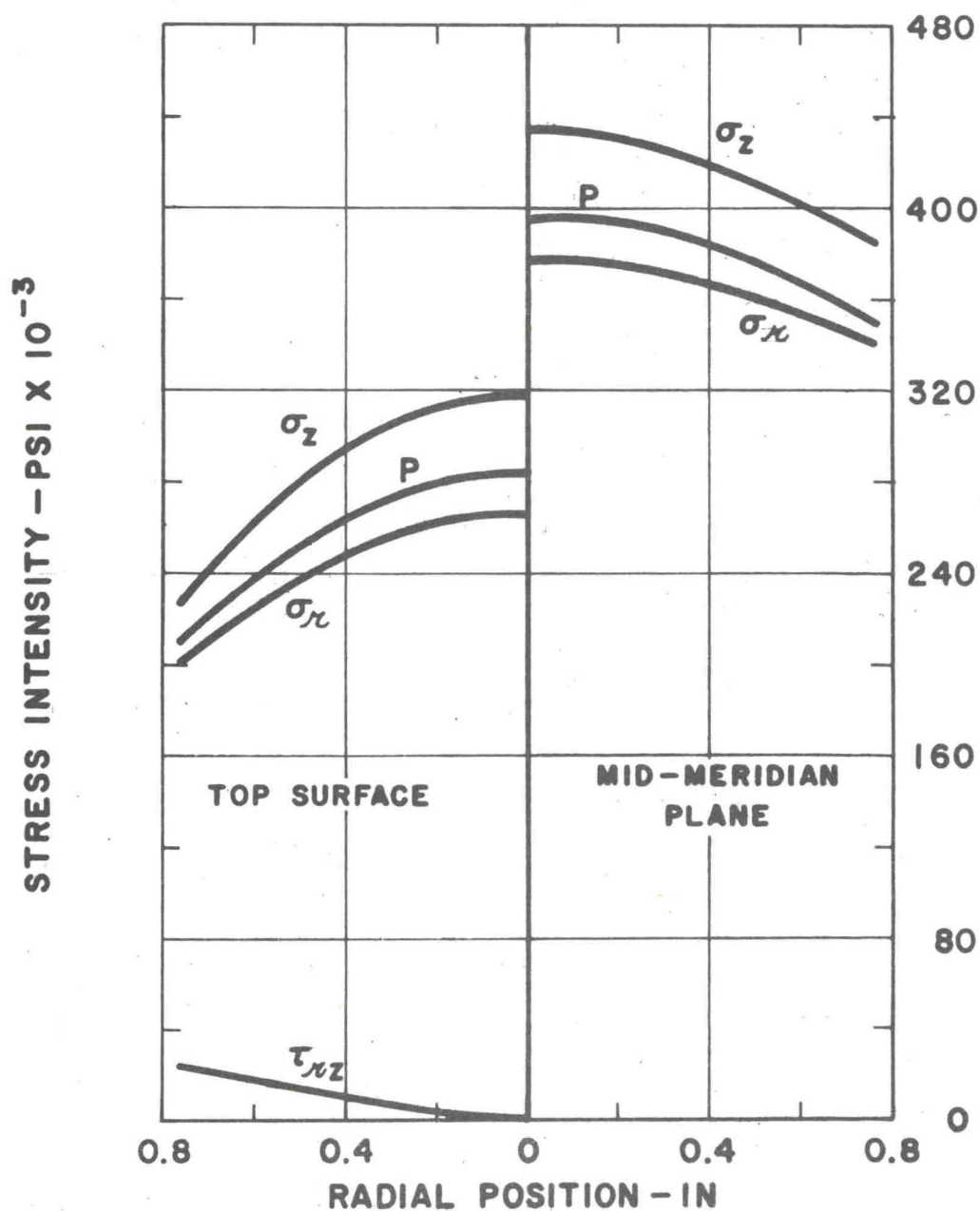


FIG. 15 STRESS DISTRIBUTION FOR 303  
 STAINLESS STEEL. CASE II-A  
 $R_c/R_0 = 1.024$ .

CASE II-A SOLID WAFER, CONFINED  
 COEF. OF FRICTION = 0.04  
 $R_c/R_0 = 1.024$ ,  $D/H = 6.5$

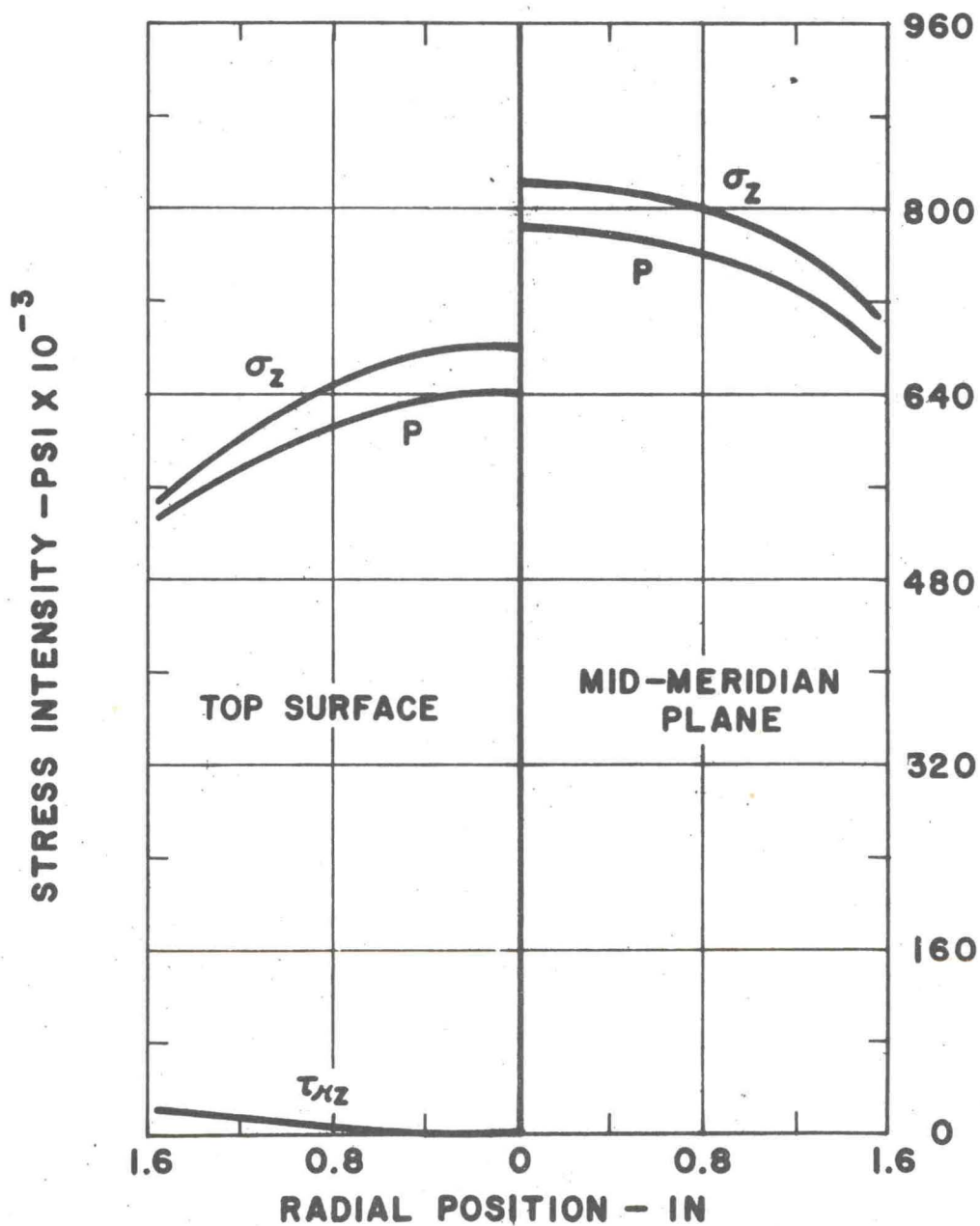


FIG. 16 STRESS DISTRIBUTION FOR 303  
 STAINLESS STEEL. CASE II-A  
 $D/H = 6.5$

CASE II-A SOLID WAFER, CONFINED  
 COEF. OF FRICTION = 0.04  
 $R_c/R_0 = 1.024$ ,  $D/H = 13$

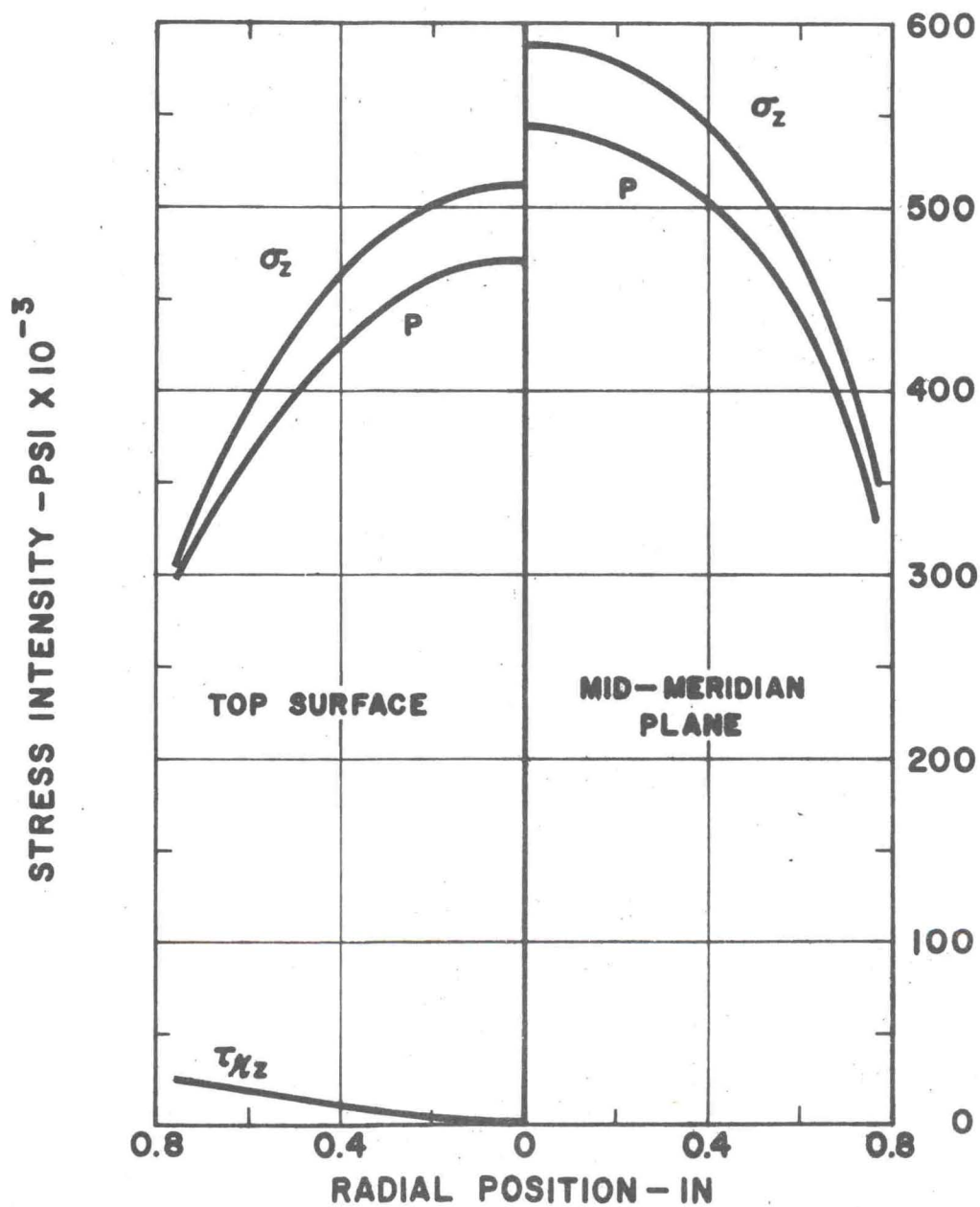
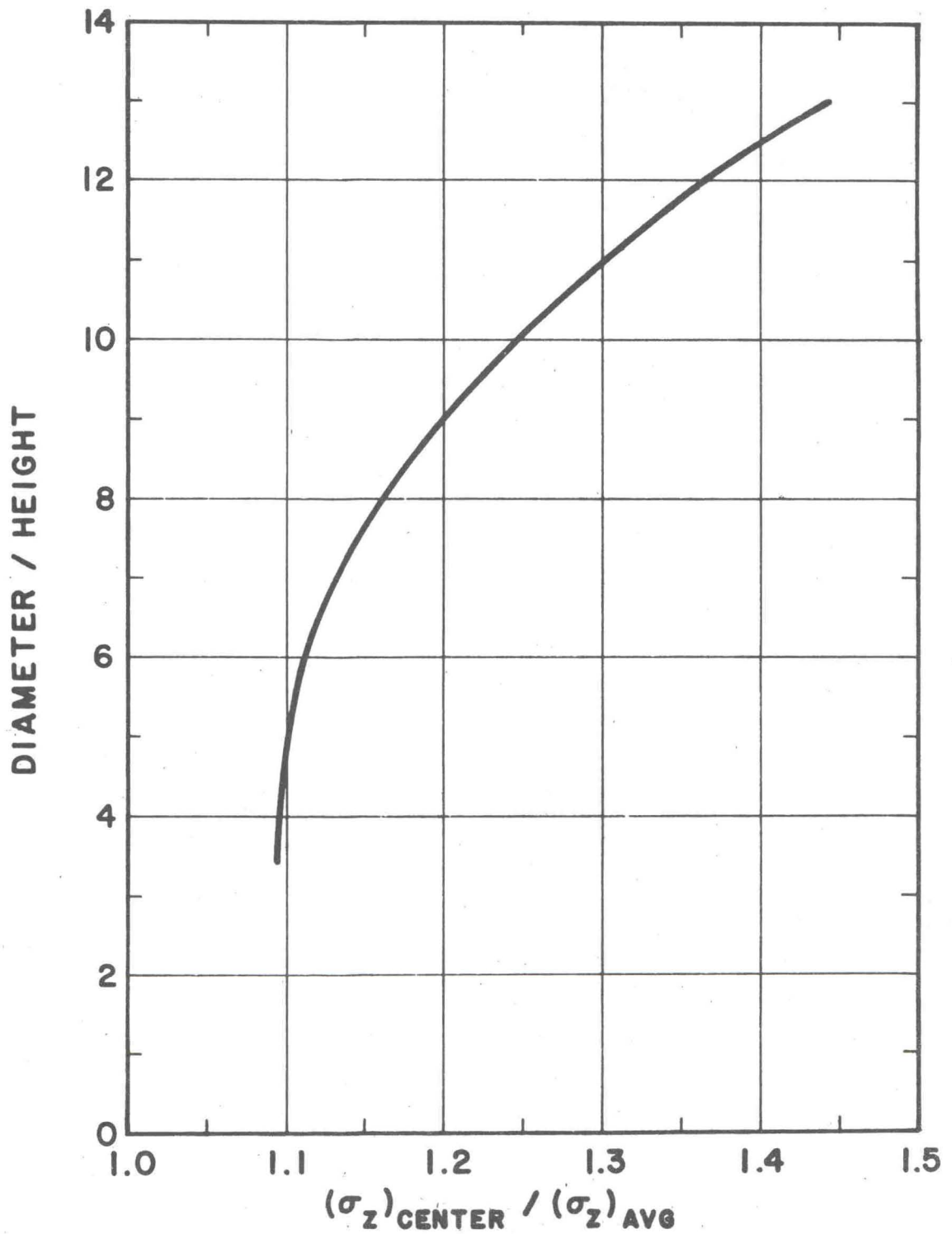


FIG. 17 STRESS DISTRIBUTION FOR 303  
 STAINLESS STEEL. CASE II-A  
 $D/H = 13$



**FIG. 18 INFLUENCE OF WAFER SHAPE ON AXIAL STRESS GRADIENT FOR 303 STAINLESS STEEL .**

maximum at the wafer center, and that the axial stress gradient in the radial direction becomes larger with increase in the wafer diameter-to-height ratio. This result is a topic of concern to many experimentors, References (a), (b), and (c), and will be discussed in more detail in the section Summary and Conclusions.

Several 2S aluminum wafers of various shapes were compressed to check the validity of the one-dimensional analysis. The non-linear stress-strain curve of 2S aluminum affords an opportunity to observe the usefulness of the Ludwig equation (63). The applied force-displacement data were arranged in the usual way, and are presented in Figure 19. The analytical results are lower than that dictated by experiments, which is as expected, since the one-dimensional analysis ignores the force required to overcome the inevitable friction existing at the wafer-anvil interface. The axial stress distributions are found from equation (66) and are shown in Figure 20. The axial stress corresponding to rigid, perfectly lubricated anvils is given in equation (71), and is shown in Figure 20 for comparison. Additional information on the one-dimensional analysis is given in Reference (1). The experimental data used in the construction of the aforementioned figures has been documented, and is shown in the following seven tables.

The agreement achieved between experimental data and the two-dimensional analysis is deemed good, and the resulting stress gradients are considered to be defensible in view of

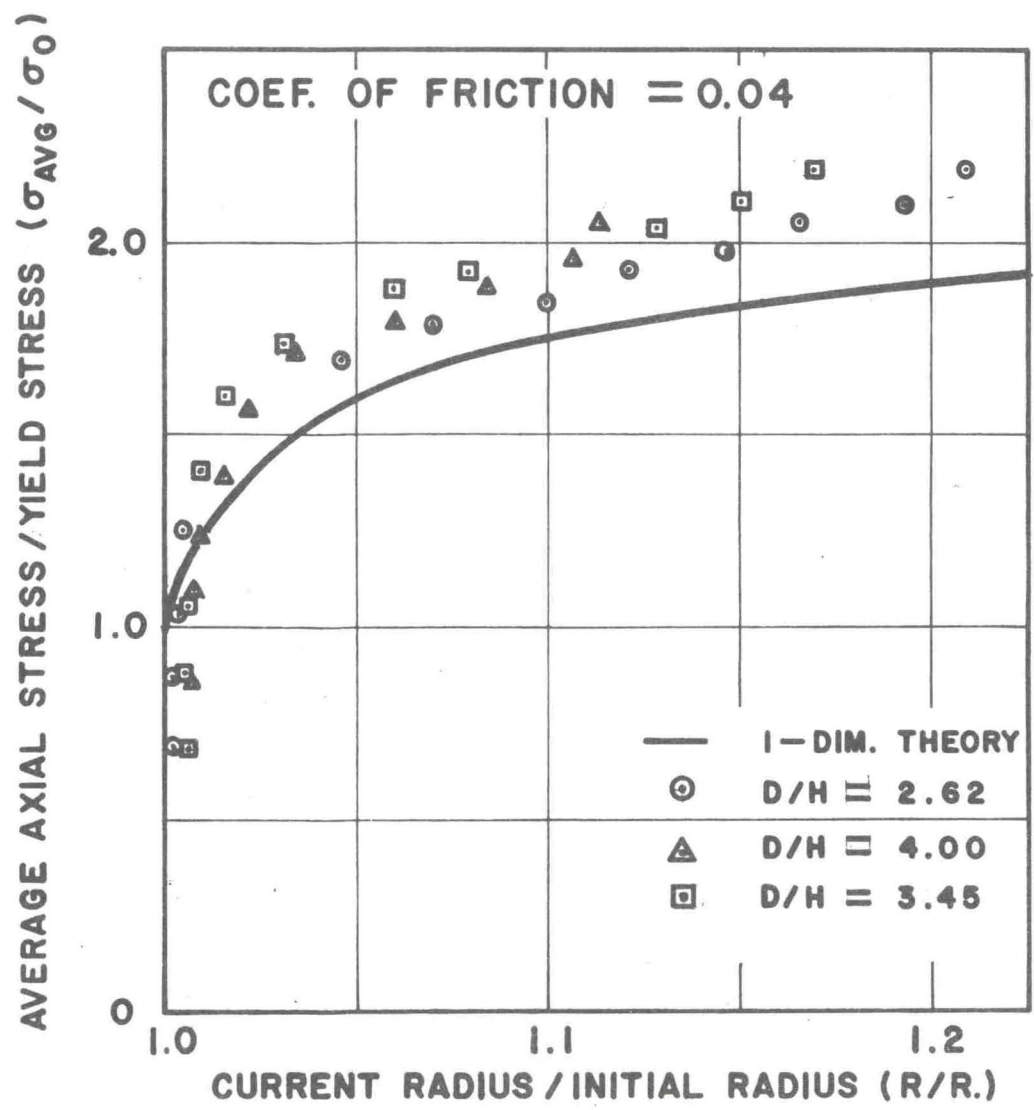


FIG. 19 APPLIED FORCE DISPLACEMENT RELATION FOR AN UNCONFINED 2S ALUMINUM WAFER.

CASE I-A SOLID WAFER, UNCONFINED  
COEF. OF FRICTION = 0.04

LEGEND:

— EQUATION 66  
- - - EQUATION 71

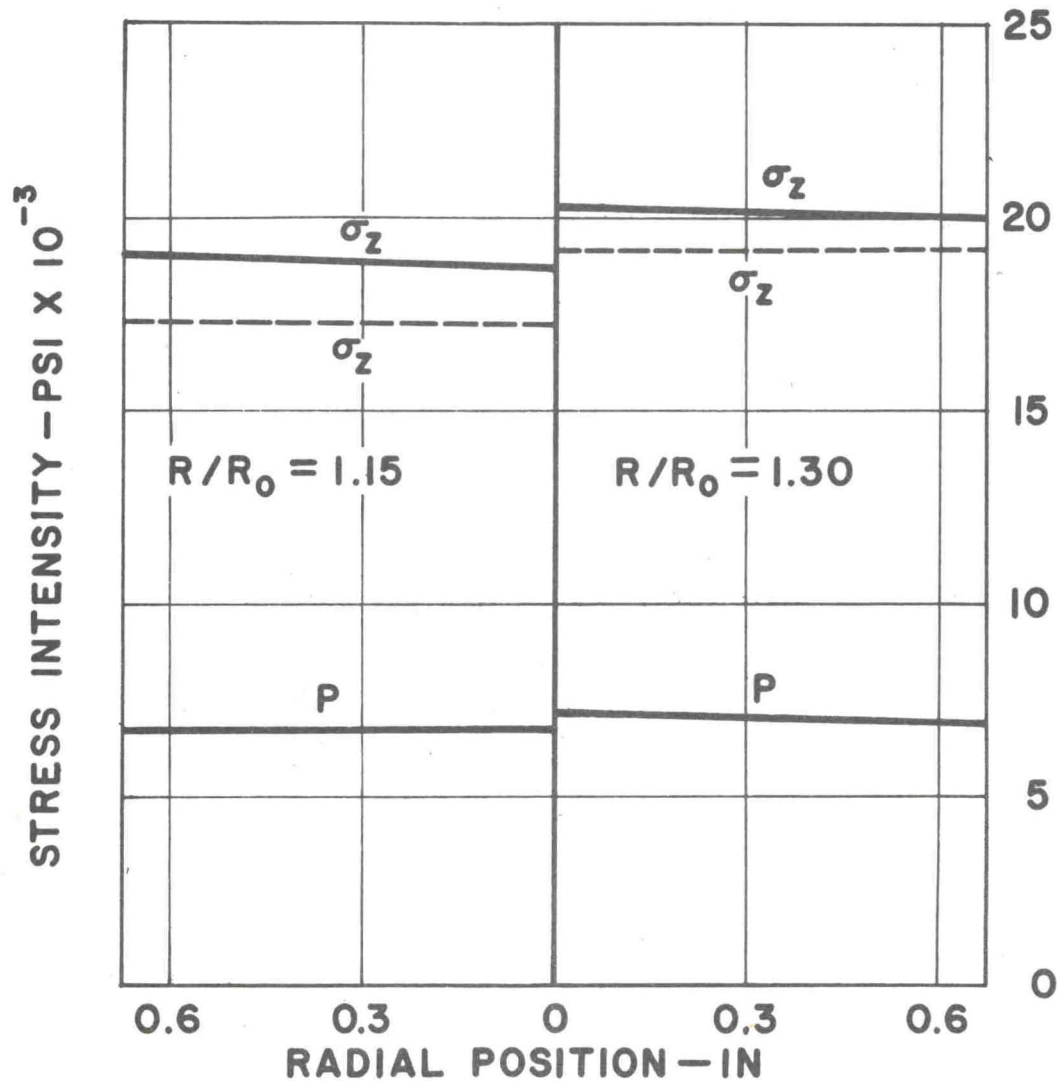


FIG. 20 ONE-DIMENSIONAL STRESS DISTRIBUTION FOR 2S ALUMINUM.  
CASE I-A.

<u>MATERIAL:</u> 303 Stainless Steel,                      D/H = 3.19 <u>WAFER:</u> Solid, Unconfined <u>INITIAL O.D.</u> = 0.997" ;    INITIAL HEIGHT = 0.313"							
ANVIL LUBRICANT Molybdenum Disulphide				ANVIL LUBRICANT Iron Oxide			
FORCE (Kips)	DIA. (in)	$\sigma_t/\sigma_o$	R/R <sub>o</sub>	FORCE (Kips)	DIA. (in)	$\sigma_t/\sigma_o$	R/R <sub>o</sub>
0	0.997	0	1.000	0	0.997	0	1.000
40	1.003	1.33	1.008	40	0.998	1.36	1.001
80	1.063	2.36	1.066	80	1.035	2.50	1.041
120	1.116	3.22	1.119	120	1.075	3.47	1.072
160	1.155	4.01	1.158	160	1.113	4.31	1.121
200	1.209	4.58	1.212	200	1.150	5.06	1.158
240	1.262	5.04	1.265	240	1.184	5.72	1.192
280	1.312	5.61	1.315	280	1.218	6.33	1.225
				320	1.247	6.88	1.254
				360	1.280	7.35	1.288

TABLE I    EXPERIMENTAL DATA FOR COMPRESSION OF SOLID, UNCONFINED 303 STAINLESS STEEL WAFERS

<u>MATERIAL:</u> 303 Stainless Steel, D/H = 3.23					
<u>WAFER:</u> Solid, Confined					
<u>INITIAL O.D.</u> = 1.500" ; <u>INITIAL HEIGHT</u> = 0.465"					
ANVIL LUBRICANT Molybdenum Disulphide			ANVIL LUBRICANT Iron Oxide		
FORCE (Kips)	STRAIN GAGE ( $10^{-6}$ in/in)		FORCE (Kips)	STRAIN GAGE ( $10^{-6}$ in/in)	
	LEFT	RIGHT		LEFT	RIGHT
110	30	10	50	10	5
200	135	95	100	15	5
300	340	260	150	35	25
400	555	475	200	115	110
500	740	690	250	200	225
600	930	840	300	280	320
700	1115	930	350	360	435
800	1235	-	400	465	475
900	1360	-			

TABLE 2 EXPERIMENTAL DATA FOR COMPRESSION OF SOLID, CONFINED 303 STAINLESS STEEL WAFERS

<u>MATERIAL:</u> 303 Stainless Steel, <span style="float: right;">D/H = 3.22</span>					
<u>WAFER:</u> Hollow, Unconfined; <span style="float: right;"><u>INITIAL I.D.</u> = 0.375"</span>					
<u>INITIAL O.D.</u> = 1.500" ; <span style="float: right;"><u>INITIAL HEIGHT</u> = 0.466"</span>					
ANVIL LUBRICANT Molybdenum Disulphide			ANVIL LUBRICANT Iron Oxide		
FORCE (Kips)	DIA. (in)	R/R <sub>0</sub>	FORCE (Kips)	DIA. (in)	R/R <sub>0</sub>
0	1.500	1.000	0	1.500	1.000
50	1.502	1.001	50	1.501	1.001
100	1.508	1.004	100	1.504	1.002
140	1.548	1.031	145	1.517	1.011
170	1.575	1.050	195	1.548	1.031
195	1.597	1.063	245	1.580	1.053
250	1.639	1.092	295	1.609	1.072
290	1.671	1.114	350	1.638	1.091
340	1.706	1.137	395	1.662	1.109
400	1.741	1.161	450	1.690	1.127
445	1.776	1.184	500	1.708	1.138
600	1.875	1.250	550	1.731	1.155
			600	1.751	1.168

Final I.D. = 0.380"

Final I.D. = 0.275"

TABLE 3 EXPERIMENTAL DATA FOR COMPRESSION OF HOLLOW, UNCONFINED 303 STAINLESS STEEL WAFERS

<u>MATERIAL:</u> 303 Stainless Steel,		D/H = 3.22			
<u>WAFER:</u> Hollow, Confined;		<u>INITIAL I.D.</u> = 0.375"			
<u>INITIAL O.D.</u> = 1.500" ;		<u>INITIAL HEIGHT</u> = 0.466"			
ANVIL LUBRICANT Molybdenum Disulphide			ANVIL LUBRICANT Iron Oxide		
FORCE (Kips)	STRAIN GAGE (10 <sup>-6</sup> in/in)		FORCE (Kips)	STRAIN GAGE (10 <sup>-6</sup> in/in)	
	LEFT	RIGHT		LEFT	RIGHT
200	15	5	200	90	100
250	150	95	250	235	255
300	320	285	300	405	445
350	500	485	350	580	635
400	665	660	400	745	755
450	820	815	450	945	935
500	1005	990	500	1145	1075
Final I.D. = 0.264"			Final I.D. = 0.293"		

TABLE 4 EXPERIMENTAL DATA FOR COMPRESSION OF HOLLOW, CONFINED 303 STAINLESS STEEL WAFERS

<u>MATERIAL:</u> Armco Iron, <span style="float: right;">D/H = 3.66</span>						
<u>WAFER:</u> Unconfined; <span style="float: right;"><u>INITIAL I.D.</u> = 0.250"</span>						
<u>ANVIL LUBRICANT:</u> Molybdenum Disulphide						
<u>INITIAL O.D.</u> = 1.008" ;				<u>INITIAL HEIGHT</u> = 0.275"		
SOLID				HOLLOW		
FORCE (Kips)	DIA. (in)	$\sigma_t/\sigma_o$	R/R <sub>o</sub>	FORCE (Kips)	DIA. (in)	R/R <sub>o</sub>
0	1.008	0	1.000	0	1.008	1.000
20	1.009	0.72	1.001	20	1.009	1.001
40	1.030	1.37	1.022	40	1.030	1.022
60	1.096	1.82	1.088	60	1.092	1.085
80	1.154	2.17	1.147	80	1.169	1.162
100	1.246	2.34	1.238	100	1.241	1.234
105	1.258	2.41	1.250	105	1.259	1.252
110	1.273	2.47	1.265	110	1.282	1.275
115	1.293	2.49	1.285	115	1.295	1.288
120	1.307	2.55	1.300	120	1.313	1.306

Final I.D. = 0.185"

TABLE 5 EXPERIMENTAL DATA FOR COMPRESSION OF SOLID AND HOLLOW, UNCONFINED ARMCO IRON WAFERS

MATERIAL: 6061 Aluminum							
WAFER: Solid, Unconfined							
ANVIL LUBRICANT: Molybdenum Disulphide							
D/H = 8.33				D/H = 4.66			
FORCE (Kips)	DIA. (in)	$\sigma_f/\sigma_0$	R/R <sub>0</sub>	FORCE (Kips)	DIA. (in)	$\sigma_f/\sigma_0$	R/R <sub>0</sub>
0	1.500	0	1.000	0	1.242	0	1.000
22	1.505	1.13	1.003	14	1.251	1.05	1.008
24	1.506	1.23	1.004	18	1.256	1.36	1.012
28	1.512	1.44	1.009	24	1.271	1.84	1.025
32	1.519	1.65	1.012	28	1.287	2.11	1.036
36	1.535	1.86	1.023	32	1.307	2.41	1.052
40	1.555	2.06	1.037	36	1.334	2.71	1.076
44	1.579	2.26	1.052	40	1.375	3.01	1.109
48	1.601	2.47	1.069	44	1.406	3.31	1.133
52	1.621	2.67	1.081	48	1.425	3.61	1.149
56	1.657	2.88	1.104	52	1.458	3.91	1.174
60	1.687	3.08	1.123	56	1.490	4.21	1.201
				60	1.509	4.52	1.217

TABLE 6 EXPERIMENTAL DATA FOR COMPRESSION OF SOLID, UNCONFINED 6061 ALUMINUM WAFERS

<u>MATERIAL:</u> 25 Aluminum <u>WAFER:</u> Solid, Unconfined <u>ANVIL LUBRICANT:</u> Molybdenum Disulphide							
D/H = 4.0				D/H = 4.0			
FORCE (Kips)	DIA. (in)	$\sigma_t/\sigma_o$	R/R <sub>o</sub>	FORCE (Kips)	DIA. (in)	$\sigma_t/\sigma_o$	R/R <sub>o</sub>
0	0.500	0	1.000	0	1.250	0	1.000
2.55	0.503	1.23	1.006	13.5	1.255	1.04	1.004
2.94	0.507	1.39	1.014	16.0	1.256	1.23	1.005
3.34	0.511	1.55	1.022	18.5	1.262	1.41	1.009
3.73	0.516	1.70	1.032	20.9	1.267	1.57	1.013
4.12	0.529	1.80	1.058	23.4	1.288	1.71	1.030
4.51	0.541	1.88	1.082	25.8	1.321	1.87	1.057
4.91	0.552	1.95	1.104	28.3	1.345	1.91	1.076
5.30	0.560	2.06	1.120	33.2	1.409	2.03	1.127
5.69	0.573	2.11	1.146	35.7	1.435	2.10	1.148
				38.1	1.458	2.18	1.166

TABLE 7 EXPERIMENTAL DATA FOR COMPRESSION OF SOLID, UNCONFINED 2S ALUMINUM WAFERS

the manner in which they were found. The many parameters that are varied in the experimental set-ups of the different experiments demands that a great deal more analytical work be done in order to correlate the results. A summary statement of the work to be continued in the near future is presented in the following section.

#### IV. FUTURE WORK

A proposal has been written requesting funds for continued research on the subject problem. A research grant would serve to aid in the investigation of the following items: (1) use of hollow wafer-containing ring system as a high-pressure generating device; (2) use of a four-term displacement function in lieu of the present maximum of three; (3) alteration of the analysis to include the effects of high surface shearing stresses; (4) exploration of wafer materials that are more common to high-pressure science (e. g., pyrophilite and silver chloride); (5) use of standard bismuth and manganin wire techniques for direct determination of pressure gradients; and (6) an evaluation of the possible effects of material compression and pressure dependent material constants.

The computer programs presented herein for the evaluation of the displacement coefficients for the compressed, hollow wafer will be tailored to meet the programming requirements for acceptance on the IBM 7090 computer. These results will be used as a guide in the optimum design of the high-pressure generating device.

## SUMMARY AND CONCLUSIONS

The method of solution used in the analysis of one- and two-dimensional parametric variations in the compression of cylindrical wafers is considered to be valid, and is adequately supported with numerous experimental data. The use of the displacement function has served to demonstrate the type of solution to be obtained with a retention of the appropriate terms. It also indicates the next term to be added if a more extensive analysis is to be performed. The solutions are limited to situations involving low shearing stresses at the anvil-wafer interface, and are somewhat cumbersome to use. However, in view of the fact that the solutions embody the effects of material strain hardening, anvil deflection, surface shear, radial constraints, magnitude of load and strain, etc., they should be regarded as useful analytical tools for determining the stress and pressure gradients existing in Bridgman-type pressure cells (a term generally adapted for confined compression wafers). In the compression of unconfined, short cylinders, these solutions should also describe the "end effects" that are commonly excluded.

The stress distributions, for confined and unconfined wafers, all indicate that the stress, and pressure, is greatest at the wafer center, and decreases with increase in radial position. This observation is consistent with the results reported in References (c), and (j), and is in partial agreement with the conclusions of Reference (b). The admittance

of a containing ring around the wafer enhances the prospect of obtaining pressures in the  $5 \times 10^5$  psi range, especially at the wafer center. Evidence is presented, Figures 14 and 15, which supports the argument that the stress state in a radially supported pressure cell approaches a hydrostatic condition with a sufficient increase in applied load. The containing ring need not remain elastic, nor should it act solely on the wafer, if the main purpose is to generate ultra-high pressures. The reason for doing such here is to obtain an experimental model that is more nearly compatible with the mathematical assumptions. The limited information obtained for high surface friction, iron oxide lubricant, indicates that the shearing stresses restrain the radial expansion of the wafer, in much the same manner as a containing ring, and serves to intensify the stress level at the wafer center, and to increase the axial variations of pressure.

This thesis entertains the effects of the variables pertinent to pressure cell constructions that have not previously been resolved. The method of solution permits a re-evaluation of the simpler analysis now available, and lends itself to an extension to problems of more complexity. The experience gained in performing this analysis should aid in extending the solutions to include the variations listed in the previous section. This work is not terminal, and will be pursued from different points of view until more elaborate and satisfactory results have been achieved.

## APPENDIX I.

### COMPUTER PROGRAMS AND SAMPLE RESULTS

As indicated earlier, the equations (45), (48), (50), (53), and (57) represent five independent equations for the determination of the three displacement coefficients,  $a_1$ ,  $a_2$ ,  $a_3$ , the mid-meridian constraining pressure,  $P_c$ , and the wafer centerline deflection,  $\Delta$ . A knowledge of these parameters allows for the determination of the normal and shearing stress distributions from equations (38), (39), (40), and (41), respectively. The applied compressive force can likewise be determined from (43).

If, at a given load, or what is equivalent, a given radius ratio  $R_c/R_o$ , values of  $a_2$  and  $\Delta$  are assumed, then  $a_3$  can be found from equation (50). Using this,  $a_1$  and  $P_c$  are found from (45) and (48), respectively. Equations (53) and (57) are utilized to check the validity of the assumed values of  $a_2$  and  $\Delta$ . A reasonably close approximation can be found for  $\Delta$  by assuming that the wafer maintains its cylindrical shape at all loads. Since the wafer expands more at the mid-meridian plane, the coefficient  $a_2$ , which is a measure of this curvature, will be some initially small negative quantity.

The computer program shown in Figure 21, written in FORTRAN language, starts with an assumed value of -0.010 for  $a_2$ , and then calculates an approximate value of  $\Delta$  from

```

C C
C DAVIS, R. TRIAL AND ERROR SOLUTION FOR COEFFICIENTS
  DIMENSION ARU(6), SIM(6), A34(50)
1  READ, RO, HO, STRO, B
2  READ, UNU, G
3  READ, DIF1, RING, A2, F
4  F1 = 1.+DIF1
5  F1 = F1 + DIF1
  NAN = 1
  CUP = 0.02
  SAM = 0.
  X = 0.
  Y = 0.
  RC = F1*RO
  DELTA = (HO*(1.-1./(F1**2.)))*2.
  PRINT, DELTA
10 A2 = -0.010
  HC = HO-DELTA/2.
  L = 1
  M = 0
  MAN = 0
  HC1 = 2.*HO - DELTA
11 A3 = DELTA/(2.*HC1)-(A2*(HC1*HC1))/4.
  M = M+1
  MAN = MAN+1
12 A1 = ((RC-RO)/(RC*RC*RC))-(A3/(RC*RC))
13 PC = (RC*RING)*(A1*RC*RC+A3)
  ALPHT = (52./3.)*A1*A1
  HAMT = 12.*A1*A2+9.*A2*A2+16.*A1*A1
  BETT = (4./3.)*(HAMT*HC*HC+12.*A1*A3)
14 BETTP = (8./3.)*(HAMT*HC)
  GAMT = 4.*(3.*A2*HC*HC+A3)*(3.*A2*HC*HC+A3)
  GAMTP = 48.*A2*(3.*A2*HC*HC+A3)*HC
  RT = RC
43 RT3 = A1*RT*RT
  RT4 = 3.*A2*HC*HC+A3
  RT1 = RO+(RT3+RT4)*RT
  RT2 = ABS(RT1-RT)
  IF(RT2-0.001)15,15,35
35 RT = 0.25*(3.*RT+RT1)
  GO TO 43

```

FIG. 21 COMPUTER PROGRAM FOR DETERMINING UNKNOWN DISPLACEMENT COEFFICIENTS. SOLID WAFER

```
15  IF(RT-RC)91,91,9
9   IF(NAN-1)1,96,93
91  HT = HC
39  HT3 = -2.*A2*HT*HT
    HT4 = 4.*A1*RT*RT+2.*A3
    HT1 = HO+(HT3-HT4)*HT
    HT2 = ABS(HT1-HT)
    IF(HT2-0.001)16,16,47
47  HT = 0.25*(3.*HT+HT1)
    GO TO 39
16  ZEKE = SQRT(ALPHT)
    BILL = SQRT(GAMT)
    COEF1 = (F*STRO/(3.*ZEKE))*(2.*A1-3.*A2)
    GRE1 = 2.*ALPHT*RT*RT+BETT
    IF(GRE1)31,31,33
31  COMP1 = 0.
    COMP3 = 0.
    GO TO 37
33  COMP1 = (GRE1/(4.*ALPHT))*(LOG(GRE1)-1.)
    COMP3 = 0.5*RT*RT*LOG(GRE1)
37  IF(BETT)32,32,36
32  COMP2 = 0.
    GO TO 38
36  COMP2 = (BETT/(4.*ALPHT))*(LOG(BETT)-1.)
38  RIGH1 = COEF1*(COMP1-COMP2-COMP3)
    COEF2 = 2.*F*STRO/3.
    EPSIT = SQRT(ALPHT*RT*RT*RT*RT+BETT*RT*RT+GAMT)
17  COMP4 = (7.*A1*EPSIT)/(2.*ALPHT)
    BALL1 = (BETT/(2.*ZEKE))+ZEKE*RT*RT+EPSIT
    IF(BALL1)6,6,7
6   GRE2 = 0.
    GO TO 8
7   GRE2 = LOG(BALL1)
8   COMP5 = (7.*A1*BETT/(4.*ALPHT**1.5))*GRE2
    COMP6 = (7.*A1*BILL)/(2.*ALPHT)
    BALL2 = (BETT/(2.*ZEKE))+BILL
    IF(BALL2)19,19,21
19  GRE3 = 0.
    GO TO 25
21  GRE3 = LOG(BALL2)
25  GRE4 = BETT/(4.*ALPHT**1.5)
```

FIG. 21 (CONTINUED)

```

COMP7 = GRE4*GRE3*7.*A1
GRE5 = 9.*A2*HC*HC+3.*A3
COMP8 = (GRE5/(2.*ZEKE))*GRE2
COMP9 = (GRE5/(2.*ZEKE))*GRE3
RIGH2 = COEF2*(COMP4-COMP5-COMP6+COMP7)+COEF2*(COMP8-COMP9)
SAM1 = F*STRO*HC*(3.*A2-4.*A1)
SAM2 = 3.*(BETT*BETT-4.*ALPHT*GAMT)
COEF3 = SAM1/SAM2
GRE6 = BETT*BETTP-2.*ALPHT*GAMTP
ELEM1 = (GRE6/(2.*ALPHT))*EPSIT
ELEM2 = GRE6*GRE4*GRE2
ELEM3 = GRE6*BILL/(2.*ALPHT)
ELEM4 = GRE6*GRE4*GRE3
GRE7 = BETT*GAMTP-2.*GAMT*BETTP
ELEM5 = (GRE7/(2.*ZEKE))*GRE3
ELEM6 = (GRE7/(2.*ZEKE))*GRE2
ELEM7 = ((GRE6*RT*RT-GRE7)/EPSIT)*0.5*RT*RT
RIGHA = ELEM1-ELEM2-ELEM3+ELEM4
RIGHB = ELEM5-ELEM6+ELEM7
RIGH3 = COEF3*(RIGHA+RIGHB)
RIGH4 = 0.25*F*B*RT*RT*RT*RT*(4.*A1+A2)
COEF5 = 0.5*F*RT*RT
TERM1 = (2./3.)*A1*B*RT*RT
TERM2 = A2*B*RT*RT
TERM3 = 6.*A2*B*HC*HC
TERM4 = 2.*A3*B
PT = RT*RING*(A1*RT*RT+3.*A2*HC*HC+A3)
PT1 = (RT-RO)*RING
PT = 0.5*(PT+PT1)
RIGH5 = COEF5*(TERM1-TERM2+TERM3+TERM4+PT)
SIDER = RIGH1-RIGH2+RIGH3-RIGH4-RIGH5
ZEK2 = SQRT(ZEKE)
BIL2 = SQRT(BILL)
BALL3 = (BIL2+RT*ZEK2)/(BIL2-RT*ZEK2)
IF(BALL3)26,26,27
26 BALL4 = 0.
GO TO 28
27 BALL4 = LOG(BALL3)
28 R = 0.-RT/10.
BOY3 = (GAMT/(ALPHT*ALPHT*ALPHT))*0.25
18 R = R + RT/10.

```

FIG. 21 (CONTINUED)

```

SHEA1 = (2./3.)*B*(3.*A2-4.*A1)*R*HT
EPSI = SQRT(ALPHT*R*R*R*R+BETT*R*R+GAMT)
SHEA2 = (2./3.)*STRO*(3.*A2-4.*A1)*R*HT/EPSI
TAUNO = (1./2.)*STRO+(1./2.)*B*EPSI
TAURZ = SHEA1+SHEA2
IF(RT-R)24,20,20
20  TAUNO = ABS(TAUNO)
    TAURZ = ABS(TAURZ)
    IF(TAUNO-TAURZ)23,23,22
22  GO TO 18
23  RA = R
    GO TO 34
24  BOY1 = (2./3.)*STRO*(3.*A2-4.*A1)*HC
    BOY2 = RT/ZEKE
    BOY4 = 0.5*BOY3*BALL4
    BOY5 = BOY1*(BOY2-BOY4)
    BOY6 = (2./9.)*B*HC*RT*RT*RT
    BOY7 = (SIDER-BOY5)/BOY6
    A21 = (4.*A1+BOY7)/3.
    GO TO 44
34  GIRL1 = (2./3.)*STRO*(3.*A2-4.*A1)*HC
    GIRL3 = GIRL1*(RA/ZEKE-BOY3*0.5*BALL4)
    GIRL4 = 0.25*STRO*(RT*RT-RA*RA)
    GIRL5 = ((0.5*B*GRE1)/(8.*ALPHT))*EPSIT
    GRE8 = (4.*ALPHT*GAMT-BETT*BETT)/(16.*ALPHT**1.5)
    BALL5 = 2.*ALPHT*RT*RT+BETT+2.*ZEKE*EPSIT
    IF(BALL5)29,29,30
29  BALL6 = 0.
    GO TO 51
30  BALL6 = LOG(BALL5)
51  GIRL6 = 0.5*B*GRE8*BALL6
    CAR1 = 2.*ALPHT*RA*RA+BETT
    CAR2 = SQRT(ALPHT*RA*RA*RA*RA+BETT*RA*RA+GAMT)
    GIRL7 = 0.5*B*CAR1*CAR2/(8.*ALPHT)
    BALL7 = CAR1+2.*ZEKE*CAR2
    IF(BALL7)52,52,53
52  BALL8 = 0.
    GO TO 55
53  BALL8 = LOG(BALL7)
55  GIRL8 = 0.5*B*GRE8*BALL8
    SIDEL = GIRL3+GIRL4+GIRL5+GIRL6-GIRL7-GIRL8

```

FIG. 21 (CONTINUED)

```
CAR3 = (2./9.)*B*HC*RA*RA*RA
A21 = ((SIDER-SIDEL)/CAR3+4.*A1)/3.
44  A22 = ABS(A21)
    IF(A22+A21)1,46,45
46  A23 = ABS(A2)
    IF(A23+A2)1,61,62
61  A24 = ABS(A21-A2)
63  IF(A24/ABS(A2)-0.01)60,60,65
65  A34(L) = A24
    IF(L-2)64,64,66
66  IF(A34(L)-A34(L-2))64,9,9
64  IF(M-10)40,40,49
40  A2 = 0.5*(A2+A21)
    PRINT, A2, A21
    L = L+1
    GO TO 11
49  IF(MAN-20)86,86,87
86  A2 = 0.25*(3.*A2+A21)
    PRINT, A2, A21
    L = L+1
    GO TO 11
87  A2 = 0.1*(9.*A2+A21)
    PRINT, A2, A21
    L = L+1
    GO TO 11
62  A24 = ABS(A21+A2)
    GO TO 63
45  A23 = ABS(A2)
    IF(A23+A2)1,62,61
60  RSC01 = (STRO/(3.*ZEKE))*(2.*A1-3.*A2)
    NAN = NAN+1
    C = 0.
    DO 83 I=1,5
    ARU(I) = 2.*ALPHT*RT*RT*C*C+BETT
    IF(ARU(I))81,81,82
81  SIM(I) = 0.
    GO TO 83
82  SIM(I) = LOG(ARU(I))
83  C = C+0.25
    RST1 = SIM(1)+4.*SIM(2)+2.*SIM(3)+4.*SIM(4)+SIM(5)
    RST2 = RT*SIM(5)
```

FIG. 21 (CONTINUED)

```

R51 = R5C01*((1./12.)*RT*R5T1-R5T2)
R5C02 = (2./3.)*STRO
R5T3 = 7.*A1*(RT/ZEKE-0.5*BOY3*BALL4)
BOY8 = 1./(2.*(ALPHT*GAMT)**0.25)
R5T4 = (9.*A2*HC*HC+3.*A3)*BOY8*BALL4
R52 = R5C02*(R5T3-R5T4)
R5C03 = COEF3/F
R5T5 = GRE6*R5T3/(7.*A1)
R5T6 = GRE7*BOY8*BALL4
R5T7 = RT*((GRE6*RT*RT-GRE7)/EPSIT)
R53 = R5C03*(R5T5+R5T6-R5T7)
R54 = (1./3.)*B*RT*RT*RT*(4.*A1+A2)
R5T8 = (2./3.)*A1*B*RT*RT-A2*B*RT*RT+2.*A3*B+PT
R55 = (R5T8+6.*A2*B*HC*HC)*RT
R56 = SIDER/(F*RT)
R5SIDE = R51-R52+R53-R54-R55-R56
DELT1 = 2.*((HO-HT)-((1.-UNU)/G)*R5SIDE)
DELT2 = ABS(DELT1)
IF(DELT2+DELT1)1,76,75
76 DELT3 = ABS(DELTA)
IF(DELT3+DELTA)1,71,72
71 DELT5 = DELT1-DELTA
DELT4 = ABS(DELT5)
73 IF(DELT4/DELTA-0.01)90,90,79
93 IF(DELT5)98,90,99
98 DELTA = DELTA+SAM
CUP = 0.25*CUP
GO TO 79
99 DELTA = DELTA-SAM
CUP = 0.25*CUP
GO TO 79
79 PRINT, DELTA, A2, A24, CUP, DELT5
PRINT, A1, A2, A3, A24
PRINT, RC, RT, HC, HT
IF(DELT5)96,90,97
96 SAM = CUP*DELTA
Y = Y+1.
IF(X)1,84,88
84 DELTA = DELTA-SAM
PRINT, DELTA
GO TO 10

```

FIG. 21 (CONTINUED)

```
88  CUP = 0.5*CUP
    SAM = CUP*DELTA
    GO TO 84
97  SAM = CUP*DELTA
    X = X+1.
    IF(Y)1,89,77
89  DELTA = DELTA+SAM
    PRINT, DELTA
    GO TO 10
77  CUP = 0.5*CUP
    SAM = CUP*DELTA
    GO TO 89
72  DELT5 = DELT1+DELTA
    DELT4 = ABS(DELT5)
    GO TO 73
75  DELT3 = ABS(DELTA)
    IF(DELT3+DELTA)1,72,71
90  PUNCH, A1, A2, A3, A24
    PUNCH, DELTA, PC, DELT4, F1
    PUNCH, ALPHT, BETT, GAMT
    PUNCH, RC, RT, HC, HT
    IF(1.+DIF1*10.-F1)92,92,5
92  PUNCH, RO, HO, STRO, B
    PUNCH, UNU, G
    PUNCH, F, DIF1, RING
    GO TO 1
    END
```

FIG. 21 (CONTINUED)

the assumed cylindrical expansion of the wafer. The two values are used, as stated above, to determine the remaining three parameters. With this information, a new value of  $a_2$  is computed from equation (53). Note here that a check is made to assure that the shearing stress existing at the top surface of the wafer does not exceed the shear strength  $\tau_0$  of the wafer material. The computed and original values of  $a_2$  are compared, and a new selection of  $a_2$  is made and the computing starts again. This iteration scheme is repeated until such time that the computed and original values differ by less than 1%. Once this result has been accomplished, equation (57) is employed for the calculation of a new value of the wafer centerline deflection,  $\Delta$ . If the value differs by more than 1% from the value used in its calculation, then the entire procedure listed above is repeated again, with a new selection for  $\Delta$ , until the results are within the 1% margin. Fortunately, the ability to determine an approximate value for  $\Delta$  at the outset, appreciably shortens the iteration process.

After all parameters have been computed within the indicated margin of error, the results are punched in card form, and the machine advances to the next load level, as indicated by an appropriate increase in the radius ratio, and commences to compute a new set of parameters. This procedure is continued, at equal increments, until the wafer achieves a 32% expansion, or up to the load limit of the containing ring; if one is used. The time required for a complete evaluation

of the five parameter, at eight increments of radial strain, on the IFM 1620 digital computer, is  $3\frac{1}{2}$  to 4 hours. The long computer times involved suggested that a series of print-out statements be inserted in the program to keep the operator informed of the machine progress. In the solution of those problems where a containing ring was involved, a pair of accept statements, with a means for returning to them at will, were also placed in the program. The reason for this is that a small change in the assumed parameters ( $a_2$  and  $\Delta$ ) caused very erratic changes in their computed values; hence, the method previously used in the unconfined case for selecting new values did not provide the necessary convergence. The accept statements permitted the operator to insert new data as deemed necessary. After the desired results were obtained, the selection pattern became apparent; however, the purpose of this program is not to find an easier approach for obtaining the same solution over again, but rather to establish a method for determining the unknown parameters under any given set of conditions.

With the displacement coefficients, constraining pressure, and centerline deflection now known, the coefficients  $\alpha_1$ ,  $\beta_1$ , and  $\gamma_1$ , and their derivatives, can be found from an application of equations (36) and (37), respectively. This information is sufficient for finding the applied compressive force as defined in equation (43). The computer program used in the evaluation of (43) is shown in Figure 22 and is

```

C C
C DAVIS, ROBERT, APPLIED FORCE VERSUS RADIUS RATIO
  DIMENSION A1(30), A2(30), A3(30)
  DIMENSION DELTA(30), PC(30), F1(30)
1  READ, RO, HO, STRO, B
  READ, UNU, G
  READ, F, RING, STRAC
  DO 4 I=1,8
  READ, A1(I), A2(I), A3(I)
4  READ, DELTA(I), PC(I), F1(I)
  DO 40 I=1,8
  ALPHC = (52./3.)*A1(I)*A1(I)
  BETC = 16.*A1(I)*A3(I)
  GAMC = 4.*A3(I)*A3(I)
  RC = F1(I)*RO
  BAB1 = 2.*ALPHC*RC*RC+BETC
  EPSIC = SQRT(ALPHC*RC*RC*RC*RC+BETC*RC*RC+GAMC)
  ZEKE = SQRT(ALPHC)
  BILL = SQRT(GAMC)
  BAB2 = (BETC/(2.*ZEKE))+ZEKE*RC*RC
  COEF1 = (2.*3.14159/(3.*ZEKE))*STRO*(2.*A1(I)-3.*A2(I))
  IF(BETC)8,8,7
8  RIGH2 = 0.
  GO TO 9
7  RIGH2 = (BETC/(4.*ALPHC))*(LOG(BETC)-1.)
9  IF(BAB1)10,10,11
10 RIGH1 = 0.
  RIGH3 = 0.
  GO TO 12
11 RIGH1 = (BAB1/(4.*ALPHC))*(LOG(BAB1)-1.)
  RIGH3 = (0.5*RC*RC)*LOG(BAB1)
12 TERM1 = COEF1*(RIGH1-RIGH2-RIGH3)
  TERM2 = (0.5*3.14159*B*RC*RC*RC*RC)*(4.*A1(I)+A2(I))
  COEF2 = (4./3.)*3.14159*STRO
  RIGH4 = (7.*A1(I)*EPSIC)/(2.*ALPHC)
  IF(BAB2+EPSIC)14,14,15
14 BAB3 = 0.
  GO TO 16
15 BAB3 = LOG(BAB2+EPSIC)
16 BAB4 = BETC/(4.*ALPHC**1.5)
  RIGH5 = 7.*A1(I)*BAB4*BAB3

```

FIG. 22 COMPUTER PROGRAM FOR EVALUATING APPLIED FORCE ON WAFER

```

RIGH6 = 7.*A1(I)*BILL/(2.*ALPHC)
IF((BETC/(2.*ZEKE))+BILL)17,17,18
17 BAB5 = 0.
GO TO 19
18 BAB5 = LOG(BETC/(2.*ZEKE)+BILL)
19 RIGH7 = 7.*A1(I)*BAB4*BAB5
RIGH8 = (3.*A3(I)*BAB3)/(2.*ZEKE)
RIGH9 = (3.*A3(I)*BAB5)/(2.*ZEKE)
TERM3 = COEF2*(RIGH4-RIGH5-RIGH6+RIGH7+RIGH8-RIGH9)
BLAS = ((2./3.)*A1(I)-A2(I))*B*RC*RC+2.*A3(I)*B+PC(I)
TERM4 = (3.14159*RC*RC)*BLAS
FORCE = TERM1-TERM2-TERM3-TERM4
STRA = FORCE/(3.14159*RC*RC*STRO)
ESTO = STRAC*PC(I)
PUNCH, STRA, F1(I), RC
40 PUNCH, FORCE, ESTO, PC(I)
PUNCH, RO, HO, STRO, B
PUNCH, UNU, G
PUNCH, F, RING, STRAC
GO TO 1
END
```

FIG. 22 (CONTINUED)

written such that the output from the coefficients program is directly adapted for input data. The output of the force program is in terms of the applied force and the radius ratio, or containing ring strain  $\epsilon_{\theta\theta}$ ; if the wafer is confined. The data obtained from the coefficients program is also used in Figure 23, which is the required computer program for determining the normal and shearing stresses as given in equations (38), (39), (40), and (41). The stress distributions are determined for two distinct values of radial deformation in order to illustrate the effect of increased load on the stress gradients. The axial variations of the stresses are shown by comparing the results obtained at the mid-meridian plane ( $Z=0$ ) with those at the top surface. Since the pressure is defined herein as the average of the orthogonal stress state at a point, it is recorded concurrently with the documenting of the normal stresses.

In order to illustrate more clearly the operation of the computer programs just described, the information entered and received in the evaluation of the compression of an unconfined 303 stainless steel wafer is shown in Figures 24, 25, and 26. The interpretation of the location and meaning of the input and output data is best described by referring to the appropriate written program, and cross examining the "read" and "punch" statements, respectively. The output of Figure 24 is used in computing applied force in Figure 25, and the desired stress distributions in Figure 26. The results of Figures 25 and 26 were employed in the construction of

```

C C
C DAVIS, ROBERT, GENERAL STRESS DISTRIBUTION IN SOLID WAFERS
  DIMENSION A1(30), A2(30), A3(30)
  DIMENSION DELTA(30), PC(30), F1(30)
1  READ, RO, HO, STRO, B
  READ, UNU, G
  READ, F, RING, STRAC
  DO 4 I=1,2
  READ, A1(I), A2(I), A3(I)
4  READ, DELTA(I), PC(I), F1(I)
  DO 40 I=1,2
  HC = HO-DELTA(I)/2.
  Z = 0.-HC
6  Z = Z+HC
  RC = RO*F1(I)
  R1 = RC
7  RA1 = RO+A1(I)*R1*R1*R1
  R11 = RA1+3.*A2(I)*Z*Z*R1+A3(I)*R1
  R12 = ABS(R11-R1)
  IF(R12-0.001)9,9,10
10 R1 = (R11+R1)/2.
  GO TO 7
9  R = 0.-R1/10.
8  R = R+R1/10.
  ALPHA = (52./3.)*A1(I)*A1(I)
  BLU1 = 12.*A1(I)*A2(I)+9.*A2(I)*A2(I)+16.*A1(I)*A1(I)
  BETA = (4./3.)*(BLU1*Z*Z+12.*A1(I)*A3(I))
  BETAP = (8./3.)*BLU1*Z
  BLU2 = 3.*A2(I)*Z*Z+A3(I)
  GAMA = 4.*BLU2*BLU2
  GAMAP = 48.*A2(I)*BLU2*Z
  EPSI = SQRT(ALPHA*R*R*R*R+BETA*R*R+GAMA)
  EPSI1 = SQRT(ALPHA*R1*R1*R1*R1+BETA*R1*R1+GAMA)
  GIRL1 = 2.*ALPHA*R*R+BETA
  GIRL2 = 2.*ALPHA*R1*R1+BETA
  ZEKE = SQRT(ALPHA)
  DOG1 = GIRL1+2.*ZEKE*EPSI
  DOG2 = GIRL2+2.*ZEKE*EPSI1
  COEF1 = STRO*(2.*A1(I)-3.*A2(I))/(3.*ZEKE)
  DOG3 = DOG1/DOG2
  IF(DOG3)12,12,13

```

FIG. 23 COMPUTER PROGRAM FOR DETERMINING STRESS DISTRIBUTION IN WAFER

```

12  TERM1 = 0.
    GO TO 14
13  TERM1 = COEF1*LOG(DOG3)
14  COW1 = BETA*BETAP-2.*ALPHA*GAMAP
    COW2 = BETA*GAMAP-2.*GAMA*BETAP
    RIGH1 = (COW1*R*R-COW2)/EPSI
    RIGH2 = (COW1*R1*R1-COW2)/EPSI1
    PIG1 = BETA*BETA-4.*ALPHA*GAMA
    IF(PIG1)16,15,16
15  TERM2 = 0.
    GO TO 17
16  COEF2 = STRO*Z*(3.*A2(I)-4.*A1(I))/(3.*PIG1)
    TERM2 = COEF2*(RIGH1-RIGH2)
17  P1 = R1*RING*(A1(I)*R1*R1+3.*A2(I)*Z*Z+A3(I))
    TERM3 = (B/3.)*(2.*A1(I)-3.*A2(I))*(R*R-R1*R1)
    STRR = TERM1+TERM2+TERM3-P1
    TERM4 = ((4./3.)*A1(I)*STRO*R*R)/EPSI
    TERM5 = (2./3.)*A1(I)*B*(R*R+R1*R1)
    TERM6 = A2(I)*B*(R*R-R1*R1)
    STRT = TERM1+TERM2-TERM4-TERM5-TERM6-P1
    PIG2 = 7.*A1(I)*R*R+9.*A2(I)*Z*Z+3.*A3(I)
    TERM7 = ((2./3.)*STRO*PIG2)/EPSI
    TERM8 = (2./3.)*A1(I)*B*(6.*R*R+R1*R1)
    TERM9 = 6.*A2(I)*B*Z*Z
    STRZ = TERM1+TERM2-TERM7-TERM8-TERM6-TERM9-2.*A3(I)*B-P1
    PRESS = (1./3.)*(STRR+STRT+STRZ)
    PIG3 = (2./3.)*R*Z*(3.*A2(I)-4.*A1(I))
    TAURZ = B*PIG3+(STRO*PIG3)/EPSI
    TAUNO = (1./2.)*STRO+(1./2.)*B*EPSI
    TAURZ = ABS(TAURZ)
    TAUNO = ABS(TAUNO)
    IF(TAUNO-TAURZ)31,33,33
31  TAURZ = TAUNO
33  PUNCH, STRR, STRT, STRZ, R
    PUNCH, PRESS, TAURZ
    IF(R-R1)8,37,37
37  PUNCH, R1, P1, Z, HC
    IF(Z-HC)6,40,40
40  CONTINUE
    PUNCH, RO, HO, STRO, B
    PUNCH, UNU, G
    PUNCH, F, RING, STRAC
    GO TO 1
    END

```

FIG. 23 (CONTINUED)

0.750 0.232 38000. 340000.  
 0.30 12500000.  
 0.040 0. -0.010 0.04

-1.0123E-02	-6.2075E-02	8.0716E-02	8.3430E-05
6.2767E-02	0.0000	3.4849E-04	1.0800
1.7762E-03	-1.0719E-02	2.1445E-02	
8.1000E-01	8.0456E-01	2.0062E-01	2.0466E-01
-1.0747E-02	-6.9388E-02	1.1473E-01	4.9647E-04
8.5061E-02	0.0000	3.0956E-04	1.1200
2.0021E-03	-1.7137E-02	4.6013E-02	
8.4000E-01	8.3400E-01	1.8947E-01	1.9343E-01
-1.3557E-02	-8.8735E-02	1.4819E-01	8.2442E-04
1.0449E-01	0.0000	1.0152E-03	1.1600
3.1857E-03	-2.8343E-02	7.7942E-02	
8.7000E-01	8.6272E-01	1.7975E-01	1.8498E-01
-1.4745E-02	-1.0093E-01	1.7861E-01	5.6521E-04
1.2062E-01	0.0000	2.8540E-04	1.2000
3.7687E-03	-3.7697E-02	1.1517E-01	
9.0000E-01	8.9176E-01	1.7169E-01	1.7732E-01
-1.6893E-02	-1.1649E-01	2.0816E-01	3.4029E-04
1.3492E-01	0.0000	6.4619E-04	1.2400
4.9464E-03	-5.0837E-02	1.5792E-01	
9.3000E-01	9.2056E-01	1.6454E-01	1.7096E-01
-1.8855E-02	-1.3176E-01	2.3613E-01	4.1257E-04
1.4742E-01	0.0000	6.9421E-04	1.2800
6.1621E-03	-6.4828E-02	2.0471E-01	
9.6000E-01	9.4962E-01	1.5829E-01	1.6546E-01
-1.9038E-02	-1.4052E-01	2.6108E-01	3.8408E-04
1.5785E-01	0.0000	1.1836E-03	1.3200
6.2824E-03	-7.2792E-02	2.5242E-01	
9.9000E-01	9.7887E-01	1.5308E-01	1.6034E-01
-2.2936E-02	-1.6226E-01	2.8857E-01	3.8029E-04
1.6847E-01	0.0000	1.0410E-03	1.3600
9.1181E-03	-9.7452E-02	3.0900E-01	
1.0200	1.0075	1.4777E-01	1.5657E-01

FIG. 24 SAMPLE INPUT-OUTPUT DATA  
 FOR COEFFICIENTS PROGRAM.  
 303 STAINLESS STEEL WAFER.  
 CASE I-A

```

0.750 0.232 38000. 340000.
*.30 1250000.
*.04 0. 0.
-1.0123E-02 -6.2075E-02 8.0716E-02
6.2767E-02 0.0000 1.0800
-1.0747E-02 -6.9388E-02 1.1473E-01
8.5061E-02 0.0000 1.1200
-1.3557E-02 -8.8735E-02 1.4819E-01
1.0449E-01 0.0000 1.1600
-1.4745E-02 -1.0093E-01 1.7861E-01
1.2062E-01 0.0000 1.2000
-1.6893E-02 -1.1649E-01 2.0816E-01
1.3492E-01 0.0000 1.2400
-1.8855E-02 -1.3176E-01 2.3613E-01
1.4742E-01 0.0000 1.2800
-1.9038E-02 -1.4052E-01 2.6108E-01
1.5785E-01 0.0000 1.3200
-2.2936E-02 -1.6226E-01 2.8857E-01
1.6847E-01 0.0000 1.3600

```

```

-2.4522 1.0800 8.1000E-01
-1.9207E+05 0.0000 0.0000
-3.0788 1.1200 8.4000E-01
-2.5934E+05 0.0000 0.0000
-3.6944 1.1600 8.7000E-01
-3.3382E+05 0.0000 0.0000
-4.2644 1.2000 9.0000E-01
-4.1236E+05 0.0000 0.0000
-4.8138 1.2400 9.3000E-01
-4.9704E+05 0.0000 0.0000
-5.3401 1.2800 9.6000E-01
-5.8753E+05 0.0000 0.0000
-5.8294 1.3200 9.9000E-01
-6.8206E+05 0.0000 0.0000
-6.3338 1.3600 1.0200
-7.8667E+05 0.0000 0.0000
7.5000E-01 2.3200E-01 3.8000E+04 3.4000E+05
3.0000E-01 1.2500E+06
4.0000E-02 0.0000 0.0000

```

FIG. 25 SAMPLE INPUT-OUTPUT DATA  
FOR APPLIED FORCE PROGRAM.  
INFORMATION USED IN FIG. 6

```

0.750 0.232 38000. 340000.
.30 12500000.
.04 0. 0.
-1.3557E-02 -8.8735E-02 1.4819E-01
1.0449E-01 0.0000 1.1600
-1.9038E-02 -1.4052E-01 2.6108E-01
1.5785E-01 0.0000 1.3200

-2.8832E+04 -2.8832E+04 -1.6760E+05 0.0000
-7.5088E+04 0.0000
-2.8550E+04 -2.8485E+04 -1.6715E+05 8.7000E-02
-7.4727E+04 0.0000
-2.7701E+04 -2.7445E+04 -1.6578E+05 1.7400E-01
-7.3643E+04 0.0000
-2.6286E+04 -2.5707E+04 -1.6351E+05 2.6100E-01
-7.1834E+04 0.0000
-2.4299E+04 -2.3268E+04 -1.6032E+05 3.4800E-01
-6.9295E+04 0.0000
-2.1737E+04 -2.0120E+04 -1.5621E+05 4.3500E-01
-6.6021E+04 0.0000
-1.8593E+04 -1.6253E+04 -1.5116E+05 5.2200E-01
-6.2003E+04 0.0000
-1.4858E+04 -1.1657E+04 -1.4518E+05 6.0900E-01
-5.7232E+04 0.0000
-1.0523E+04 -6.3146E+03 -1.3824E+05 6.9600E-01
-5.1693E+04 0.0000
-5.5756E+03 -2.0828E+02 -1.3033E+05 7.8300E-01
-4.5372E+04 0.0000
1.6097E-02 6.6858E+03 -1.2143E+05 8.7000E-01
-3.8248E+04 0.0000
8.7000E-01 0.0000 0.0000 1.7976E-01

-2.9736E+04 -2.9736E+04 -1.6266E+05 0.0000
-7.4043E+04 0.0000
-2.9445E+04 -2.9381E+04 -1.6219E+05 8.6239E-02
-7.3673E+04 1.0434E+03
-2.8571E+04 -2.8314E+04 -1.6080E+05 1.7248E-01

```

FIG. 26 SAMPLE INPUT-OUTPUT DATA FOR  
STRESS DISTRIBUTION PROGRAM.  
INFORMATION USED IN FIG. 7

-7.2562E+04	2.0893E+03		
-2.7112E+04	-2.6534E+04	-1.5848E+05	2.5872E-01
-7.0707E+04	3.1401E+03		
-2.5064E+04	-2.4034E+04	-1.5522E+05	3.4496E-01
-6.8104E+04	4.1984E+03		
-2.2423E+04	-2.0806E+04	-1.5101E+05	4.3120E-01
-6.4746E+04	5.2671E+03		
-1.9180E+04	-1.6842E+04	-1.4585E+05	5.1744E-01
-6.0624E+04	6.3491E+03		
-8.5328E+04	-1.2129E+04	-1.3972E+05	6.0368E-01
-5.5727E+04	7.4480E+03		
-1.0857E+04	-6.6507E+03	-1.3261E+05	6.8991E-01
-5.0040E+04	8.5675E+03		
-5.7522E+03	-3.8835E+02	-1.2450E+05	7.7615E-01
-4.3546E+04	9.7120E+03		
1.4200E-02	6.6807E+03	-1.1535E+05	8.6239E-01
-3.6224E+04	1.0887E+04		
6.4175E+03	1.4584E+04	-1.0515E+05	9.4863E-01
-2.8050E+04	1.2097E+04		
8.6239E-01	0.0000	1.7976E-01	1.7976E-01
-5.2432E+04	-5.2432E+04	-2.6797E+05	0.0000
-1.2428E+05	0.0000		
-1.1915E+04	-5.1812E+04	-2.6714E+05	9.9000E-02
-1.2362E+05	0.0000		
-5.0363E+04	-4.9951E+04	-2.6468E+05	1.9800E-01
-1.2166E+05	0.0000		
-4.7773E+04	-4.6846E+04	-2.6056E+05	2.9700E-01
-1.1839E+05	0.0000		
-4.4141E+04	-4.2491E+04	-2.5479E+05	3.9600E-01
-1.1381E+05	0.0000		
-3.9462E+04	-3.6878E+04	-2.4736E+05	4.9500E-01
-1.0790E+05	0.0000		
-3.3728E+04	-2.9995E+04	-2.3826E+05	5.9400E-01
-1.0066E+05	0.0000		
-2.6928E+04	-2.1830E+04	-2.2747E+05	6.9300E-01
-9.2076E+04	0.0000		
-8.9051E+04	-1.2363E+04	-2.1498E+05	7.9200E-01
-8.2133E+04	0.0000		
-1.0081E+04	-1.5724E+03	-2.0078E+05	8.9100E-01

FIG. 26 (CONTINUED)

+7.0811E+04	0.0000		
1.8385E-02	1.0569E+04	-1.8483E+05	9.9000E-01
-5.8087E+04	0.0000		
9.9000E-01	0.0000	0.0000	1.5308E-01
-5.2272E+04	-5.2272E+04	-2.6109E+05	0.0000
-1.2188E+05	0.0000		
-5.1757E+04	-5.1655E+04	-2.6027E+05	9.7877E-02
-1.2123E+05	1.4343E+03		
-5.0209E+04	-4.9804E+04	-2.5782E+05	1.9575E-01
-1.1928E+05	2.8708E+03		
-4.7627E+04	-4.6715E+04	-2.5373E+05	2.9363E-01
-1.1602E+05	4.3117E+03		
-4.4006E+04	-4.2382E+04	-2.4800E+05	3.9151E-01
1.1146E+05	5.7594E+03		
-3.9341E+04	-3.6798E+04	-2.4061E+05	4.8938E-01
-1.0558E+05	7.2163E+03		
-3.3624E+04	-2.9951E+04	-2.3156E+05	5.8726E-01
9.8379E+04	8.6853E+03		
-2.6844E+04	-2.1827E+04	-2.2084E+05	6.8514E-01
8.9837E+04	1.0169E+04		
-1.8991E+04	-1.2409E+04	-2.0842E+05	7.8301E-01
-7.9940E+04	1.1672E+04		
-1.0049E+04	-1.6766E+03	-1.9428E+05	8.8089E-01
-6.8670E+04	1.3197E+04		
1.8385E-02	1.0397E+04	-1.7841E+05	9.7877E-01
-5.6004E+04	1.4750E+04		
9.7877E-01	0.0000	1.5308E-01	1.5308E-01
7.5000E-01	2.3200E-01	3.8000E+04	3.4000E+05
3.0000E-01	1.2500E+06		
4.0000E-02	0.0000	0.0000	

FIG. 26 (CONTINUED)

Figures 6 and 7, respectively.

The method of solution for a hollow wafer was described in an earlier section, and its discussion was resumed in the section "Future Work". The merits of having this solution have been pointed out, and a continuing effort will be made to carry it to completion. The program for use in computing the displacement coefficients is shown in Figure 27, and is completely analogous to that contained in Figure 21. The exception being that the added length of the boundary condition equations creates an overflow in the memory storage of the IBM 1620 computer. With an appropriate change in the input-output statements of the current program, it can be run on the IBM 7090, and it is the present intent to do so in the near future. The required stress and force programs have not been shown since their operation depends upon the availability of the output data from the coefficients program.

```

C C
C DAVIS, R. TRIAL AND ERROR SOLUTION FOR COEFFICIENTS
C WAFER WITH HOLE ALONG AXIS
  DIMENSION A34(4)
1  READ, RO, RIO, HO, STRO, B
  READ, UNU, G
  READ, DIF1, RING, F
  READ, VO, VO1, VO2
  READ, C1, C2, C3
  READ, AK1, AK2, AK3
  F1 = 1.
5  F1 = F1+2.*DIF1
  CUP = 0.03
  NAN = 1
  SAM = 0.
  RIM = RIO
  RIT = RIO
  RIC = RIO
  X = 0.
  Y = 0.
  RC = F1*RO
  DELTA = (HO*(1.-1./(F1*F1)))*2.
  HC = HO-DELTA/2.
  PRINT, DELTA
  HT = HC
10 A2 = -0.010
  L = 1
  M = 0
  MAN = 0
  HC1 = 2.*HO-DELTA
11 A3 = DELTA/(2.*HC1)-(A2*(HC1*HC1))/4.
  M = M+1
  MAN = MAN+1
12 A1 = ((RC-RO)/(RC*RC*RC))-(A3/(RC*RC))
15 RIT3 = A1*RIT*RIT
  RIT4 = 3.*A2*HC*HC+A3
  RIT1 = RIO-(RIT3+RIT4)*RIT
  RIT2 = ABS(RIT1-RIT)
  IF(RIT2-0.001)20,20,17
17 RIT = 0.25*(3.*RIT+RIT1)
  GO TO 15

```

FIG. 27 COMPUTER PROGRAM FOR DETERMINING UNKNOWN DISPLACEMENT COEFFICIENTS. HOLLOW WAFER

```

20  RIT1 = 1./((1.-2.*(RIT/RC)*(RIT/RC))
    RIT2 = (2.*(RC-RO)*RIT*RIT)/(RC*RC*RC)
    RIT3 = DELTA/(4.*HC)-A2*HC*HC
    RIT4 = RIT1*(RIT3-RIT2)
    RIT5 = ABS(RIT4-A3)
    IF(ABS(RIT5/RIT4)-0.01)25,25,22
22  A3 = 0.25*(3.*A3+RIT4)
    GO TO 12
25  PC = (RC*RING)*(A1*RC*RC+A3)
    ALPHT = (52./3.)*A1*A1
    HAMT = 12.*A1*A2+9.*A2*A2+16.*A1*A1
    BETT = (4./3.)*(HAMT*HC*HC+12.*A1*A3)
    BETTP = (8./3.)*(HAMT*HC)
    GAMT = 4.*(3.*A2*HC*HC+A3)*(3.*A2*HC*HC+A3)
    GAMTP = 48.*A2*(3.*A2*HC*HC+A3)*HC
    RT = RC
30  RIT3 = A1*RT*RT
    RIT4 = 3.*A2*HT*HT+A3
    RIT1 = RO+(RIT3+RIT4)*RT
    RIT2 = ABS(RIT1-RT)
    IF(RIT2-0.001)35,35,31
31  RT = 0.25*(3.*RT+RIT1)
    GO TO 30
35  RIT3 = -2.*A2*HT*HT
    RIT4 = 4.*A1*RT*RT+2.*A3
    RIT1 = HO+(RIT3-RIT4)*HT
    RIT2 = ABS(RIT1-RT)
    IF(RIT2-0.001)41,41,37
37  HT = 0.25*(3.*HT+RIT1)
    GO TO 35
41  RIT3 = A1*RIC*RIC+A3
    RIT1 = RIO-RIT3*RIC
    RIT2 = ABS(RIT1-RIC)
    IF(RIT2-0.001)45,45,43
43  RIC = 0.25*(3.*RIC+RIT1)
    GO TO 41
45  RIT3 = A1*RIM*RIM
    RIT4 = 0.75*A2*HC*HC+A3
    RIT1 = RIO-(RIT3+RIT4)*RIM
    RIT2 = ABS(RIT1-RIM)
    PIC = 0.

```

FIG. 27 (CONTINUED)

```

IF(RIT2-0.001)50,50,48
48 RIM = 0.25*(3.*RIM+RIT1)
GO TO 45
50 CAV1 = RIT*RIT+RIC*RIC+4.*RIM*RIM
CAV2 = (AK1+AK2*PIC+AK3*PIC*PIC)*V01
CAV3 = (C1+C2*PIC+C3*PIC*PIC)*V02
PI1 = -((3.14159*HC/3.)*CAV1-V0)/(CAV2+CAV3)
ERR = (ABS(PI1-PIC))/PI1
IF(ABS(ERR)-0.01)52,52,51
51 PIC = 0.25*(3.*PIC+PI1)
GO TO 50
52 ZEKE = SQRT(ALPHT)
BILL = SQRT(GAMT)
ALPHC = ALPHT
BETC = 16.*A1*A3
GAMC = 4.*A3*A3
RIT1 = 2.*ALPHC*RIC*RIC+BETC
EPSIC = SQRT(ALPHC*RIC*RIC*RIC*RIC+BETC*RIC*RIC+GAMC)
EPSC = SQRT(ALPHC*RC*RC*RC*RC+BETC*RC*RC+GAMC)
ZEKEC = SQRT(ALPHC)
RIT2 = 2.*ALPHC*RC*RC+BETC
BOY21 = STRO*(2.*A1-3.*A2)/(3.*ZEKEC)
BOY22 = (RIT1+2.*ZEKEC*EPSIC)/(RIT2+2.*ZEKEC*EPSC)
IF(BOY22)53,53,54
53 BOY23 = 0.
GO TO 55
54 BOY23 = BOY21*LOG(BOY22)
55 BOY24 = B*(RIC*RIC-RC*RC)/3.
BOY25 = (PIC+BOY23-PC)/BOY24
A21 = (BOY25+2.*A1)/3.
A22 = ABS(A21)
IF(A22+A21)1,56,67
56 A23 = ABS(A2)
IF(A23+A2)1,57,66
57 A24 = ABS(A21-A2)
58 R = RIT-RT/10.
IF(A24/ABS(A2)-0.01)71,71,59
59 A34(L) = A24
IF(L-2)61,61,60
60 IF(A34(L)-A34(L-2))95,33,33
33 IF(NAN-1)1,96,93

```

FIG. 27 (CONTINUED)

```

95     L = L-1
61     IF(M-10)62,62,63
62     A2 = 0.5*(A2+A21)
        PRINT, A2, A21
        L = L+1
        GO TO 11
63     A2 = 0.25*(3.*A2+A21)
        PRINT, A2, A21
        L = L+1
        GO TO 11
66     A24 = ABS(A21+A2)
        GO TO 58
67     A23 = ABS(A2)
        IF(A23+A2)1,66,57
71     R = R+RT/10.
        SHEA1 = (2./3.)*B*(3.*A2-4.*A1)*R*HT
        EPSI = SQRT(ALPHT*R*R*R*R+BETT*R*R+GAMT)
        SHEA2 = (2./3.)*STRO*(3.*A2-4.*A1)*R*HT/EPSI
        TAUNO = 0.5*(STRO+B*EPSI)
        TAURZ = SHEA1+SHEA2
        IF(RT-R)75,72,72
72     TAUNO = ABS(TAUNO)
        TAURZ = ABS(TAURZ)
        IF(TAUNO-TAURZ)73,73,71
75     BOY1 = (2./9.)*B*((HC+HT)/2.)*(3.*A2-4.*A1)
        BOY2 = BOY1*(RT*RT*RT-RIT*RIT*RIT)
        BUG7 = 4.*ALPHT*GAMT-BETT*BETT
        IF(GAMT)14,14,13
13     BOY21 = GAMT**0.25
        GO TO 16
14     BOY21 = 0.
16     IF(ALPHT)19,19,18
18     BOY22 = ALPHT**0.25
        BUG8 = BUG7/(16.*ALPHT**1.5)
        GO TO 21
19     BOY22 = 0.
        BUG8 = 0.
21     BOY23 = (BOY21+RT*BOY22)/(BOY21-RT*BOY22)
        IF(GAMT/ALPHT)24,24,23
23     BOY24 = 0.5*(GAMT/(ALPHT*ALPHT*ALPHT))**0.25
        GO TO 26

```

FIG. 27 (CONTINUED)

```

24     BOY24 = 0.
26     IF(BOY23)28,28,27
27     BOY25 = RT/ZEKE-BOY24*LOG(BOY23)
        GO TO 29
28     BOY25 = RT/ZEKE
29     BOY3 = (2./3.)*STRO*((HC+HT)/2.)*(3.*A2-4.*A1)
        BOY26 = (BOY21+RIT*BOY22)/(BOY21-RIT*BOY22)
        IF(BOY26)38,38,36
36     BOY27 = -RIT/ZEKE+BOY24*LOG(BOY26)
        GO TO 39
38     BOY27 = RIT/ZEKE
39     BOY4 = BOY3*(BOY25+BOY27)
        SIDEL = BOY2+BOY4
        GO TO 80
73     RA = R
        GIRL1 = 0.25*STRO*(RT*RT-RA*RA)
        BOY1 = 2.*ALPHT*RT*RT+BETT
        EPST = SQRT(ALPHT*RT*RT*RT*RT+BETT*RT*RT+GAMT)
        BOY2 = BOY1*EPST/(8.*ALPHT)
        BOY3 = 2.*ZEKE*EPST+BOY1
        BOY4 = 2.*ALPHT*RA*RA+BETT
        EPSA = SQRT(ALPHT*RA*RA*RA*RA+BETT*RA*RA+GAMT)
        BOY5 = 2.*ZEKE*EPSA+BOY4
        IF(BOY3/BOY5)42,42,46
42     BOY6 = 0.
        GO TO 47
46     BOY6 = LOG(BOY3/BOY5)
47     BOY9 = BUG8*BOY6
        BOY10 = BOY4*EPSA/(8.*ALPHT)
        GIRL2 = 0.5*B*(BOY2+BOY9-BOY10)
        GUN1 = (2./9.)*B*((HC+HT)/2.)*(3.*A2-4.*A1)
        GIRL3 = GUN1*(RA*RA*RA-RIT*RIT*RIT)
        GUN4 = (BOY21+RA*BOY22)/(BOY21-RA*BOY22)
        IF(GUN4)82,82,83
82     GUN5 = 0.
        GO TO 84
83     GUN5 = LOG(GUN4)
84     GUN7 = RA/ZEKE-BOY24*GUN5
        GUN9 = (BOY21+RIT*BOY22)/(BOY21-RIT*BOY22)
        IF(GUN9)88,88,89
88     GUN10 = 0.

```

FIG. 27 (CONTINUED)

```

GO TO 2
89 GUN10 = LOG(GUN9)
2 GUN11 = -RIT/ZEKE+BOY24*GUN10
GUN12 = (2./3.)*STRO*((HC+HT)/2.)*(3.*A2-4.*A1)
GIRL4 = GUN12*(GUN7+GUN11)
SIDEL = GIRL1+GIRL2+GIRL3+GIRL4
80 COEF1 = (F*STRO/(3.*ZEKE))*(2.*A1-3.*A2)
RIT1 = 2.*ALPHT*RT*RT+BETT
IF(RIT1)34,34,32
32 A32 = LOG(RIT1)
RIT2 = (RIT1/(4.*ALPHT))*(A32-1.)
GO TO 40
34 RIT2 = 0.
A32 = 0.
40 RIT3 = 2.*ALPHT*RIT*RIT+BETT
IF(RIT3)65,65,64
64 A35 = LOG(RIT3)
RIT4 = (RIT3/(4.*ALPHT))*(A35-1.)
GO TO 68
65 RIT4 = 0.
A35 = 0.
68 A31 = 0.5*(RT*RT-RIT*RIT)*A32
BOY1 = COEF1*(RIT2-RIT4-A31)
COEF1 = 2.*STRO*F/3.
BOY21 = 7.*A1*EPST/(2.*ALPHT)
HT2 = (28.*A1*BETT/BUG7)*BUG8
HT3 = BETT/(2.*ZEKE)+ZEKE*RT*RT+EPST
IF(HT3)70,70,69
69 HT4 = LOG(HT3)
GO TO 74
70 HT4 = 0.
74 BOY22 = HT2*HT4
EPSIT = SQRT(ALPHT*RIT*RIT*RIT*RIT+BETT*RIT*RIT+GAMT)
BOY23 = (7.*A1/(2.*ALPHT))*EPSIT
A33 = BETT/(2.*ZEKE)+ZEKE*RIT*RIT+EPSIT
IF(A33)77,77,76
76 BOY24 = LOG(A33)
GO TO 78
77 BOY24 = 0.
78 BOY29 = HT2*BOY24
COEF2 = 9.*A2*((HC+HT)/2.)*((HC+HT)/2.)+3.*A3

```

FIG. 27 (CONTINUED)

```

BOY25 = (1./(2.*ZEKE))*HT4
BOY26 = (1./(2.*ZEKE))*BOY24
BOY27 = COEF2*(BOY25-BOY26)
BOY2 = COEF1*(BOY21-BOY22-BOY23+BOY29+BOY27)
COEF2 = (STRO*F*((HC+HT)/2.)*(3.*A2-4.*A1))/3.
COEF1 = COEF2/(BETT*BETT-4.*ALPHT*GAMT)
COEF2 = BETT*BETTP-2.*ALPHT*GAMTP
BOY21 = (1./(2.*ALPHT))*EPST
BOY23 = BOY22+(1./(2.*ALPHT))*EPSIT-BOY29
BOY24 = COEF2*(BOY21-BOY23)
COEF3 = BETT*GAMTP-2.*GAMT*BETTP
BOY21 = BOY25-BOY26
BOY23 = 0.5*(COEF2*RT*RT-COEF3)/EPST
BOY24 = BOY23*(RT*RT-RIT*RIT)
BOY3 = COEF1*(BOY24-COEF3*BOY21-BOY24)
BOY4 = B*F*(4.*A1+A2)*(RT*RT*RT*RT-RIT*RIT*RIT*RIT)/4.
BOY21 = 0.5*F*(B*RT*RT*((2./3.)*A1-A2))
PT = RING*(RT-RO)
BOY23 = 0.5*F*(6.*A2*B*(HC+HT)/2.+PT)
BOY24 = RT*RT-RIT*RIT
BOY5 = (BOY21+BOY23)*BOY24
BOY6 = -F*B*A3
SIDER = BOY1-BOY2+BOY3-BOY4-BOY5
A3 = -(SIDEL-SIDER)/(F*B)
BOY1 = (HC+HT)/2.
DELT1 = 4.*BOY1*(2.*A1*RIT*RIT+A2*BOY1*BOY1+A3)
DELT2 = ABS(DELT1)
IF(DELT2+DELT1)1,44,49
44  DELT3 = ABS(DELTA)
IF(DELT3+DELTA)1,81,85
81  DELT5 = DELT1-DELTA
DELT4 = ABS(DELT5)
3   IF(DELT4/DELTA-0.01)90,90,79
93  IF(DELT5)98,90,99
98  DELTA = DELTA+SAM
CUP = 0.25*CUP
GO TO 79
99  DELTA = DELTA-SAM
CUP = 0.25*CUP
79  PRINT, DELTA, A2, A24, CUP, DELT5
PRINT, A1, A2, A3, A24

```

FIG. 27 (CONTINUED)

```
PRINT, RC, RT, HC, HT
IF(DELT5)96,90,97
96 SAM = CUP*DELTA
   Y = Y+1.
   IF(X)1,7,8
7   DELTA = DELTA-SAM
   PRINT, DELTA
   GO TO 10
8   CUP = 0.25*CUP
   SAM = CUP*DELTA
   GO TO 7
97  SAM = CUP*DELTA
   X = X+1.
   IF(Y)1,9,6
9   DELTA = DELTA+SAM
   PRINT, DELTA
   GO TO 10
6   CUP = 0.25*CUP
   SAM = CUP*DELTA
   GO TO 9
85  DELT5 = DELT1+DELTA
   DELT4 = ABS(DELT5)
   GO TO 3
49  DELT3 = ABS(DELTA)
   IF(DELT3+DELTA)1,85,81
90  PUNCH, A1, A2, A3, A4
   PUNCH, DELTA, PC, DELT4, F1
   PUNCH, ALPHT, BETT, GAMT
   PUNCH, RC, RT, HC, HT
   PUNCH, EPSC, EPSIC, EPST, EPSIT
   IF(1.+DIF1*8.-F1)92,92,5
92  PUNCH, RO, HO, STRO, B
   PUNCH, UNU, G
   PUNCH, F, DIF1, RING
   GO TO 1
END
```

FIG. 27 (CONTINUED)

## REFERENCES

- (a) Stromberg, H., et al, Calibration of Bridgman Anvils, A Pressure Scale to 125 Kb. High-Pressure Measurement Symposium. New York. Butterworths. 1963
- (b) Roy, R., et.al, Contribution to Calibration of High-Pressure Systems from Studies in an Opposed-Anvil Apparatus. High-Pressure Measurement Symposium. New York. Butterworths. 1963
- (c) Tydings, J.E., and Giardini, A.A., A Study of Stress Homogeneity in Cylindrical Cavities at High Pressures. High-Pressure Measurement Symposium. New York. Butterworths. 1963
- (d) Zeitlin, A., Annotated Bibliography on High-Pressure Technology. ASME Research Committee on Pressure Technology. Washington. Butterworths. 1964
- (e) Jackson, J.W., and Waxman, M., An Analysis of Pressure and Stress Distribution Under Rigid Bridgman-Type Anvils. High-Pressure Measurement Symposium. New York. Butterworths. 1963
- (f) Mellor, P.B., and Johnson, W., Plasticity for Mechanical Engineers. New York. D. Van Nostrand. 1962

- (g) Nadai, A., Theory of Flow and Fracture of Solids.  
Vol. 2. New York. McGraw-Hill. 1963
- (h) Hill, R., The Mathematical Theory of Plasticity.  
New York. Oxford University Press. 1950
- (i) Carson, R.L., Compression of a Viscoplastic Disk.  
ASME Paper No. 63-WA-28. New York. 1963
- (j) Lippincott, E.R., and Duecker, H.C., Distribution  
of Pressure in an Opposed-Anvil, High-Pressure Cell.  
Pressure Technology Session, ASME Winter Annual  
Meeting. New York. Paper No. 64-WA/PT-15. 1964
- (k) Hoffman, O., and Sachs, G., Theory of Plasticity  
for Engineers. New York. McGraw-Hill. 1953
- (l) Jackson, J.W., and Davis, R.L., An Analysis of the  
Stress Distribution Under Elastically Deformable  
Bridgman-Type Pressure Anvils. Pressure Technology  
Session, ASME Winter Annual Meeting. New York.  
Paper No. 64-WA/PT-27. 1964
- (m) Wentorf, R.H., Jr., Modern Very High Pressure Tech-  
niques. Washington. Butterworths. 1962
- (n) Ludwig, P., Elemente der Technologischen Mechanik.  
Springer. Berlin

## SELECTED BIBLIOGRAPHY

## Mechanics

- Nadai, A. Theory of Flow and Fracture of Solids. Vol 2.  
New York. McGraw-Hill. 1963
- Hoffman, O., and Sachs, G. Theory of Plasticity for  
Engineers. New York. McGraw-Hill. 1953
- Mellor, P.B., and Johnson, W. Plasticity for Mechanical  
Engineers. New York. D. VanNostrand. 1962
- Hill, R. The Mathematical Theory of Plasticity. Oxford  
University Press. New York. 1950
- Timoshenko, S., and Goodier, J.N. Theory of Elasticity.  
2nd ed. New York. McGraw-Hill. 1951
- Bridgman, P.W. The Physics of High Pressure. London.  
G. Bell & Sons. 1958

## Mathematics

- Sneddon, I.N. Elements of Partial Differential Equations.  
New York. McGraw-Hill. 1957
- Hodgman, C.D. Standard Mathematical Tables. Cleveland.  
Chemical Rubber Company. 1954